PERFORMANCE CHARACTERISTICS OF A KITE POWERED PUMP

A Thesis Submitted
In Partial Fulfilment of the Requirements
For the Degree of

MASTER OF TECHNOLOGY

by

R. VIJAYAKUMAR

to the

DEPARTMENT OF MECHANICAL ENGINEERING
INDIAN INSTITUTE OF TECHNOLOGY, KANPUR
APRIL, 1984

CERTIFICATE

CERTIFIED that the work entitled, "PERFORMANCE CHARACTERISTICS OF A KITE POWERED PUMP" has been carried out under my supervision by Sri R. Vijayakumar and this has not been submitted elsewhere for award of a degree.

Kanpur
April 1984

J.S. Goela
Assistant Professor
Mechanical Engineering Department
Indian Institute of Technology
Kanpur 208016

ACKNOWLEDGEMENTS

I am deeply indeb ted to Dr. J. S. Goela for the way in which he guided me through this work. His deep involvement in the problem and willingness to discuss it at any time of the day made it possible to complete this thesis by now. I cannot express my sense of gratitude to him in words.

Thanks are due to Dr. V. K. Garg for his advices on the numerical solution of differential equations using computers. The numerical calculations had been done by the DEC-1090 system at Indian Institute of Technology, Kanpur.

I am thankful to Mr. H. K. Nathani for typing the manuscript, Mr. J.C. Verma for preparing the tracings and Mr. Ayodhya Prasad for cyclostyling work.

Finally I would like to thank all my friends in IIT Kanpur, especially Sri George Kurian for their help.

Kanpur
April 1984

- R. Vijayakumar

TABLE OF CONTENTS

LIST OF FIGURES

NOMENCLATURE

a - radius of pulley

A_k - Kite area

C_D - Coefficient of drag

C_L - Coefficient of lift

C_{LA} - Coefficient of lift during ascension

C_{LD} - Coefficient of lift during descension

$(C_L/C_D)_A$ - C_L/C_D during ascension

$(C_L/C_D)_D$ - C_L/C_D during descension

$(C_L/C_D)_{eq}$ - C_L/C_D corresponding to equilibrium

F_{DK} - Drag force on kite

F_{Dt} - drag on tether

F_{LK} - Lift force on kite

F_{Lt} - lift on tether

F_{LO} - Initial lift on kite

g - acceleration due to gravity

I_t - moment of inertia of tether

K, K' - Constants to determine drag on tether (Used in Appendix A)

K_f - $\exp\{\mu(\pi/2-\theta)\}$

L - length of tether from kite to pulley

L_l - Length of tether from pulley to load

L_o - initial tether length from kite to pulley

m_k - mass of kite

m_L - mass of load

S - Stroke

ABSTRACT

In this work, a kite powered pump is theoretically investigated to determine its performance characteristics. This pump directly converts the to and fro motion of the kite into up and down motion of a load which consists of water payload and container dead weight. In particular, feasibility of cyclic operation (comprising a power stroke starting from rest followed by a return stroke also starting from rest) of this pump has been investigated. The governing equations describing the motion of the system in both power and return strokes were developed assuming that the tether profile is a straight line. These equations were solved numerically on a computer.

The results show that power during power stroke is maximized when the kite moves cross wind. However, this mode of pump operation was not considered for detailed analyses due to several associated practical problems. Optimization of power output during ascension stroke (power stroke) was carried out when the tether is 70°. It turns out that gross load 1.68 times the static lift force gives the maximum power during ascension stroke. Corresponding

to this optimum, a return stroke bringing the kite back to its initial starting position can be designed by selecting a combination of load and C_L/C_D. From the point of view of cycle power, the best combination during descension stroke is the least possible load and a corresponding C_L/C_D to match the kite path profile. Further there is an optimum kite weight which maximizes the cycle power. For tether angle = 70°, length = 1000m, C_L/C_D = 6.5 during ascension, and = 2.0 during descension, wind velocity = 10m/s and kite area = $10m^2$, it turns out that a kite weight of 8 kg will maximize the power output.

I. INTRODUCTION

The present world depends heavily on earth's supply of non-renewable sources of energy to meet its power demand. The energy available from such sources is cheap, relatively easy to obtain and has high energy concentration. But such sources will inevitably be exhausted. This has led to a renewed interest in alternative sources of energy; especially wind energy.

Wind energy is considered an attractive source because it is renewable, non polluting and in a form (kinectic energy) that can be readily converted to other forms of energy. In spite of these attractive features this source has not yet been utilized for large scale power generation due to high capital cost of wind energy conversion systems.

Energy conversion systems making use of wind energy as its source are of two category: ground based systems and tethered systems. The altitude at which ground based systems (e.g. wind mills) can intercept wind is restricted by the constraints placed on them by the supporting structure. On the other hand there is no such restriction on the altitude at which wind is intercepted by tethered systems. This fact is important in that wind speed and hence the available wind potential is higher at larger altitudes. Due to this reason

the capacity ofasingle unit of ground based systems is much smaller than what can be generated from a single unit of tethered system.

There are two types of tethered systems. In the first type, the tether is for the purpose of anchoring a conversion system at the altitude at which it is to operate. The wind is intercepted by wind turbines mounted on supporting devices such as aerodynamic platforms [1], rotary wing platforms [2], balloons [3] and kites [4]. These devices develop enough lift to support the weight of the system. The tether has the additional function of transmitting the electricity generated on the platform to the ground.

In the second type of tethered energy conversion systems, the wind potential is intercepted by a kite or an aerodynamic body at higher altitude while the energy conversion is done on the ground. The tether not only supports the kite, but also serves as a means of transmitting motion of the kite to the ground for eventual conversion into other more useful forms of motion [5-8]. The kite motion as a consequence of the wind can either be converted into rotary motion or it can be used directly to pull loads on the ground. The latter mode of operation is best suited for pumping water from a well. Pumping water with the help of kites is an important application for irrigation of farms.

Though an economic analysis of a kite powered pump has not yet been done, it appears that such a system will probably incur less capital and maintenance costs in comparison to other wind energy systems.

In this study, an attempt has been made to investigate theoretically a kite powered pump and to determine its performance characteristics. For this purpose a system study taking into account kite, tether and the load together has been carried out to explore if the cyclic operation of the pump is feasible. To the best of the knowledge of the author such a system study emphasizing the dynamical aspects has not yet been carried out, though one can find simplified analyses which considers only the dynamics of the kite [7,8]. In our study, dynamical equationsboth in ascension and descension havebeen developed assuming that the tether profile is a straight line. Important parameters affecting the performance of the kite powered pump havebeen identified and optimization done with respect to them. In particular it will be seen if an increase in kite weight will affect the performance adversely. In Section II, the literature on tethered wind energy conversion systems is reviewed. Section III presents the details about the kite powered pump and the governing equations. In Section IV the method of solution of the governing equations is given. The results of the analysis are presented in Section V followed by conclusions in Section VI.

II. REVIEW OF LITERATURE ON TETHERED SYSTEMS

Simple kites had been in use for the purpose of pulling loads for hundreds of years. But they never competed with wind turbines for power generation [10]. In the early part of the 19th century, G. Pocock refined the use of kites as much as was then possible [11]. Until recently, the kite powered systems had been virtually ignored due to the invasion of more attractive energy sources. The following is a brief survey of the various tethered systems so far suggested.

In locations where very high speed (jet stream) wind is available, Fletcher and Roberts [1] suggest the use of aerodynamic platforms to intercept it. The aerodynamic platform consists of a glider like structure with high lift devices permanently deployed. Incorporated into the aerodynamic platform are wind turbines coupled to generators. The platform is held in position by two tethers each with an inner core of kevlar surrounded by an aluminium sheath to carry the generated electricity. The availability of jet stream wind in Australia and the feasibility of the suggestion has been established.

The purpose of the high lift platforms is to generate sufficient lift to support the machinery mounted

on them. Four designs of aerodynamic platforms are compared for the cost of electricity generation by Fletcher, Honan and Sapuppo [2]. The four configurations are Integrated diffuser Augmented Wind Turbines (IDAWT), Separated Diffuser Augmented Wind Turbines (SDAWT), Separated Unshrounded Wind Turbine (SUWT), and Rotary Wing Concept (RWC). The first three are modifications in the wind turbines locations on the platform so as to increase the mass flow through the turbines while the fourth configuration necessarily means the use of the turbines themselves for the purpose of providing the necessary lift.

The IDAWT configuration is one in which, the lift producing parts of the platform also assist the power extraction function via the generation of additional circulation. In SDAWT concept the diffusers are separated from the lift generating wings resulting in a lighter structure. When turbines are used without shrouds larger diameter turbines are required. But this is somewhat offset by the absence of the weight of the shrouds. This is the basis of SUWT. In RWC, the conventional horizontal axis turbines are tilted forward. As a result, the turbines both generate power and provide lift to support platforms. On the basis of the economic analysis, it is pointed out that RWC is unsuitable for the purpose due to its high operating cost. Reigler, Riedler and Horvath [3] have suggested a similar scheme but use a balloon instead of the aerodynamic platform.

Loyd [4] shows how the power generating capacity of a tethered system can be increased artificially by rotating the kite about the lower end of the tether at high speeds. His analysis is based on a kite designed in the shape of a C-5A aircraft. These kites are aerodynamically efficient and generate sufficient lift to support the machinery mounted on them. The scheme is to allow the kites to move in large circles transverse to the wind. This motion increases the wind speed relative to the system, thereby increasing the energy potential. It is claimed that a single kite based on the C-5A design is capable of generating 6.7MW from a 10 m/s wind. Although the suggestion appears very attractive, it is doubtful whether the cross wind motion can be sustained, particularly if the wind speed changes.

All the systems mentioned above use wind turbines for conversion of wind energy. The kite (or its equivalent) is used solely for the purpose of enabling the turbine generator combination to remain at an altitude so as to intercept increased velocity wind.

Goela has suggested that the to and fro motion of a kite can be utilized for power generation [5-8]. In this scheme, the tether acts as a connecting link and transmits kite motion to the ground where a suitable mechanism converts this motion into a desired form. One method of converting the motion of the tether into rotary

motion of a shaft is to employ a mechanism similar in function to the crank of an IC engine [5]. In this method, the lower end of the tether is attached to a rotor. There are two strokes: power stroke when the kite is let out and the rotor rotates through half a revolution, and the return stroke when the kite is pulled in and the rotor completes the other half revolution. There is a net gain of power if the power developed in power stroke is larger than that consumed during the return stroke.

In another configuration called the reeling arrangement, the kite tether is fed from a reel during the power stroke and is wound around it when the kite executes its return stroke [7,8]. The reel is so mounted on the shaft that during the power stroke the reel drives the shaft, while during the return stroke the shaft drives the reel in the opposite direction to bring the kite back. A drawback of the above scheme is the absence of power generation from the system during the return stroke. To generate power continously, a two kite system has been suggested [7]. The two kites are attached to tethers on two different reels mounted on the same shaft. The system can be so designed that, while one kite is executing the power stroke the other is returning. This way continuity of power generation can be ensured.

A single kite reeling system can be used to pump water from a well, by attaching the bucket to the reel directly by a string. While the kite executes power stroke, the reel rotates such that the string attached to the bucket is wound around it and consequently the bucket with water is lifted up. At the end of the power stroke, the kite angle of attack is reduced and the water payload is removed from the bucket. Then the bucket weight causes the reel to rotate in the opposite direction, the tether attached to the kite is wound on the reel, but the string attached to the bucket is unwound and the bucket moves down [7].

When the bucket to carry water from a well is attached directly to the end of the tether, without any reeling arrangement, the conversion system becomes the simplest. This is a kite powered pump [8]. In this system the to and fro motion of the kite is converted directly into up and down motion of the pump.

In all the above systems which employ the to and fro motion of a kite to generate power, it is necessary that the attitude of the kite relative to the wind be changed at the end of each stroke. Of the mechanisms suggested for this purpose [7,8] one design employs a servomotor mounted on the kite to alter the kite attitude. The servo mechanism is activated by a radio signal transmitted from the ground at the end of a stroke. The servo-mechanism

can tilt the kite directly [7] or it can control a flapper at the tail of the kite [7]. The lift on the flapper can be adjusted so as to exert a moment on the kite to rotate it. In another mechanism, two tethers are employed. The relative movement of the two tethers caused by a tripping mechanism in the ground equipment causes the necessary tilting of the kite. The tripping mechanism is actuated when the load reaches a dead centre [9].

III. FORMULATION OF THE PROBLEM

3-1. A Kite Powered Pump

A kite powered pump consists essentially of a kite, its tether going around a pulley and a mechanism to change the attitude of the kite when desired. Fig. 1 shows schematically the arrangement of the system. (The kite attitude changing mechanism is excluded.)

The kite intercepts wind at a desired altitude. The wind while passing over the kite generates lift and drag. If the lift and drag are sufficient to overcome the weight of the system including the load (consisting of a bucket dead weight and water payload), the kite moves up. This is the ascension stroke. On the other hand if the weight of the system overcomes the lift and drag, the kite moves down. This is descension stroke. The lift and drag on the kite is a function of its attitude (angle of attack) with respect to the wind.

At the start of each cycle of operations, the mechanism which changes the angle of attack α, positions the kite so that the lift to drag ratio (C_L/C_D) is a maximum. This enables the kite to produce sufficiently large lift and drag to ascend. During ascension the load (bucket and water) also moves up. At the end of the ascension stroke the mechanism is activated to change the angle of

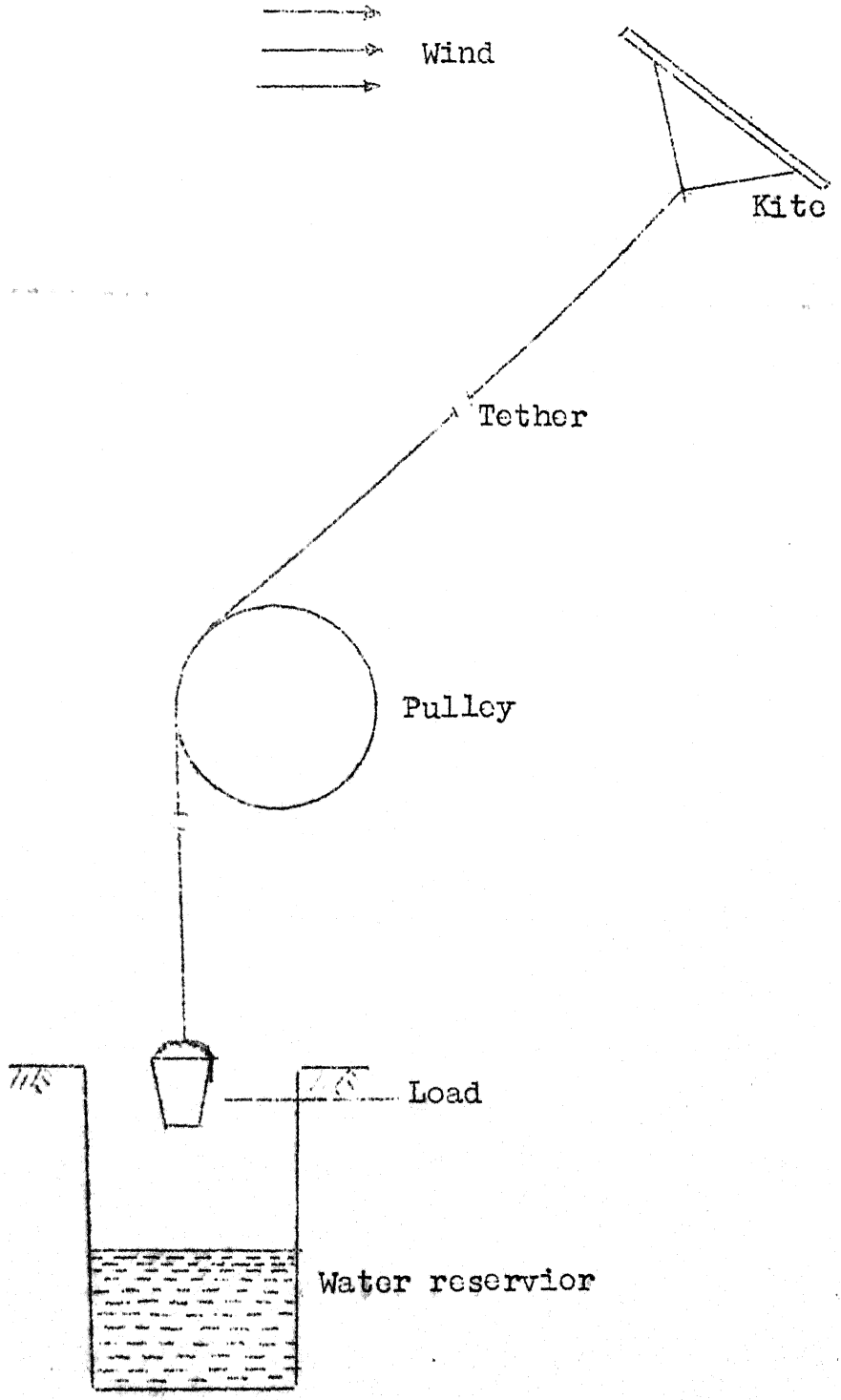

Fig. 1: Schematic arrangement of a kite powered pump.

attack to a small value so that C_L/C_D is small. The mechanism also trips the bucket to deliver water to a channel or a tank. Now the lift is very small and so is the load at the end of the tether (bucket alone). Still, this dead weight can overcome the lift and drag, so that the kite is pulled back to its original position. At the end of the descension stroke once again the mechanism is activated to increase angle of attack. At the same time the bucket is tipped to fill itself with another load of water. A new cycle of operations ensues.

3-2. Governing Equations

For the purpose of analysis the mechanism which changes the angle of attack is not considered. We assume that C_L/C_D does not change during a stroke, air density and wind speed are functions of neither altitude nor time, and tether profile is a straight line. This later assumption is reasonable as shown through calculations in Appendix A.

Consider the kite moving with a velocity V_k in a direction making an angle β with the horizontal. The relative wind velocity in the rest frame of the kite is V_R (refer Fig. 2), in a direction making an angle Φ with the horizontal. The tether is at an inclination θ with the horizontal. The lift F_{LK} and drag F_{DK} on the kite can be calculated as

$$F_{LK} = \frac{1}{2} \rho C_L A_K V_R^2 \qquad (1)$$

$$F_{DK} = \frac{1}{2} \rho C_D A_K V_R^2 \qquad (2)$$

where ρ, C_L, C_D, A_K, and V are the air density coefficient of lift, coefficient of drag, the surface area of the kite and the wind speed and

$$V_R^2 = V^2 + V_K^2 - 2V V_k \cos\beta \qquad (3)$$

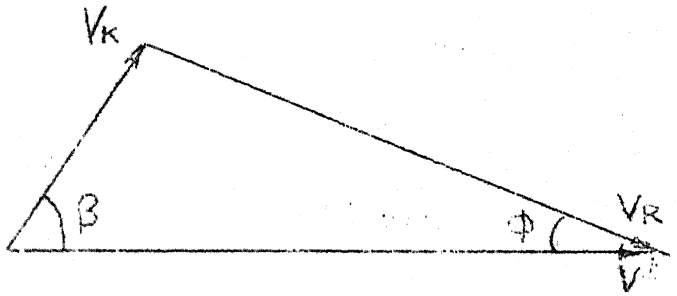

Fig. 2: Velocity in the rest frame of the kite.

The angle Φ is calculated from

$$\tan \phi = \frac{V_K \sin\beta}{V - V_K \cos\beta} \qquad (4)$$

The equation of motion is derived by making a force balance in any direction. If V_1 and V_2 are the components of V_K along and perpendicular to the direction of the tether, force balance in the direction

of V_1 (refer Fig. 3) yields

$$(m_k + w_t L)\frac{dV_1}{dt} = F_{LK}\,\mathrm{Sin}\,(\theta+\Phi) + F_{DK}\,\mathrm{Cos}(\theta+\Phi) -$$

$$(W_k + w_t L\,g + F_{Lt})\,\mathrm{Sin}\,\theta + F_{Dt}\,\mathrm{Cos}\,\theta - T_p \qquad (5)$$

where m_k, w_t, L, W_k, F_{Lt}, F_{Dt} and T_p are the mass of kite, mass density of tether per unit length, length of tether from the kite to pulley, weight of kite, lift and drag on the tether, and the tension at the pulley end of the tether respectively.

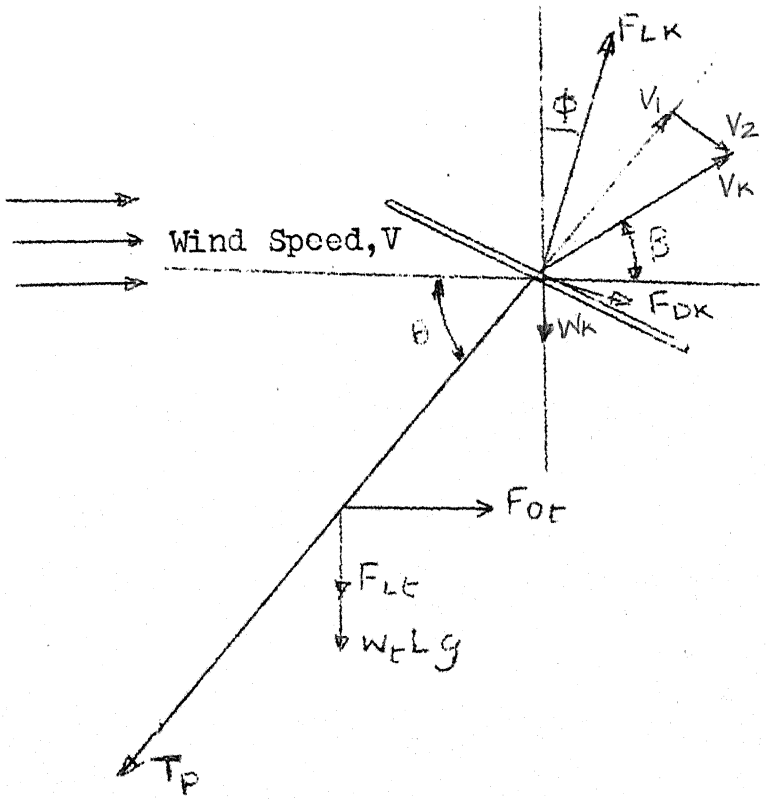

Fig. 3: Forces on the kite and kite tether upto pulley.

Moment balance about the pulley end of the tether provides the equation of motion perpendicular to it

$$(m_K L^2 + I_t)\frac{d^2\theta}{dt^2} = \left\{F_{LK}\,\mathrm{Cos}(\theta+\Phi) - F_{DK}\,\mathrm{Sin}(\theta+\Phi) - W_k\,\mathrm{Cos}\,\theta\right\} L - \left\{(W_t L\, g + F_{Lt})\,\mathrm{Cos}\theta - F_{Dt}\,\mathrm{Sin}\,\theta\right\}\frac{L}{2} \qquad (6)$$

where I_t is the moment of inertia of the tether about its end.

In order to get a relation in terms of V_2, the kite velocity perpendicular to the tether, $\frac{d^2\theta}{dt^2}$ can be evaluated from the following. Referring to Fig. 4 we obtain the geometric relations

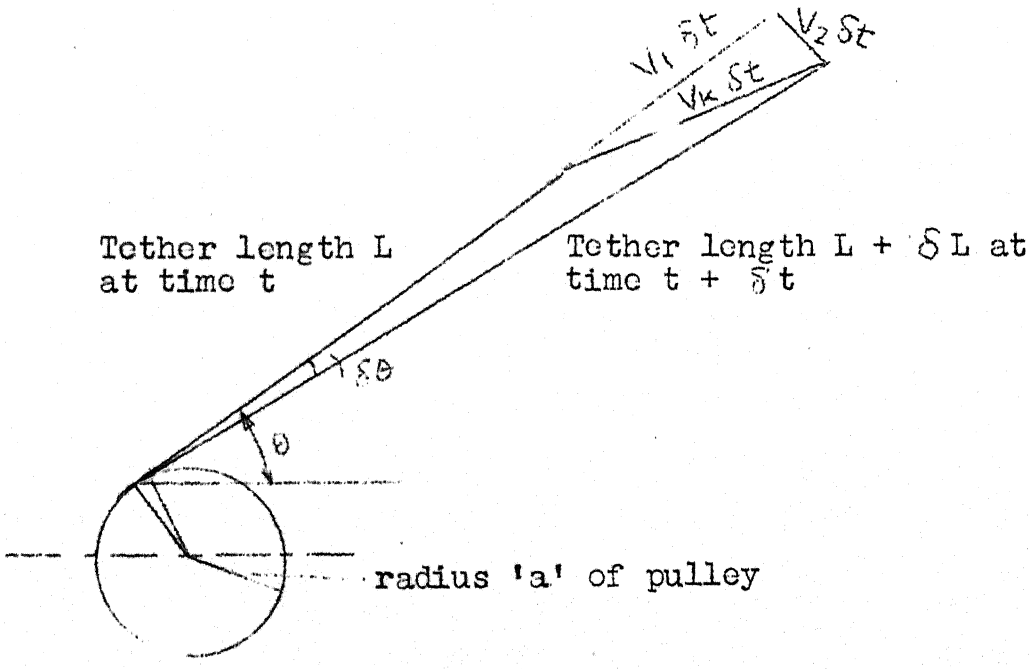

Fig. 4: Movement of tether in a small time interval δt.

$$L + \delta L = L + V_1 \delta t - a\ \delta\theta$$

or

$$\frac{\delta L}{\delta t} = V_1 - a\frac{\delta\theta}{\delta t} \qquad (7)$$

and

$$\frac{\delta\theta}{\delta t} = \frac{V_2}{L} \qquad (8)$$

Noticing that $\delta\theta$ is negative, equation (7) and (8) will become

$$\frac{dL}{dt} = V_1 - a\frac{d\theta}{dt} \qquad (9)$$

and $$\frac{d\theta}{dt} = -\frac{V_2}{L^2} \qquad (10)$$

respectively as $\delta\theta$, δL and $\delta t \longrightarrow 0$

Differentiation of eqn (10) yields

$$\frac{d^2\theta}{dt^2} = -\frac{1}{L}\frac{dV_2}{dt} + \frac{V_2}{L^2}\frac{dL}{dt}$$

which gives after substitution for $\frac{dL}{dt}$

$$\frac{d^2\theta}{dt^2} = -\frac{1}{L}\frac{dV_2}{dt} + \frac{V_1V_2}{L^2} + \frac{aV_2^2}{L^3} \qquad (11)$$

Equation (5) contains an unknown tension T_p which can be expressed in terms of the load. If we assume the pulley to be rotating and frictionless $T_p = T_L$. However if the pulley is fixed then T_p and T_L are related as: (refer fig 5)

$$\frac{T_p}{T_L} = \exp\left(\mu\left(\frac{\pi}{2} - \theta\right)\right) \qquad (12)$$

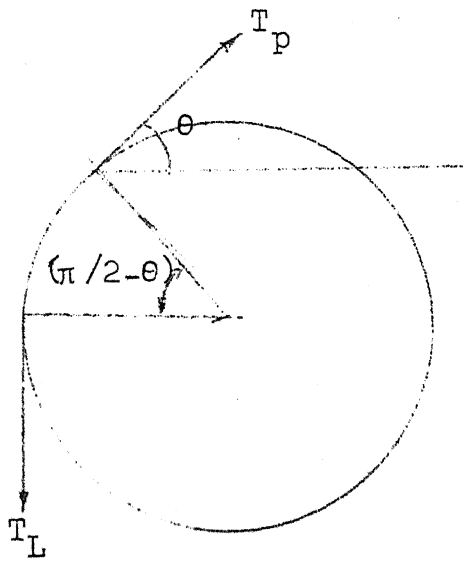

Fig. 5: Force transmission around the pulley.

where T_L is the tension at the load end of the pulley, and μ is the coefficient of friction between tether and pulley.

Fig. 6 shows the forces at the load end of the system. Force balance for this gives,

$$(m_L + w_t L_1) \frac{dV_2}{dt} = T_L - W_L - w_t L_1 g \qquad (13)$$

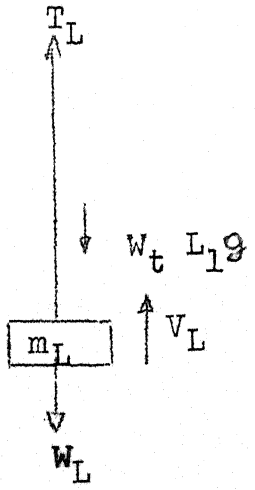

Fig. 6: Forces at the load end of the system.

where m_L, L_1, V_L and W_L are the mass of the load, length of tether from pulley to load, the load velocity and load respectively.

From Eqn. (12, 13) we can calculate T_p as

$$T_p = \left\{(m_L + w_t L_1) \frac{dV_L}{dt} + W_L + w_t L_1 g\right\} e^{\mu(\frac{\pi}{2} - \theta)} \qquad (14)$$

It may be noted that load velocity V_L and V_1 will be numerically equal. Using this fact and substituting for the value of T_p from Eqn. (14) into Eqn. (5) we get

$$(m_k + w_t L) \frac{dV_1}{dt} = F_{LK} \operatorname{Sin}(\theta+\Phi) + F_{DK} \operatorname{Cos}(\theta+\Phi)$$

$$- (W_K + w_t L g + F_{Lt}) \operatorname{Sin} \theta + F_{Dt} \operatorname{Cos} \theta - \left\{(m_L + w_t L_1) \frac{dV_1}{dt} + W_L + w_t L_1 g\right\} \exp(\mu(\tfrac{\pi}{2} - \theta),$$

which when rearranged gives

$$\frac{dV_1}{dt} = [F_{LK} \operatorname{Sin}(\theta+\Phi) + F_{DK} \operatorname{Cos}(\theta + \Phi) - (W_K + w_t L g + F_{Lt}) \operatorname{Sin} \theta + F_{Dt} \operatorname{Cos} \theta - (W_L + w_t L_1 g) \exp\left\{\mu(\tfrac{\pi}{2} - \theta)\right\}] / \left\{m_k + w_t L + (m_L + w_t L_1) e^{\mu(\frac{\pi}{2} - \theta)}\right\} \qquad (15)$$

Similarly Eqn. (6) after substitution for $\frac{d^2\theta}{dt^2}$ and rearrangement yields

$$\frac{dV_2}{dt} = [F_{DK} \sin(\theta+\Phi) - F_{LK} \cos(\theta-\Phi) + W_K \cos\theta +$$

$$\frac{w_t L g}{2} + F_{Lt} \cos\theta + \frac{F_{Dt}}{2} \sin\theta + (m_K + \frac{I_t}{L^2})(\frac{V_1 V_2}{L} + \frac{aV_2^2}{L^2})]/$$

$$(m_K + I_t/L^2) \qquad (16)$$

In the above equations I_t, the moment of inertia of tether at the kite side of the system is calculated as

$$I_t = w_t \frac{L^3}{3} \qquad (17)$$

It may be noticed that the length of the tether from pulley to load L_1 changes at the rate of V_L

$$\text{i.e.} \quad \frac{dL_1}{dt} = V_L = V_1 \qquad (18)$$

Equations (15, 16, 18, 9 and 10) form a closed set of first order differential equations. The boundary conditions are given as at $t = 0$,

$$\begin{aligned} L &= L_o \\ \theta &= \theta_o \\ V_1 &= 0 \\ V_2 &= 0 \\ L_1 &= L_{10} \end{aligned} \qquad (19)$$

3-3. Simplification of the Equations

The radius of the pulley 'a' is very small in comparison to L, and hence may be neglected. The lift and drag on the tether are also neglected. In our calculations with $w_t = 1.0 \times 10^{-3}$ kg/m length, and L = 1000m, mass of tether becomes small in comparison to the load (of the order of 100 kg). Hence the terms containing tether weight and mass are neglected. With these simplifying assumptions, the governing equations become

$$\frac{dL}{dt} = V_1 \tag{20}$$

$$\frac{dV_1}{dt} = \frac{F_{LK} \sin(\theta+\phi) + F_{DK} \cos(\theta+\phi) - W_K \sin\theta - W_L k_f}{m_L k_f + m_k} \tag{21}$$

$$\frac{dV_2}{dt} = \frac{F_{DK} \sin(\theta+\phi) - F_{LK} \cos(\theta+\phi) + W_k \cos\theta + (m_K + \frac{w_t L}{3}) - \frac{V_1 V_2}{L}}{m_k + w_t L/3} \tag{22}$$

where

$$K_f = \exp\{\mu(\tfrac{\pi}{2} - \theta)\} \tag{23}$$

These equations along with (10) are a closed set of differential equations which describe the system during ascension. The initial conditions are:

$$\left.\begin{aligned} L &= L_o \\ \theta &= \theta_o \\ V_1 &= 0 \\ V_2 &= 0 \end{aligned}\right\} \quad \text{at} \quad t = 0 \tag{24}$$

3-4. Equations of Motion During Descension

The above set of equations describes the motion during descension also with a minor modification in Eqn. (23). This becomes

$$K_f = \exp\left\{-\mu\left(\frac{\pi}{2} - \theta\right)\right\} \qquad (25)$$

This is because during descension, T_L is greater than T_p. It should be noted that during descension V_1 is negative.

3-5. Non Dimensionalization of the Equations

The governing equations are non-dimensionalized for identifying the parameters which affect the performance of the system. The V, L_o, t_o and F_{Lo} are defined as the characteristic velocity, length, time and force for this purpose, where

$$F_{Lo} = \frac{1}{2} \rho C_L A_K V^2 \qquad (26)$$

Non-dimensionalization of Equations (3,4,10,20,21 and 22) gives respectively,

$$\bar{V}_R^2 = 1 + \bar{V}_k^2 - 2 \bar{V}_k \cos\beta \qquad (27)$$

$$\tan\phi = \bar{V}_k \sin\beta \,/\, (1 - \bar{V}_k \cos\beta) \qquad (28)$$

$$\frac{d\theta}{d\bar{t}} = \left(\frac{V_{to}}{L_o}\right) \frac{\bar{V}_2}{\bar{L}} \qquad (29)$$

$$\frac{d\bar{L}}{d\bar{t}} = \left(\frac{V_{to}}{L_o}\right) \bar{V}_1 \qquad (30)$$

$$\frac{d\bar{V}_1}{d\bar{t}} = \frac{gt_o}{V} \left[\frac{\bar{V}_R^2 \, \mathrm{Sin}(\theta+\phi) + \frac{C_D}{C_L} \mathrm{Cos}\,(\theta+\phi) - \bar{W}_k \, \mathrm{Sin}\theta - \bar{W}_L K_f}{\bar{W}_L \, K_f + \bar{W}_k} \right] \tag{31}$$

$$\frac{d\bar{V}_2}{d\bar{t}} = \frac{gt_o}{V} \left[\left\{ \bar{V}_R^2 \left(\frac{C_D}{C_L} \mathrm{Sin}(\theta+\phi) - \mathrm{Cos}(\theta+\phi) \right) + \bar{W}_k \cos\theta + \left(\frac{\bar{W}_k}{g} + \frac{w_t L_o}{3F_{L_o}} \bar{L} \right) \frac{V^2}{L_o} \frac{\bar{V}_1 \bar{V}_2}{\bar{L}} \right\} \Big/ \left(\bar{W}_k + \frac{w_t L_o g}{3F_{Lo}} \bar{L} \right) \right] \tag{32}$$

In the above equations, the characteristic time t_o may be choosen as $\frac{S}{V}$ in Equations for V_1 and $\frac{L_o}{V}$ in equations for V_2 and θ. Then, the following dimensionless parameters emerge:

$\pi_1 = \frac{S}{L_o}$ = stroke to Length

$\pi_2 = \frac{gL_o}{V^2}$

$\pi_3 = C_L/C_D$ = Lift to drag ratio

$\pi_4 = \frac{W_k}{F_{Lo}} = \bar{W}_k$ = Kite weight parameter.

$\pi_5 = \frac{W_L}{F_{Lo}} = \bar{W}_L$ = Load parameter

$\pi_6 = \theta_o$ = Initial tether angle.

Although $\frac{V_k}{V} = \bar{V}_k$ also appears to be a parameter, it is a time dependant variable and hence not regarded as a parameter.

IV. SOLUTION OF THE EQUATIONS

The governing equations are a set of first order, coupled, non linear differential equations. They were solved simultaneously by a fourth order Runge-Kutta method (see Appendix B for program).

The data used were

$$\rho = 1.167 \text{ kg/m}^3,$$

$$V = 10 \text{ m/s},$$

$$A_k = 10\text{m}^2,$$

$$\mu = 0.25.$$

w_t was computed from the properties of tether material. The tether was designed for a tension of 500N. For 'Kevlar 29' with density = 1440 kg/m^3 and tensile strength = 2.8×10^9 Pa, the diameter of tether is 0.9 mm. (Factor of safety = 4). With this tether $w_t = 1.008 \times 10^{-3}$ kg/m. However, the same w_t was used for tensions beyond 500N also. It does not affect our results very much since this is used in the equation for V_2 only and is comparatively unimportant.

To start a Runge-Kutta scheme, the initial value of all the four dependant variables are needed. These were given as the boundary conditions at t = 0, L = 1000m, $V_1 = 0$, $V_2 = 0$. Initial tether angle θ was changed to investigate the possibility of optimisation.

Except when the performance was studied for the effect of W_k on it, m_k was taken as 1.3 kg. Similarly the initial length of tether was changed only when that parameter was being investigated. For most part of the analysis, C_L/C_D, m_L and θ were treated as parameters.

The numerical calculations were carried out in the following manner:

The initial values of L, θ, V_1, V_2 and t are known. With the help of other known parameters, the rates of change $\frac{dL}{dt}$, $\frac{d\theta}{dt}$, $\frac{dV_1}{dt}$, and $\frac{dV_2}{dt}$ are computed if F_{LK}, F_{DK} and ϕ are known (Eqns. 10, 20, 21, 22). These are calculated from the aerodynamic relations $F_{LK} = \frac{1}{2} \rho C_L A_k V_R^2$ and $F_{DK} = \frac{C_D}{C_L} F_{LK}$ where $V_R^2 = V^2 + V_K^2 - 2V V_K \cos\beta$.

Initially $\beta = 0$, $\phi = 0$ and $V_R^2 = V^2$. Hence the rates of change of the four variables are known.

[When $V_K \neq 0$, β is calculated as $\beta = \theta - \tan^{-1}\left(\frac{V_2}{V_1}\right)$ $V_K^2 = V_1^2 + V_2^2$ and $\phi = \tan^{-1} \frac{V_K \sin\beta}{V - V_k \cos\beta}$. This leads to V_R^2 and the computation of lift and drag.]

The current values of L, θ, V_1 and V_2 and their rates of change computed in the above manner are fed to the Runge-Kutta subroutine, which in turn computes the variables at the next point (i.e., after a small time interval dt). This procedure is repeated until the load is moved through a pre-determined stroke 'S'.

V. RESULTS and DISCUSSION

The performance of an energy conversion system is usually evaluated by the amount of average power it generates. In order to maximize power in cyclic operation (consisting of two strokes-ascension and discension) it is necessary to maximize power during ascension and minimize it during discension. This optimization is to be done with the condition that after one cycle, the kite comes back to the same location from where it started. In the following, first we discuss power output during ascension with an aim to maximize it with respect to various parameters, then we discuss power output during discension and finally the cyclic operation. The effect of kite weight parameter, and length of tether on the performance characteristics of the kite powered pump is discussed at the end of this section.

5-1. Kite Powered Pump in Equilibrium

Before going into the discussion of the system during ascension and discension, let us first study the system in static equilibrium. This is important because, in this thesis, we have assumed that both power and return strokes start from rest. Starting from rest does not necessarily mean that the system will be in equilibrium, but equilibrium position is one situation from where the cycle could conveniently begin.

Fig. 7 shows the various forces acting on the kite at equilibrium. From the figure it is easy to see that the tether angle 0 and tension T_K are given by

$$0 = \tan^{-1}\left(\frac{F_{LK} - W_K}{F_{DK}}\right) = \tan^{-1} \frac{C_L}{C_D}(1 - \bar{W}_K) \qquad (26)$$

and

$$T_K = (F_{LK} - W_K) \text{ Sin } 0 + F_{DK} \text{ Cos } 0 \qquad (27)$$

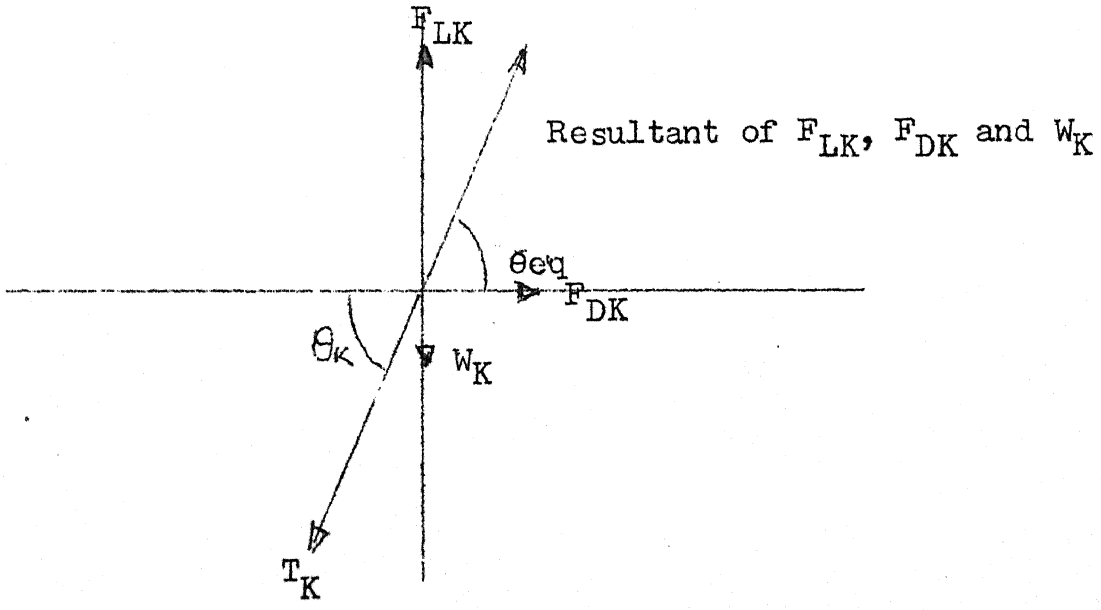

Fig. 7: Forces on the kite at equilibrium.

The angle 0 and tension T_K obtained from Equations (26) and (27) may be called 0_{eq} and $T_k eq$ respectively. Thus for a given $\frac{C_L}{C_D}$ and W_k there exists a definite 0_{eq} and $T_k eq$, at which the kite is in equilibrium. The values of 0_{eq} and $T_k eq$ for various values of $\bar{W}_K$ as a function of C_L/C_D are given in Figs. 8 and 9. From Figure 8

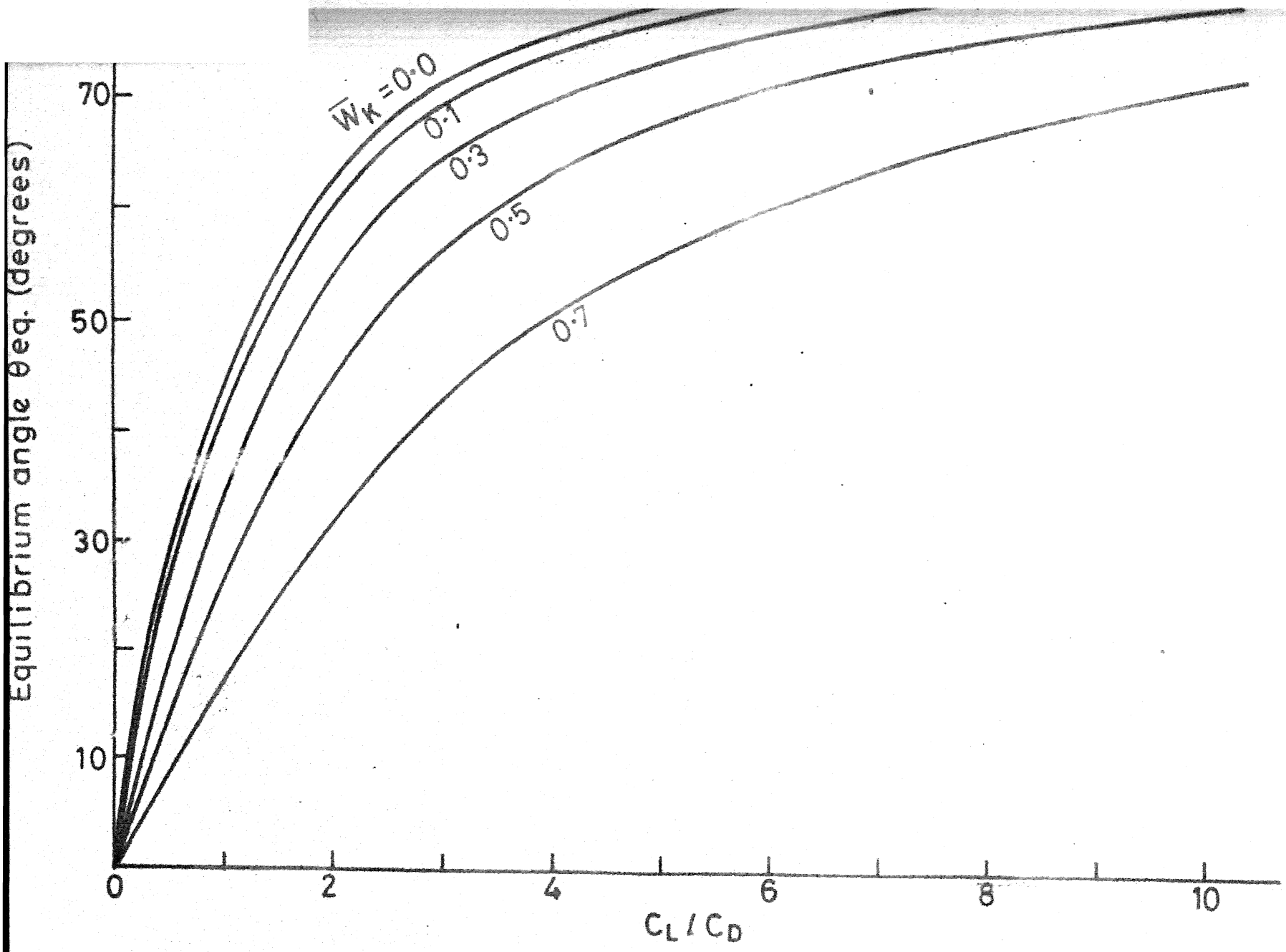

Fig.8 The equilibrium tether angle as a function of C_L/C_D for different values of $\bar{W}_K$

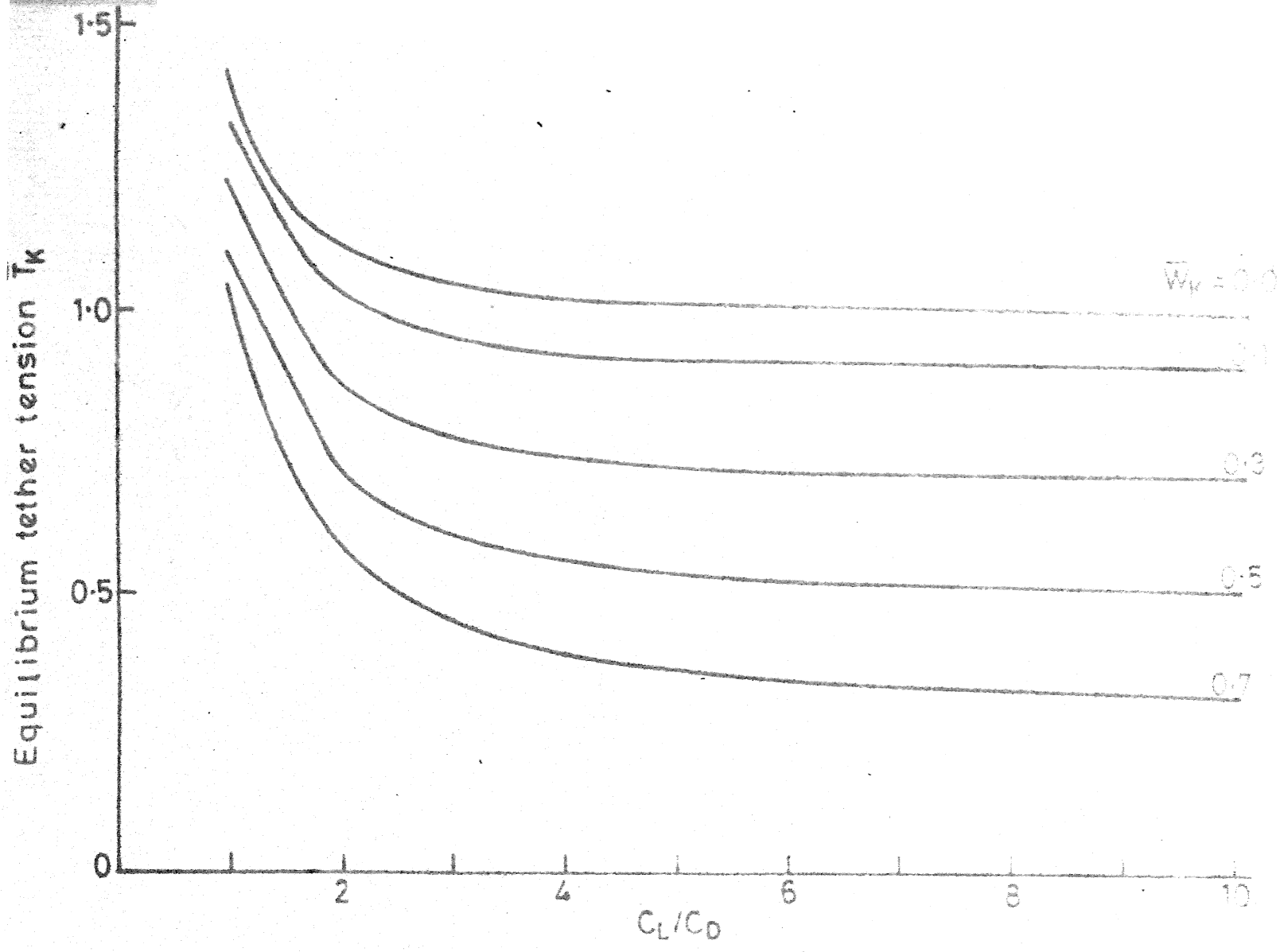

Fig.9 The equilibrium tether tension vs C_L/C_D for different values of $\bar{W}_K$

we see that, at large C_L/C_D the change in θeq is small when $\bar{W}_K$ changes from 0 to 0.5. For example, θeq changes by 9% when $\bar{W}_k$ changes from 0 to 0.5 at $C_L/C_D = 10$. But the change in θeq is significant at small C_L/C_D and at large W_k. Fig. 9 shows normalized $T_k eq$ plotted against C_L/C_D for different values of $\bar{W}_k$. No significant change in $\bar{T}_k$ is observed for large C_L/C_D. However, for $C_L/C_D < 3.0$, the change in $\bar{T}_K$ is significant.

If the actual tether angle $\theta = \theta eq$, the magnitude of actual tension T_k (in comparison to $T_k eq$) determines whether the kite will ascend or descend. For instance, if $T_k < T_k eq$, the kite will ascend and if $T_k > T_k eq$, then it will descend. At other angles, in addition to this motion in the direction of θ there will also be kite movement perpendicular to the tether.

5.2 Performance of the Kite Powered Pump During Ascension

Now we consider the performance of the kite pump in ascension. This is shown in Fig. 10-20. In Fig. 10, the normalized average power is shown as a function of normalized load. The normalization of power is done with respect to the total available wind potential ($\frac{1}{2} \rho C_L A_K V^3$) while that of the load is done with respect to the lift force ($= \frac{1}{2} \rho C_L A_K V^2$). From this figure, it can be seen that there is a maximum in average power both with respect to load as well as initial tether angle θ. The maximum

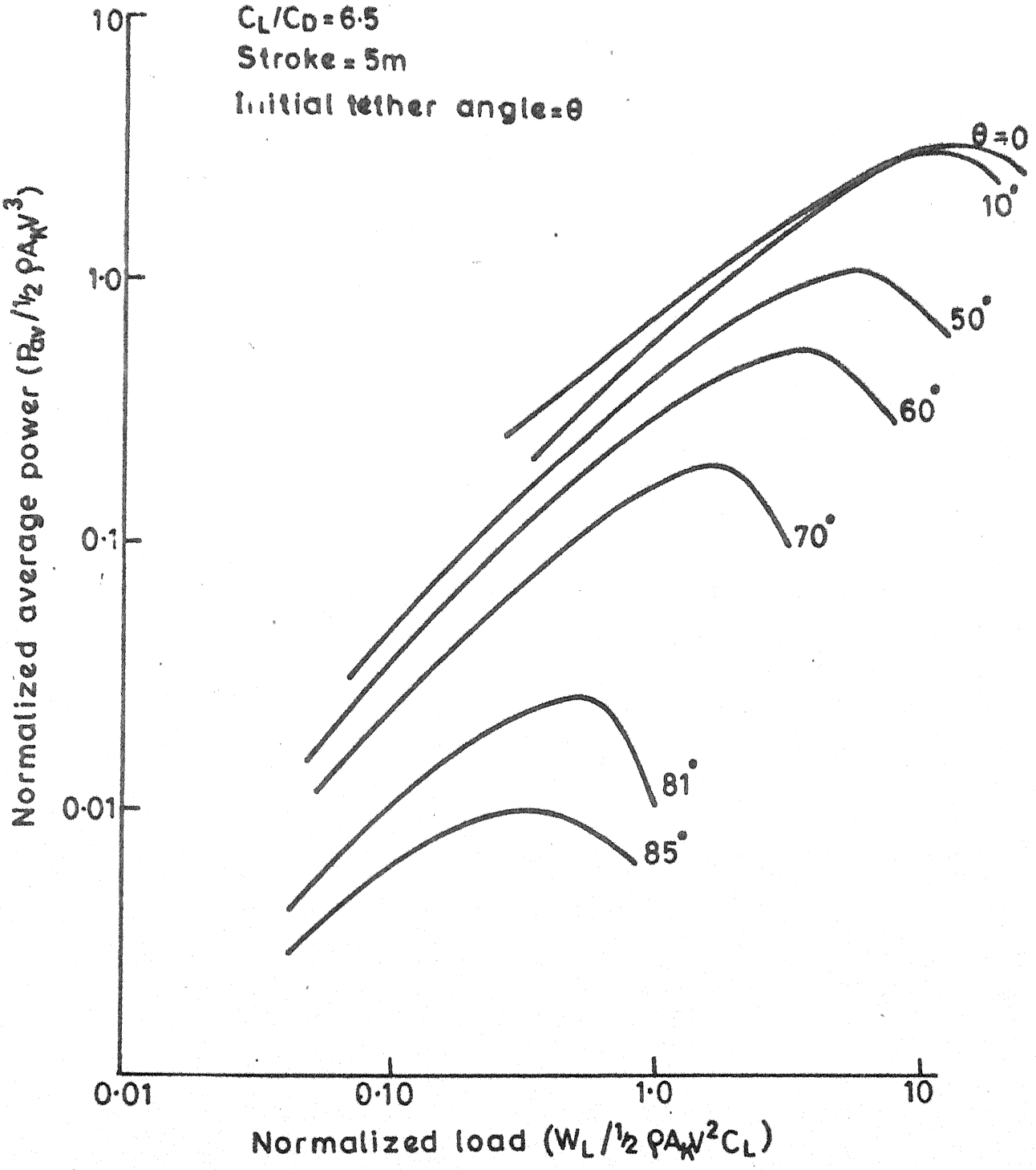

Fig.10 Variation of average power with load

power is obtained when initial tether angle $\theta = 0^{\circ}$, and $\bar{W}_L \simeq 13$. Tether angle $\theta = 0^{\circ}$, implies that the kite is moving approximately crosswind. As is discussed in Ref. [4] when a cross wind motion takes place there is a substantial increase in power output of a kite energy conversion system. Thus our results are in agreement with those of [4]. It should be noted that when the kite is in motion during ascension, it can support load which is 13 times the initial lift. This is because, as the kite moves, the relative velocity, generated is much larger than the wind velocity. Since the maximum power is obtained when the velocity in the direction of the tether is $\frac{1}{3}$rd of the wind velocity [4,8], it is essentially the velocity perpendicular to the tether that contributes towards such large relative wind velocity. For the same reasons the maximum normalized average power is greater than 1.0.

In Fig. 11, the variation of ascension time with normalized average load for different values of θ is shown. We see that as load increases the ascension time also increases. The ascension time is less for smaller angles, the time being the least for $\theta = 0^{\circ}$. At $\theta < \theta_{eq.}$, the forces in the direction perpendicular to the tether become unbalanced. This gives rise to a velocity in a direction perpendicular to the tether. The smaller the angle θ, the larger the magnitude of this force and subsequently the velocity as

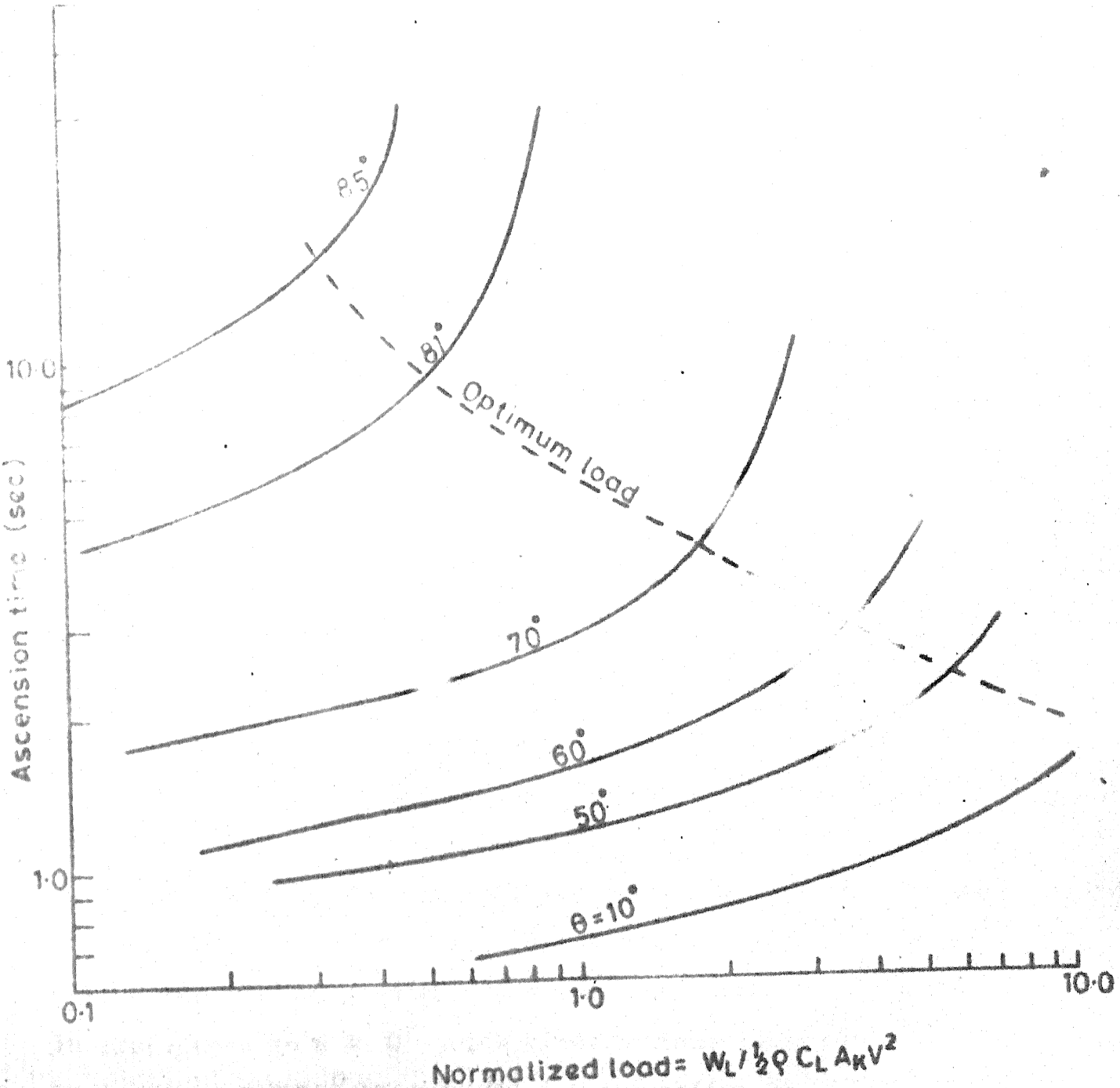

Fig.11 Time of ascension vs load at various tether angles

explained in the preceding paragraph. As a result the driving forces during ascension (lift and drag) become large and the system ascends more rapidly. But a limit reaches, when any further increase in load can not increase V_R sufficiently, to generate lift and drag to balance the increased load. Thus, the time of ascension increases, more rapidly beyond this load. This feature can be observed by the sharp increase in time beyond loads indicated by the dashed line. This behaviour also explains why the average power output decreases beyond this load. It can also be noted that, for the same average power developed, the load increases and the time decreases as θ is decreased. This indicates that the load carrying capacity of the system can be increased by operating it at smaller tether angles, without sacrificing the power output from the system. The above results were obtained for $C_L/C_D = 6.5$ and stroke = 5m.

The plot of normalized instantaneous power Vs time during ascension for different values $\bar{W}_L$ is shown in Fig. 12. In making the following calculations, we have taken $\theta = 70^\circ$. In preference to $\theta = 0^\circ$ which gives maximum power we have chosen $\theta = 70^\circ$ because (i) the assumption of a straight line tether is better satisfied when $\theta = 70^\circ$ (see Appendix) and (ii) $\theta = 70^\circ$ is more appropriate from the point of view of the system operation. As has been emphasized in Ref. [7], one would lose most of the

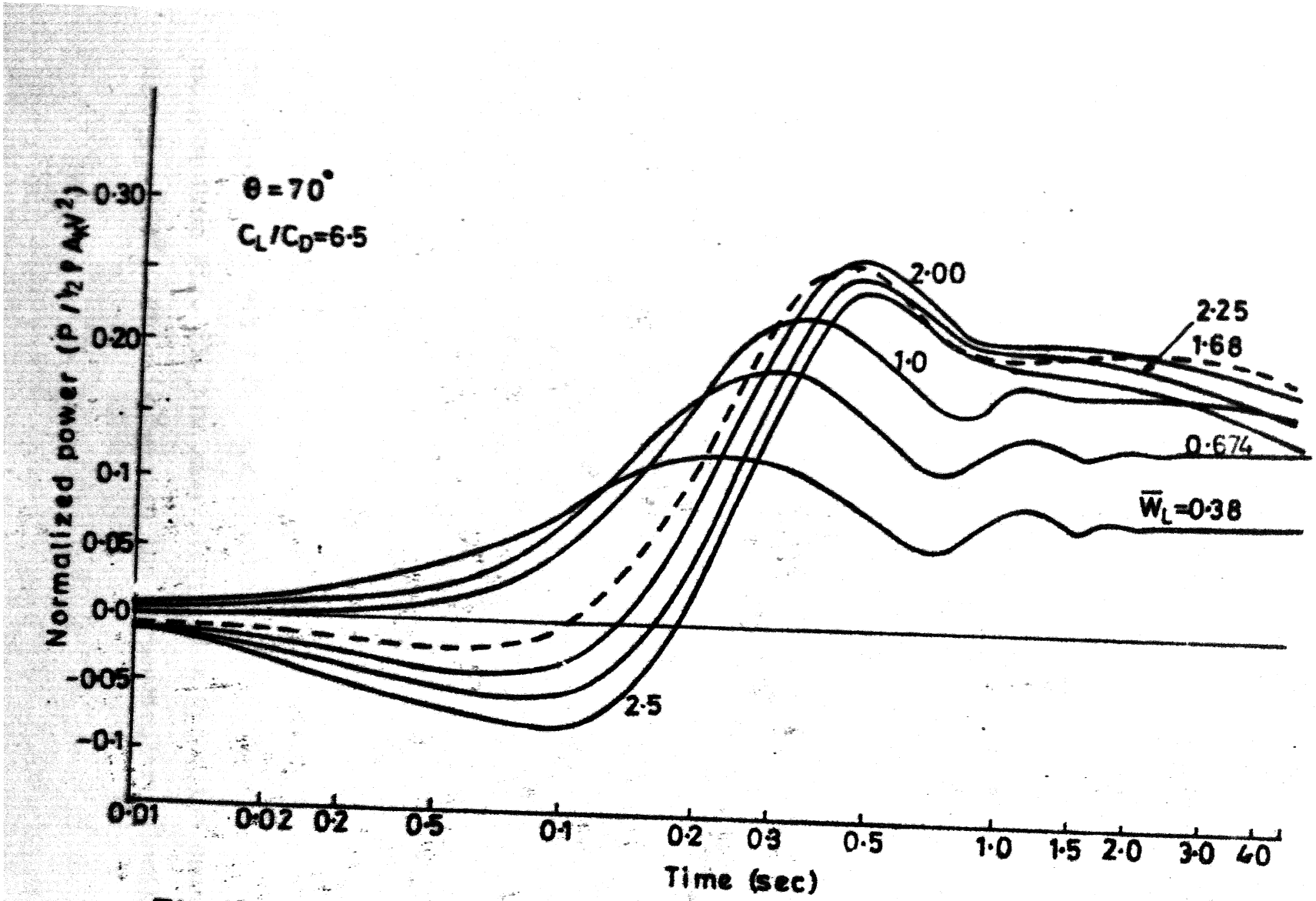

Fig.12 Normalized instantaneous power vs time for different loads

attractive features of a tethered system if the system is operated in a mode where $\theta = 0^{\circ}$.

From Fig. 12, we see that with the progress of time, the transient behaviour of power changes into the steady state pattern. (The power was calculated as the product of W_L and V_L (= V_1). Thus the behaviour of power with time is the same as the behaviour of V_1.). However, an interesting observation is that, for $\bar{W}_L > 1.0$, the pump initially starts in the descension mode. This is because, we have assumed that the system starts in the ascension mode from rest and that the maximum load the stationary system can support is given by Eqn. (27). The important point to note here is that eventhough the system initially starts in the descension mode, the magnitudd and direction of the relative velocity changes in such a manner (and consequently the lift and drag) that the system comes in ascension mode after a short time. The above results have been obtained assuming $\theta = 70^{\circ}$, but similar results have been obtained for all other angles.

Fig. 13 shows the paths through which the kite ascends. (kite profiles). Since $\theta = 70^{\circ}$ in all the cases shown in the figure and $\theta_{eq} = 81^{\circ}$ (corresponding to $C_L/C_D = 6.5$ as seen from Fig. 8), the kite starts in a direction such that $\beta = 160^{\circ}$. This is because the perpendicular velocity

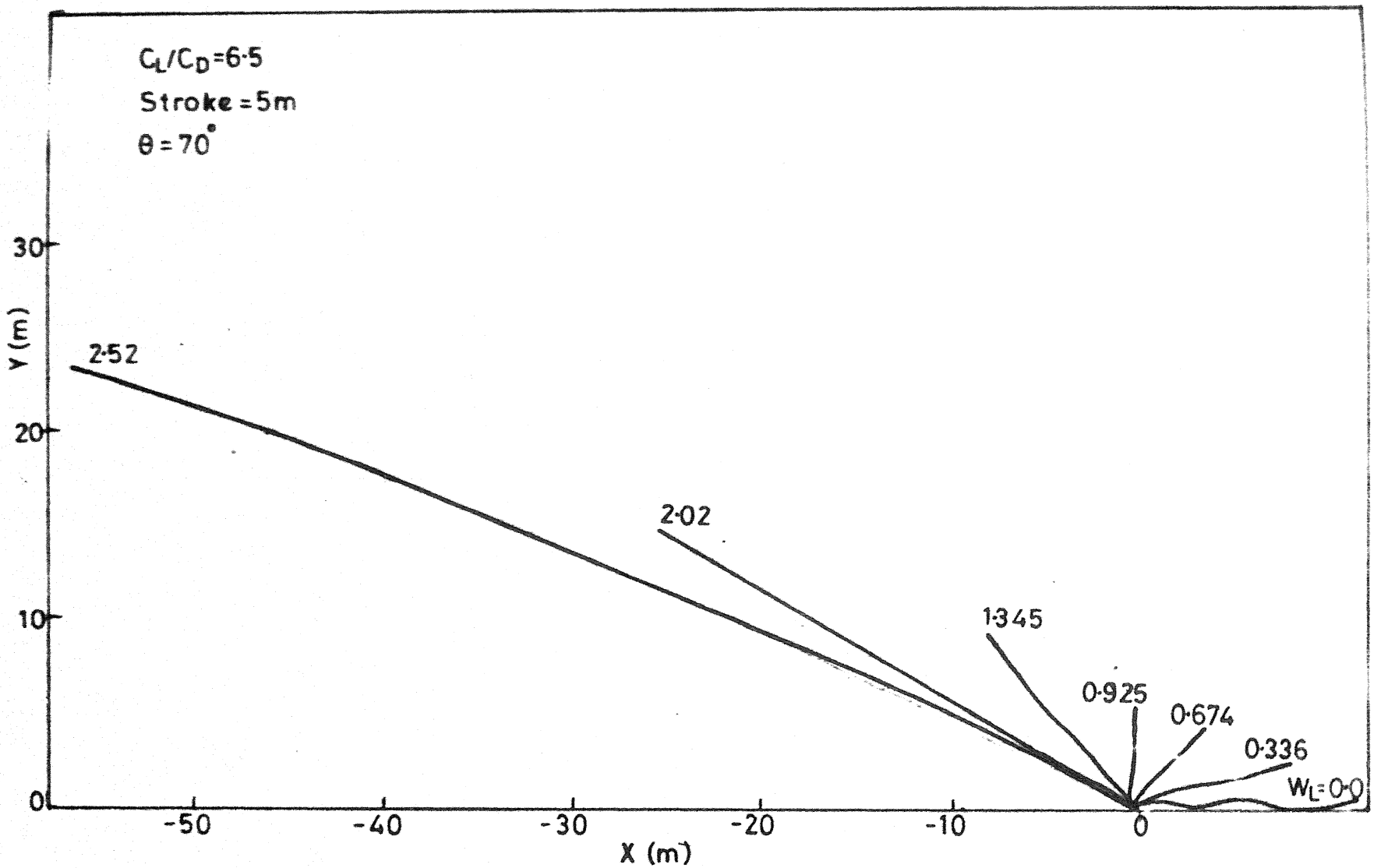

Fig. 13 Kite profiles during ascension

V_2 is much larger than the other component. From Fig. 13 it is clear that, the profiles for all the loads start in this direction but those for $\bar{W}_L < 1.0$ slowly turn towards down wind side, while those for $\bar{W}_L > 1.0$ remain in the second quadrant. This behaviour can be explained by referring to Fig. (14, 15) which shows the velocity triangle (Fig. 14) and the various forces when T_k is small Fig. (15a) and large (15b).

When the system starts from rest, eventhough the force perpendicular to the tether is small, the acceleration in that direction is large, because the mass to be accelerated in that direction is small. This is in contrast to the mass of the entire system which is to be accelerated in the direction of the tether. As a result, the velocity V_2 is much larger than V_1 and the kite starts in a direction such that $\beta = \theta + 90^\circ$. As the kite attains some velocity V_k (at angle $\beta > 90$), the lift and drag forces rotate clockwise by an angle Φ. (Refer Fig. 14, 15). This reduces the force perpendicular to the tether and increases the force along the tether causing corresponding changes in acceleration. If W_L is small, the change in V_1 is large because the system mass is small and the resultant force has a larger component (Fig. 15a) in the direction of the tether. But if W_L is large, the force component perpendicular to the tether is large (Fig. 15b). Thus for small W_L, V_1

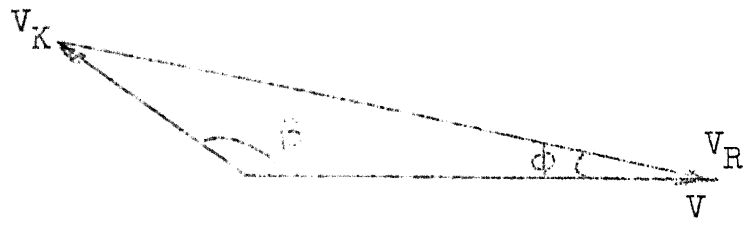

Fig. 14: Velocity triangle when the kite moves such that $\beta > 90^\circ$

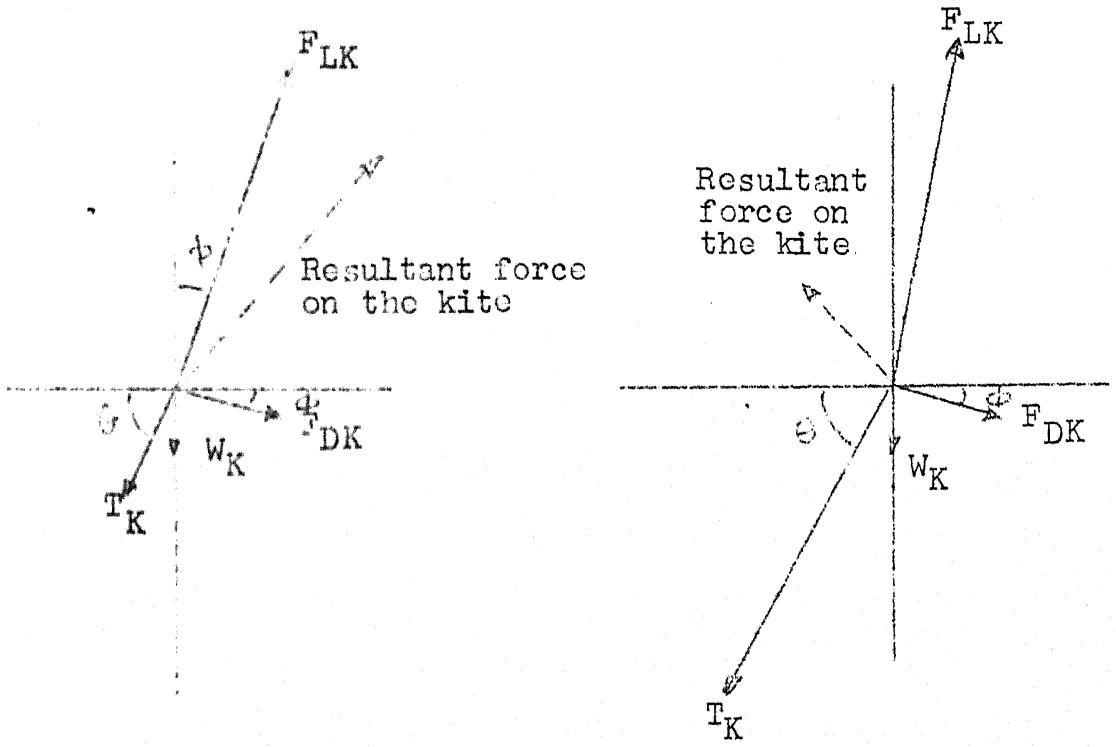

(a) T_k small

(b) T_k large

Fig. 15: Forces on the kite corresponding to the velocity triangle in Fig. 14.

becomes the dominant component of velocity and V_2 gradually decreases, while for large W_L, the magnitude of V_2 is always greater than V_1. This is the reason why the kite turns downwind for small W_L and it remains upwind for large W_L.

The instantaneous kite velocity Vs time for different loads is plotted in Fig. 16. As anticipated the kite velocity is transient in nature. It becomes more or less steady as time increases. The steady kite velocity is the minimum for $\bar{W}_L \simeq 1.0$. $\bar{W}_L = 1.0$ means that, the load is equal in magnitude to the lift, the driving force of the system during ascension. Therefore, the resultant force on the system tend to be very small, resulting in small velocity. The kite profile is more or less vertical at this load. Fig. 17, confirms the above conclusion. This shows the kite velocity at the end of a 5m stroke as a function of the normalized load. These curves have been drawn for various θ. An interesting observation that can be made from these curves is that, for $\theta = 81^\circ$ and 85°, the portion of the curve beyond $W_L = 1.$ does not exist because at these loads, the kite keeps on descending. Since $C_L/C_D = 6.5$, $\theta_{eq} = 81^\circ$ and $\theta = 85^\circ$ corresponds to tether angle > θ_{eq}.

To see how the average power output and velocity at the end of the stroke change with stroke, consider Figs. 18 and 19. In Fig. 18, the initial portion of the curve the average power is comparatively small, and increases with

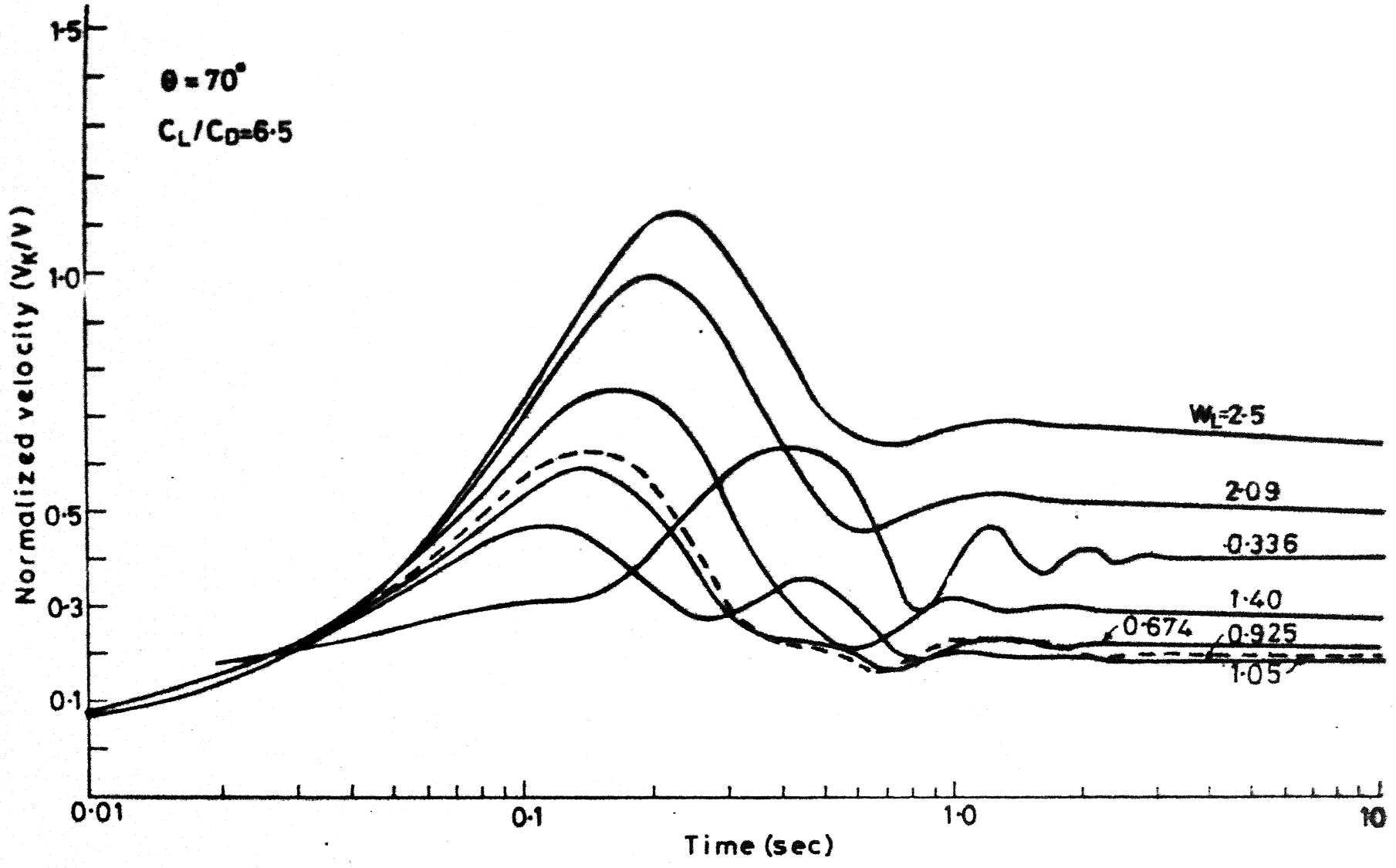

Fig.16 Instantaneous kite velocity V_K vs time for different $\bar{W}_L$

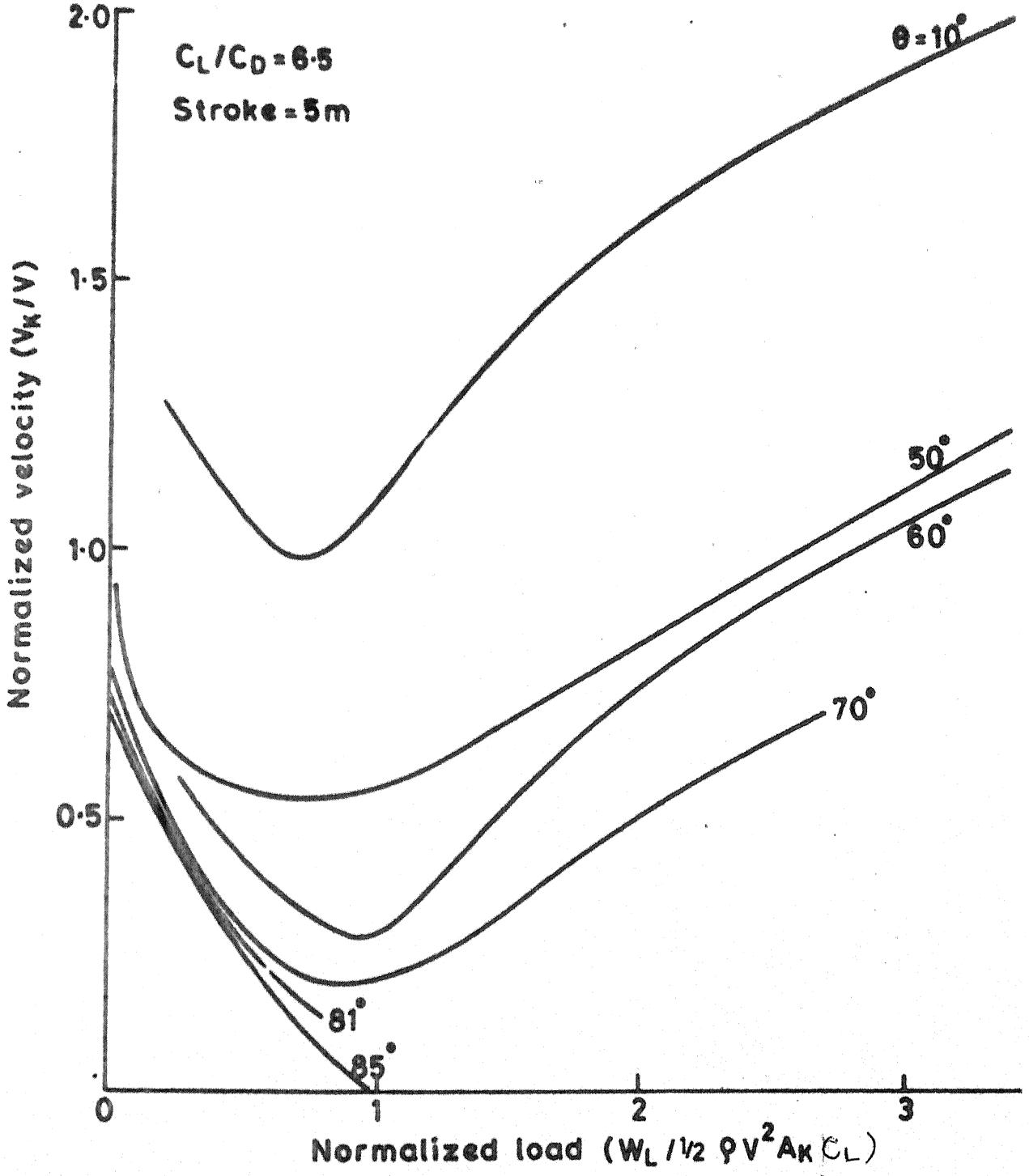

Fig.17 Load vs kite velocity at various initial tether angles

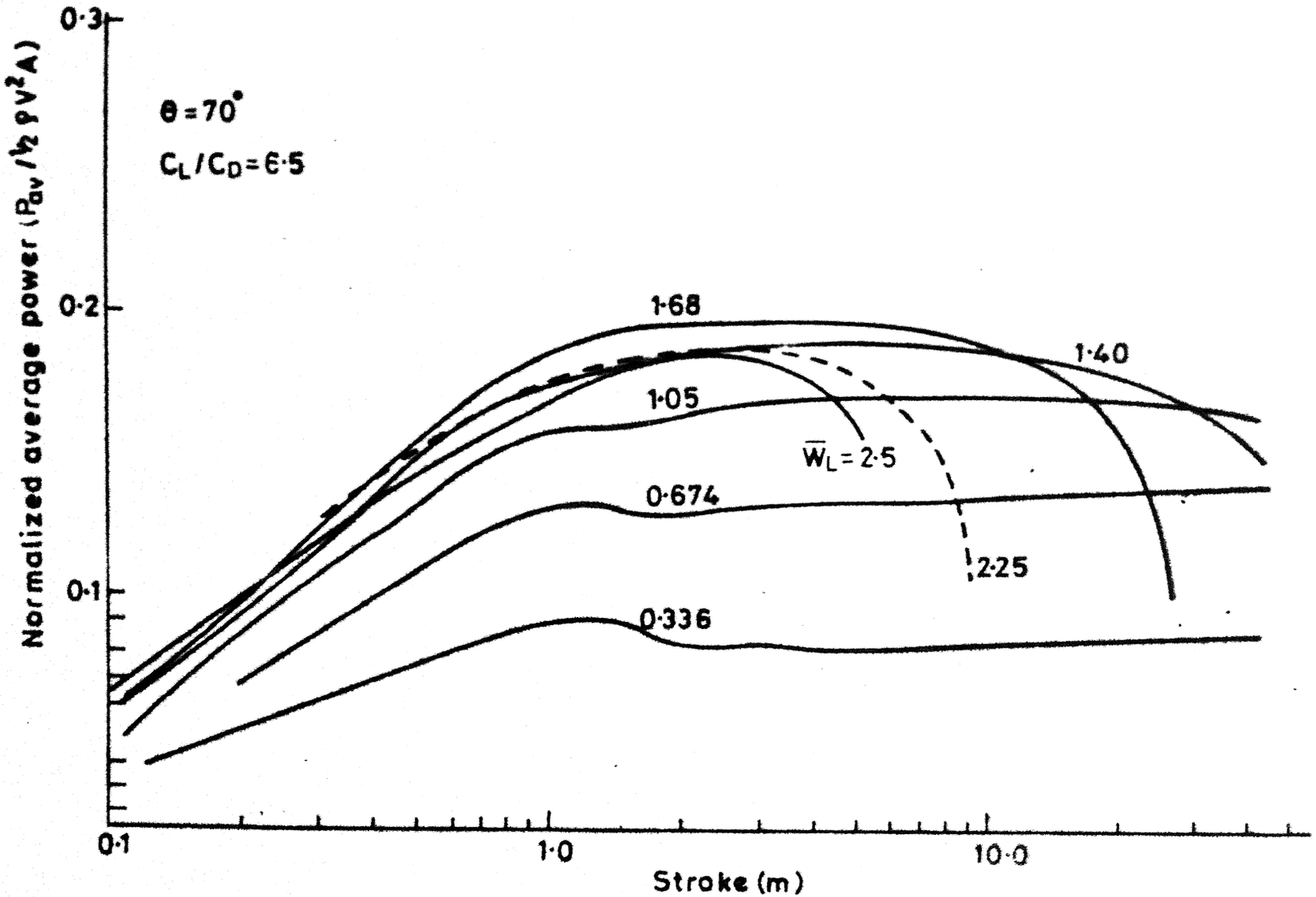

Fig.18 Normalized average power vs stroke for various loads

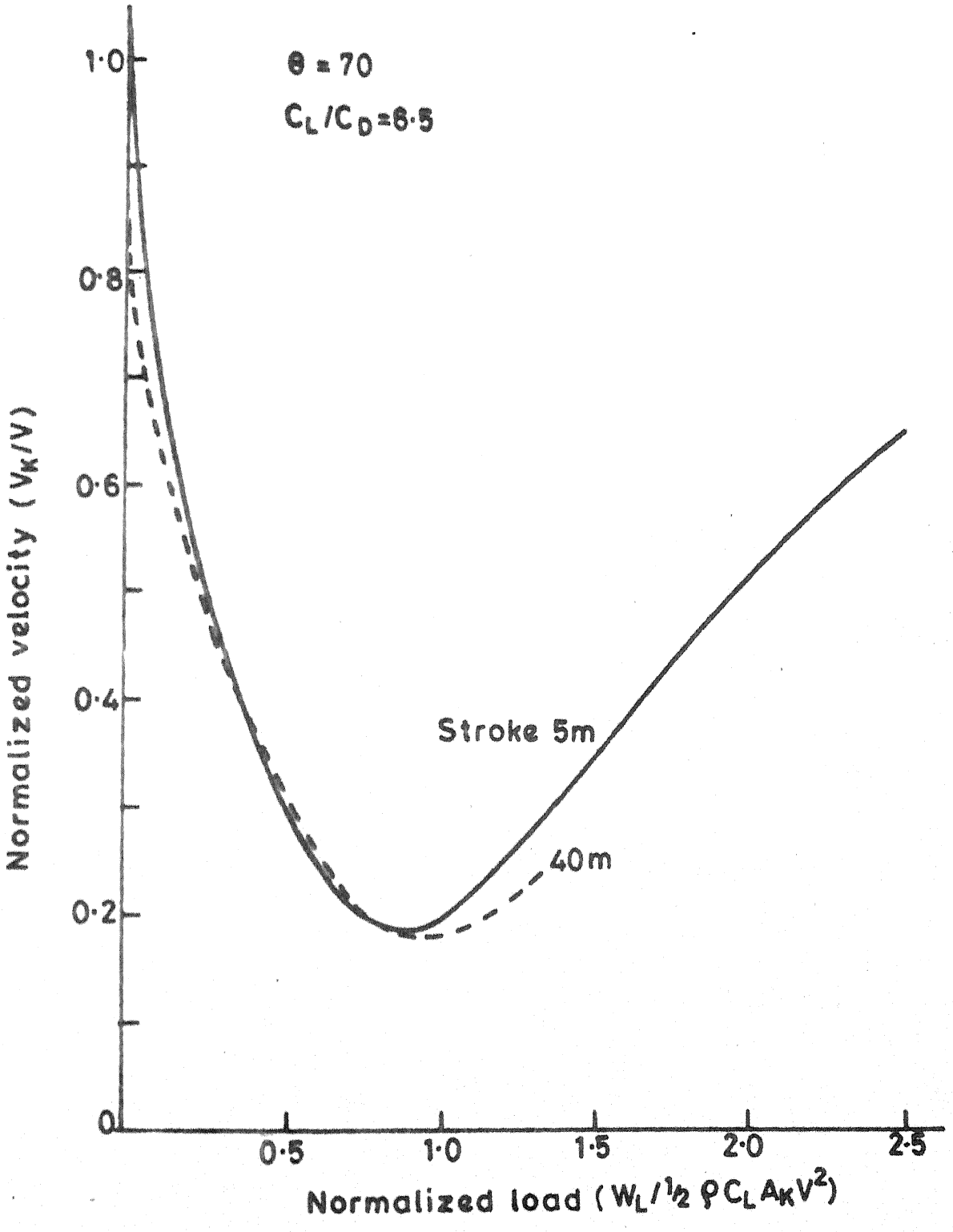

Fig.19 Velocity at the end of stroke vs load during ascension

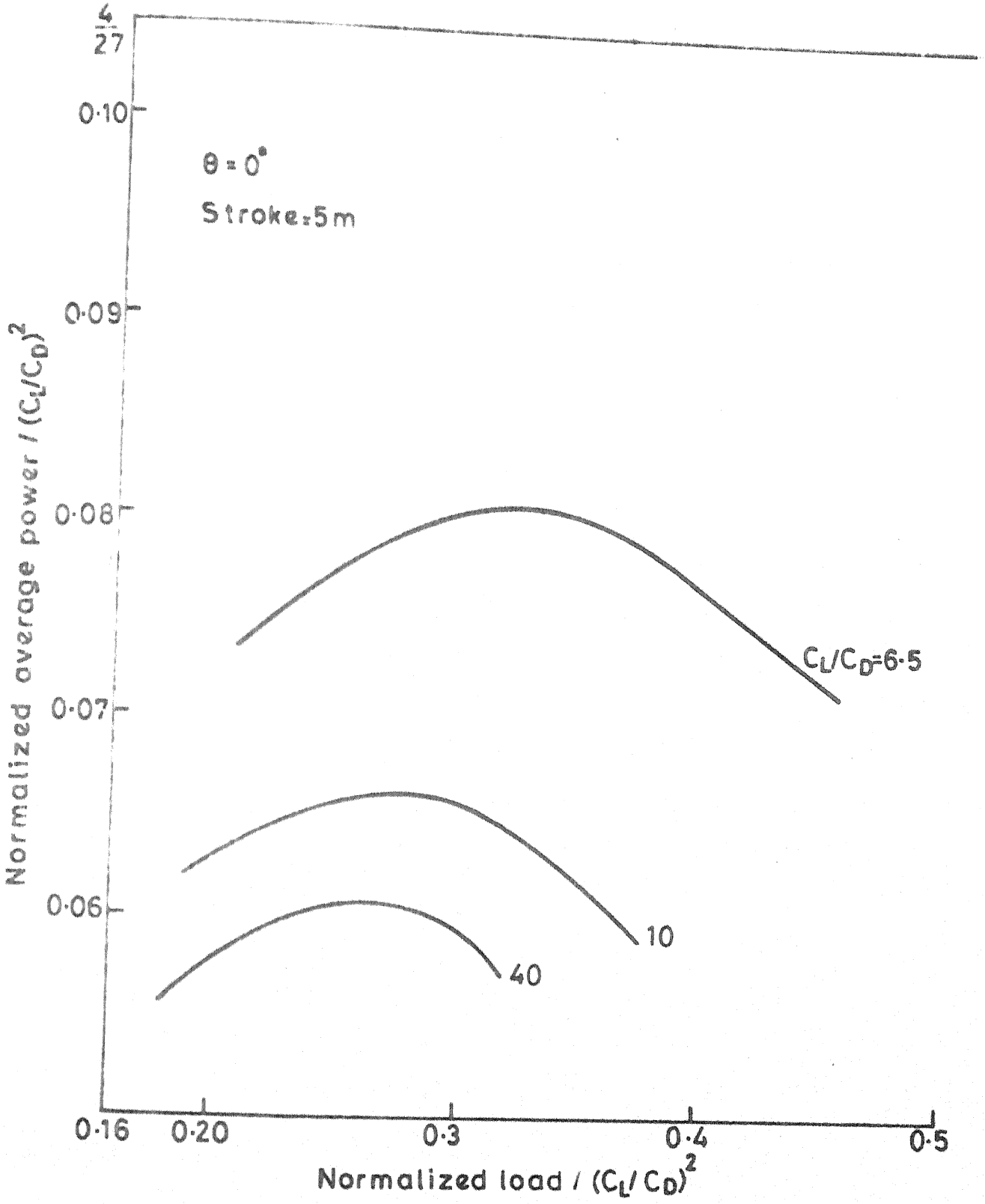

Fig.20 Average power output during ascension

stroke. This is due to the system starting from rest. After about 1m, the average power remains steady for $\bar{W}_L < 1.0$ but has a drooping characteristic for $\bar{W}_L > 1.0$. It can also be noticed that large loads ($\bar{W}_L > 1.0$) tend to decelerate the system during ascension and the system starts to descend after a certain stroke. For example, $\bar{W}_L = 1.68$ goes upto a stroke of 25m, while $\bar{W}_L = 2.5$ can barely execute a stroke of 5m. This fact is further illustrated in Fig. 19, which gives V_k at the end of a 5m stroke and 40m stroke. We note that when the load $\bar{W}_L > 1.33$, a 40m stroke is not completed. Further, for most loads, V_k at the end of a 40m stroke is less than that at the end of 5m stroke.

Fig. 20 shows how the average power output varies with load when different C_L/C_D are used for operation. These curves are drawn for initial tether angle $\theta = 0^o$. References [4,8] give the maximum power output from a tethered system as

$$\left(\frac{C_p}{C_L}\right)_{max} = \frac{4}{27} (CL/CD)^2 \qquad (28)$$

where C_p is the power coefficient defined as $C_p = \dfrac{\text{Power}}{\frac{1}{2} \rho A_k V^3}$. Fig. 20 is plotted by normalising power by $\frac{1}{2} \rho A_k V^3 C_L \left(\frac{C_L}{C_D}\right)^2$ and load by $\frac{1}{2} \rho A_k C_L V^2 \left(\frac{C_L}{C_D}\right)^2$. Then the upper limit for power generation from a kite pump becomes $\frac{4}{27}$. This upper limit is shown for the purpose of comparison in Fig. 20. It is observed that increasing C_L/C_D

does not improve the power output at the predicted rate [= $(C_L/C_D)^2$] but at a lower rate. This reduction in power may be attributed to two causes (i) our calculation of power is based on averaging over a stroke of 5m. (ii) Refs. [4 and 8] do not take into account the presence of friction as is done in this case. Table 1 compares the average power at optimum load for various θ with and without friction.

Tether angle θ (degree)	Optimum W_L	Normalized average power	
		With friction	Without friction
85	0.33625	0.0444	0.01465
81	0.4203	0.0322	0.0336
78	0.7565	0.055	0.0585
70	1.681	0.1803	0.1986
60	3.363	0.4974	0.566
50	6.136	0.9403	1.1516
10	13.45	2.78	3.85
0	13.45	2.84	4.0175
-5	13.45	2.7676	3.998

Table 1: Average power during ascension at optimum load and different θ.

The friction between pulley and tether accounts for 41.5% of the power when the tether angle is 0^o. At angles greater than zero, the friction will be less than the above figure.

5-3. Performance During Descension

At the end of the ascension stroke the payload of the system is delivered and C_L/C_D of the kite is reduced. This reduced load on the system pulls the whole system back to its original position if the lift and drag forces are not sufficient to overcome it. The results during descension as given below are obtained with a $C_L/C_D = 2.0$ ($C_L = 2/6.5$), unless otherwise specified. It was assumed that the kite again starts from rest. The performance of the system during descension is shown in Figs. (21 - 29).

In Fig. 21, the normalized average power is shown as a function of the normalized load $\bar{W}_L$. The characteristic power and load are taken as $\frac{1}{2} \rho C_L A_K V^3$ and $\frac{1}{2} \rho C_L A_K V^2$ respectively where C_L now is C_L during descension. The graphs are drawn for $\theta = 81^\circ$, 70° and 60°. Angles below $\theta = 60^\circ$ are not considered here because for $C_L/C_D = 2.0$ $\theta_{eq} = 63^\circ$ (Refer Fig. 8). Therefore any angle $\theta < \theta_{eq}$ is favourable for ascension and the kite tends to ascend at moderate loads. The curves (Fig. 21) show a monotonous decrease in power requirement as $\bar{W}_L$ increases. The dashed portion of the curves were not actually obtained; but obtained by extrapolation. This portion indicates that for loads below $\bar{W}_L$ corresponding to zero average power the systems can ascend. In descension the load is the driving force and lift and drag are opposing forces. Thus as W_L increases, the time of

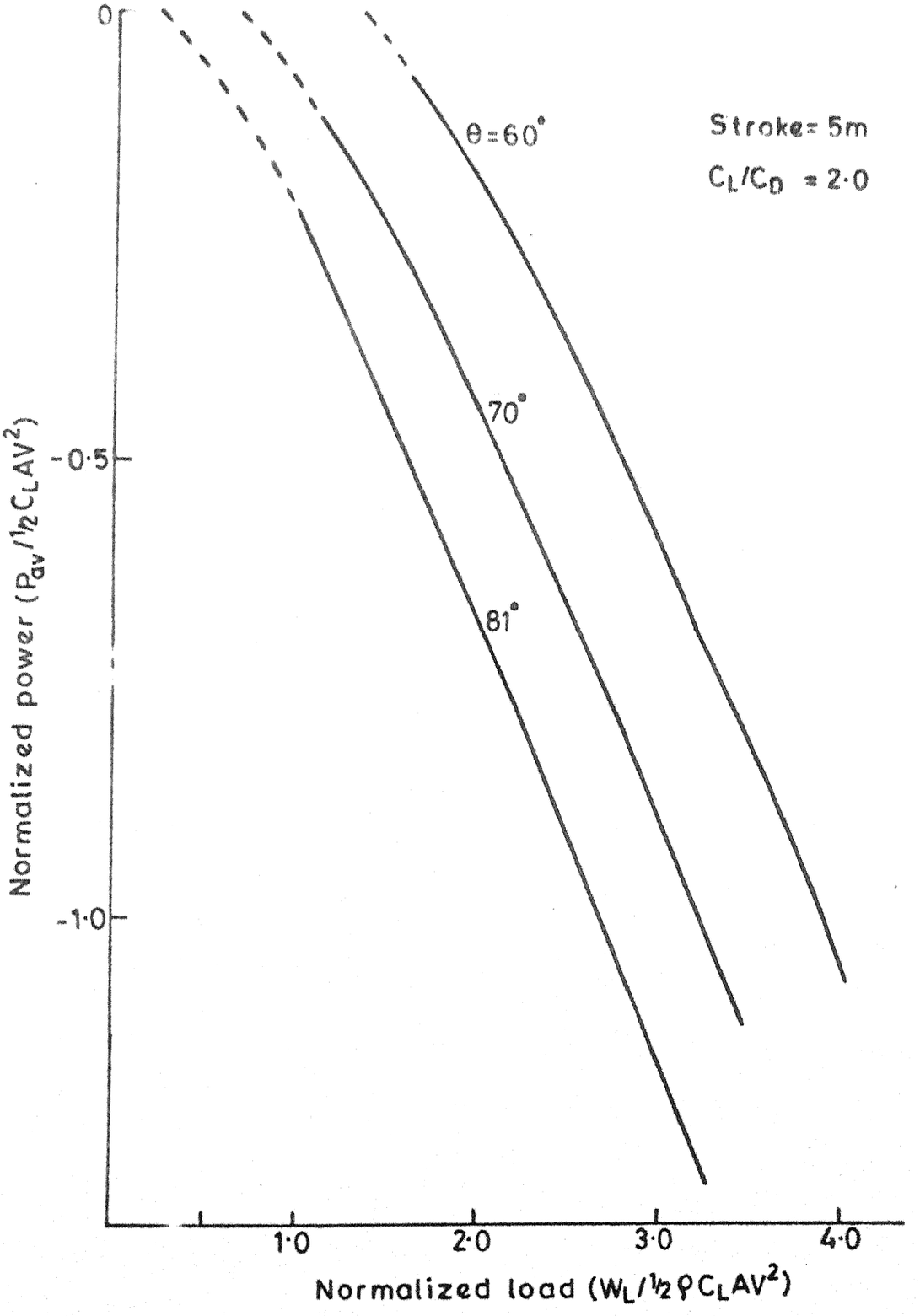

Fig. 21 Average power during descension vs load for θ = 81°, 70° and 60°

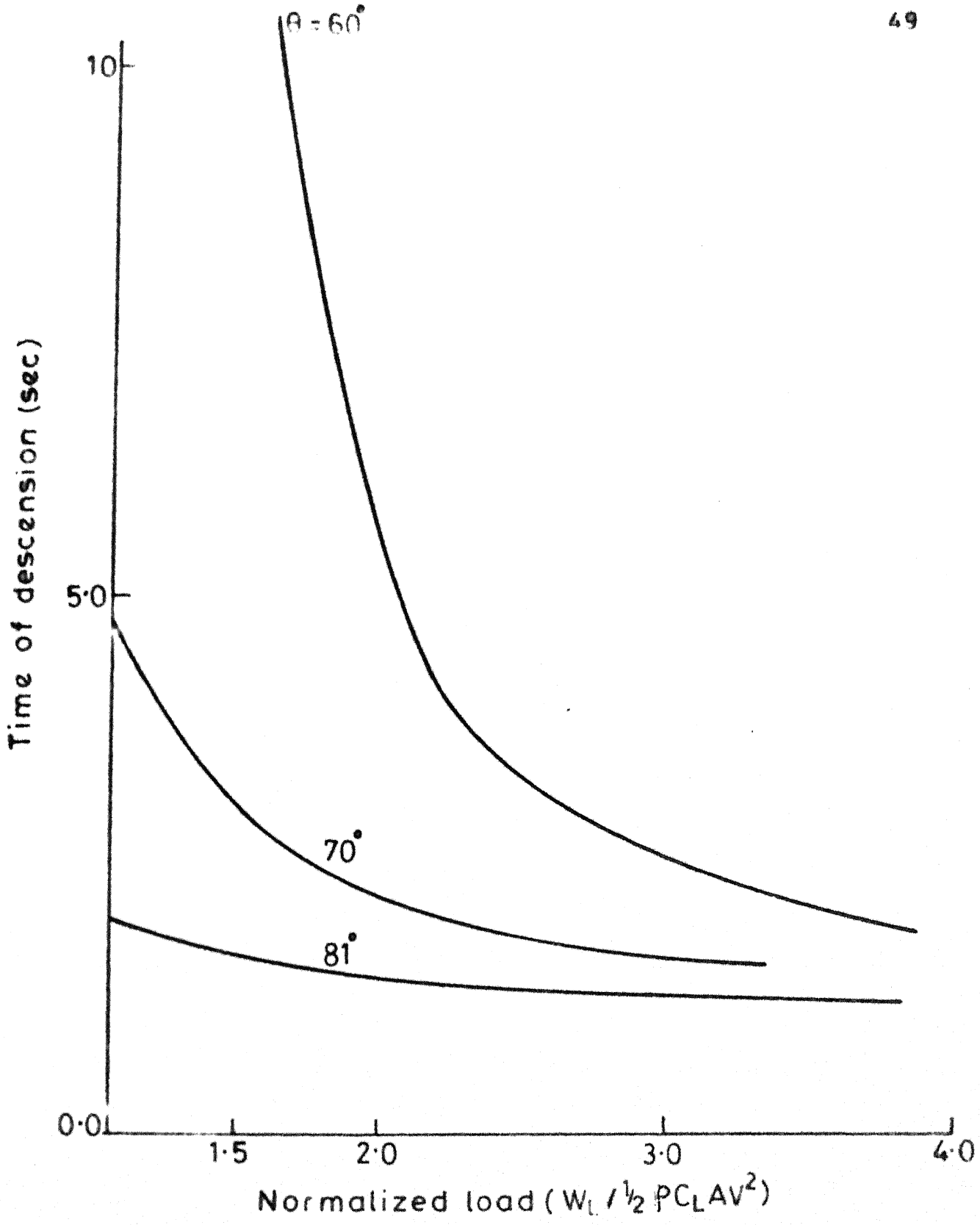

Fig.22 Descension time vs normalized load for different initial tether angle

descension decreases [Fig. 22] and the average power goes on decreasing. There is no optimum value of $\bar{W}_L$. This is in contrast to the behaviour in ascension, where there is a trade off between the load and ascension time and hence we have an optimum. However, $\theta > \theta eq$ are more suitable for descension than $\theta \leq \theta eq$ since the time of descension and the power requirement are smaller for $\theta > \theta eq$.

In Fig. 23, we observe that V_k is less when θ is nearer to θeq. This observation is in agreement with the results of ascension. Nearer to θeq the V_1 component of velocity contributes more to kite velocity than V_2 component. This is the reason why V_k is small when the initial tether angle θ is near θeq.

As mentioned earlier, $\theta = 70^\circ$ is greater than θeq corresponding to $C_L/C_D = 2.0$. Therefore, as the kite starts from rest, the rotational component of velocity (V_2) tends to take it towards the right. This behaviour at the start of descension is observed from the kite profiles during descension (Fig. 24). For $\bar{W}_L < 1.3$, the profiles are entirely in the fourth quadrant, while larger loads tend to turn the path towards left; the paths finally ending up in the 3rd quadrant. This behaviour may be explained by referring to the velocity triangle and the forces on the kite when the kite is moving such that $\beta > 270^\circ$. Fig. (25-26).

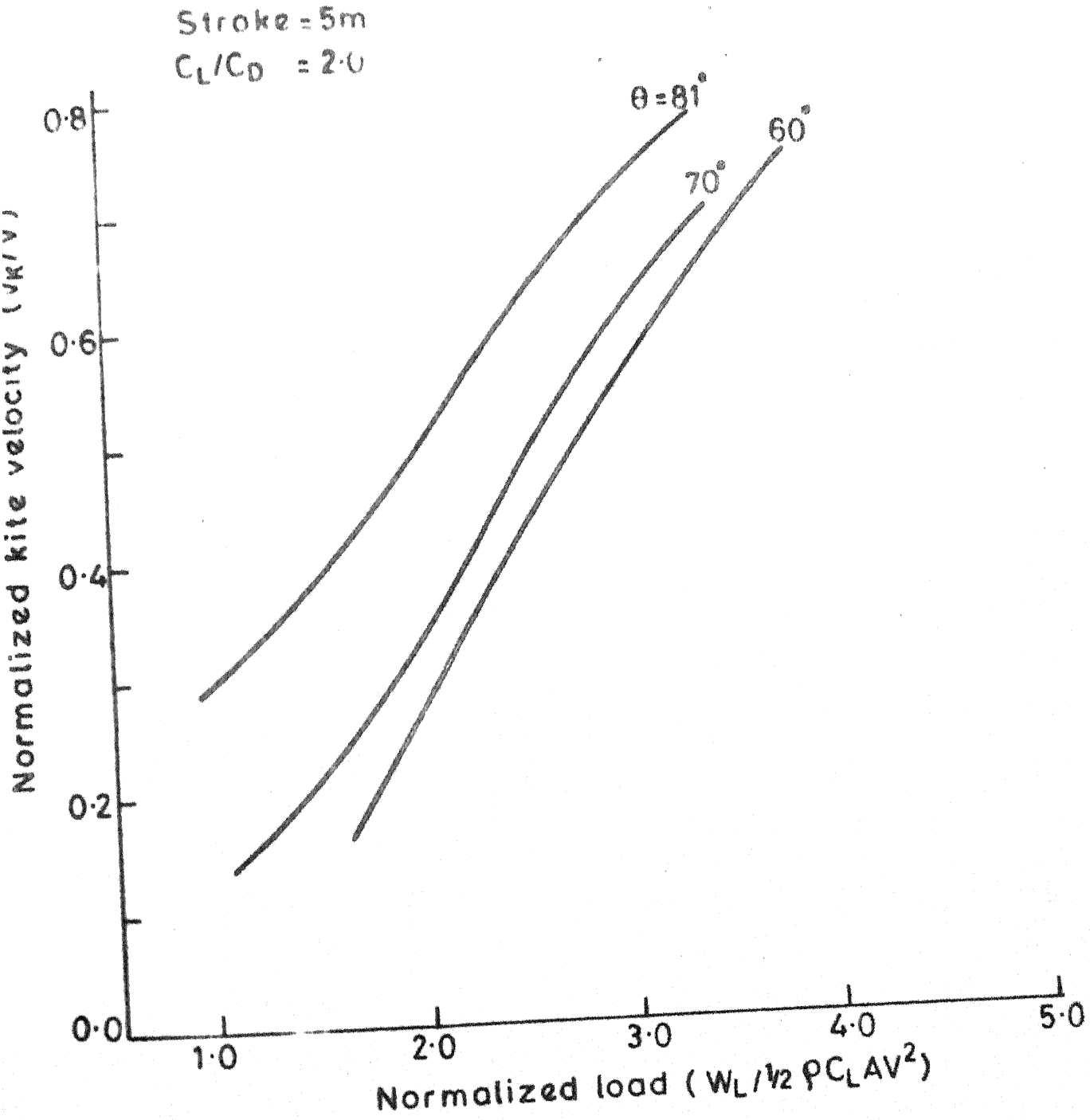

Fig.23 Kite velocity during descension vs load

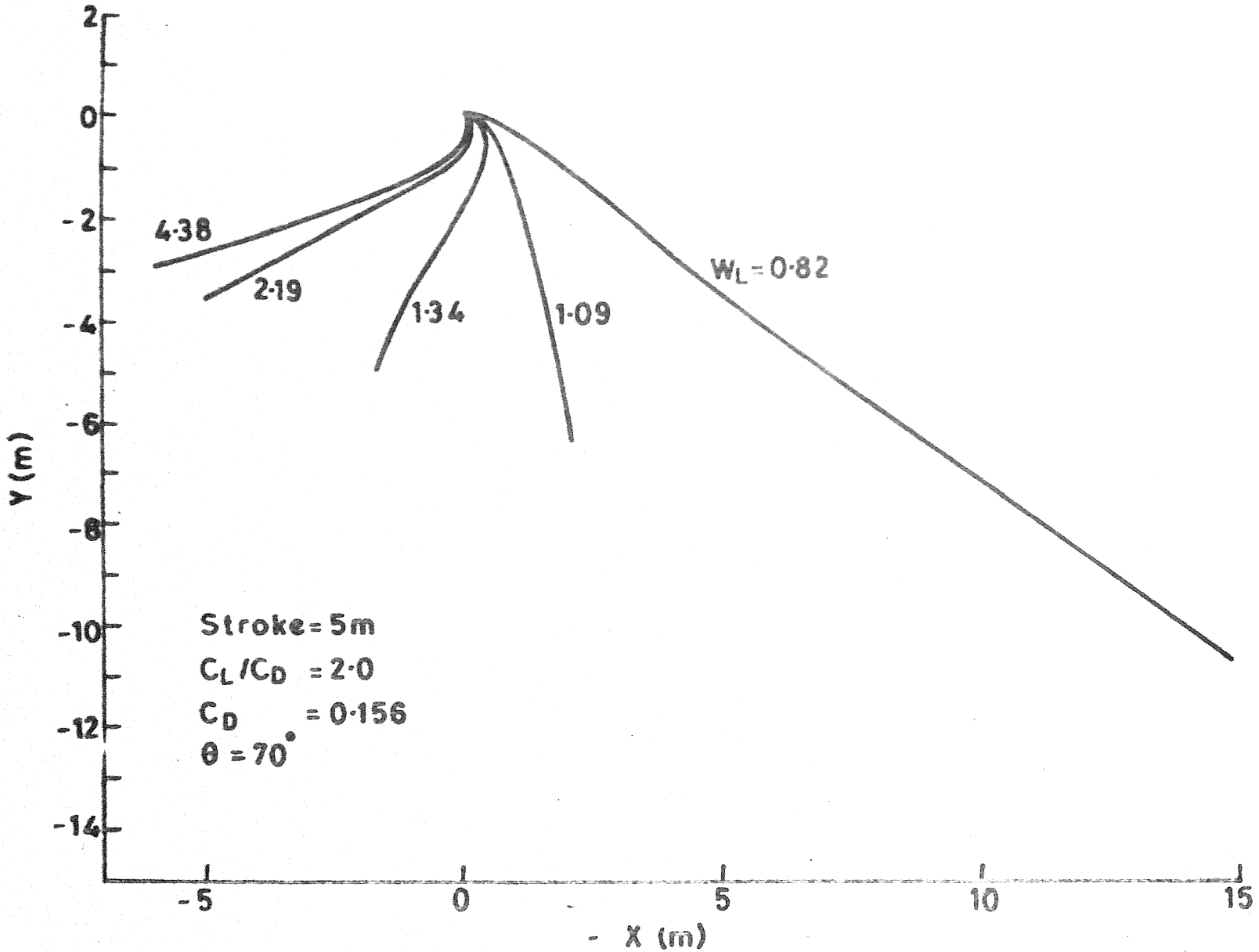

Fig. 24 Kite profiles during descension

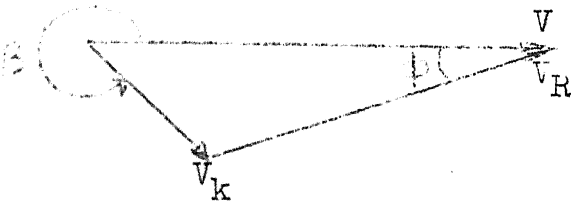

Fig. 25: Velocity triangle when $\beta > 270^\circ$.

In general, when the kite descends, the lift and drag forces rotates anticlockwise by an angle Φ. This makes an effective equllibrium angle = $\theta eq + \Phi$, at the same time the rotation of the thether is such that θ slowly increases. When the load is very small ($\bar{W}_L << 1$) and hence T_k the lift and drag together can overcome the load and the kite ascends. At moderate loads, the kite descends, but the direction of the resultant force is as shown in Fig. 26(a).

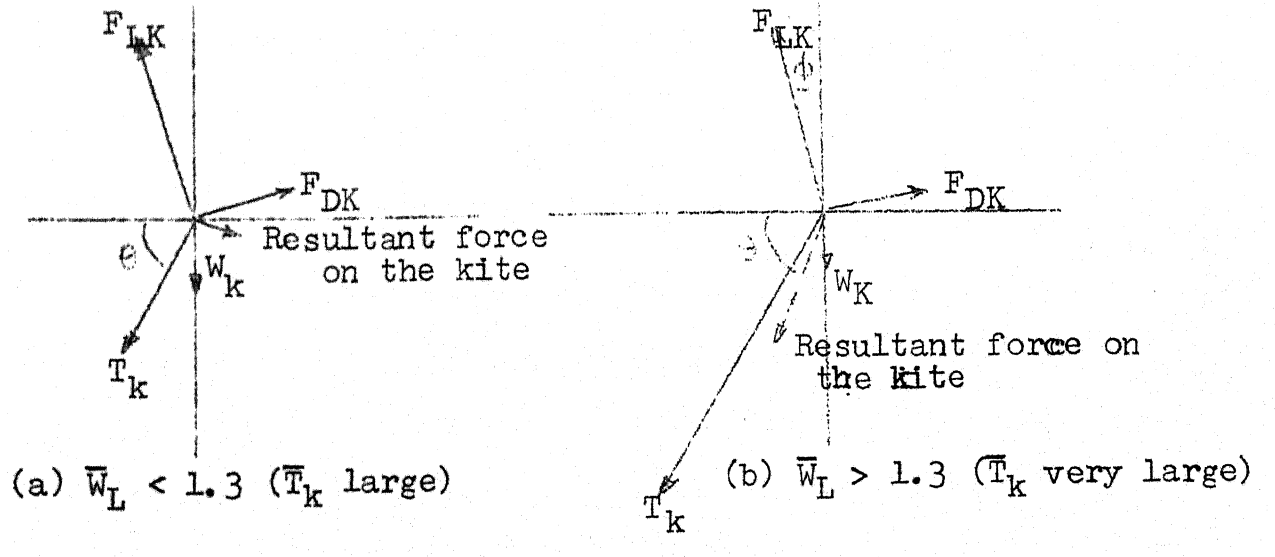

Fig. 26: Forces on the kite corresponding to the velocity triangle in Fig. 25.

The magnitude of the force along the tether is very small and therefore the component of velocity in that direction (V_1) also is small. But the component of velocity in the direction perpendicular to the tether (V_2) is comparatively large, and the kite moves, more or less in the direction of V_2 (downwind). When W_L is still large, the resultant force on the kite has a different direction as shown in Fig. 26(b). In this case it can be observed that V_2 is smaller, and V_1 is the dominant component of V_K. V_2 goes on decreasing as the kite moves, and hence it turns upwind.

The variation of the instantaneous power with time is shown in Fig. 27. The transient behaviour of instaneous power seen in ascension is absent, during descension. The power decreases monotically. However, one of the curves starts in ascension mode ($\overline{W}_L = 0.82$). This is because, the lift and drag forces at the start can overcome load when $\overline{W}_L < 1.0$. But the motion is such that V_R decreases as V_k increases. (Since β is greater than 270). As a consequence the magnitude of F_{LK} and F_{DK} decreases, and after some time the kite is not able to support the load and it descends. The descension time becomes very large due to this initial ascension. (If the load is still smaller the kite may keep moving in the ascension stroke and may never descend.) This explains the sharp change in descension time for $\overline{W}_L$ around 1.0 as shown in Fig. 28. In the figure it is also observed that the kite velocity at the end of the stroke is the smallest when $\overline{W}_L \simeq 1.0$.

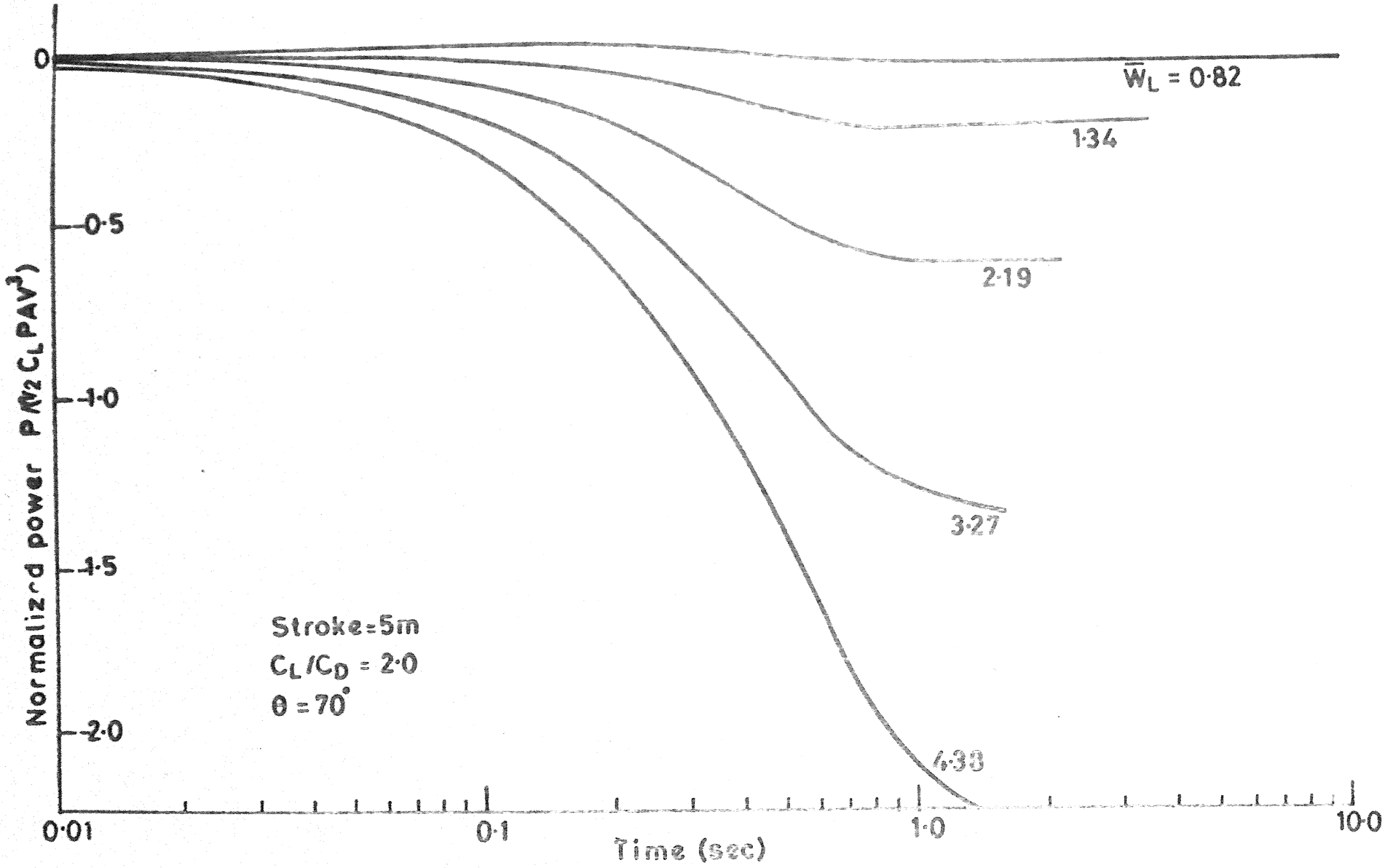

Fig. 27 Instantaneous power during descension

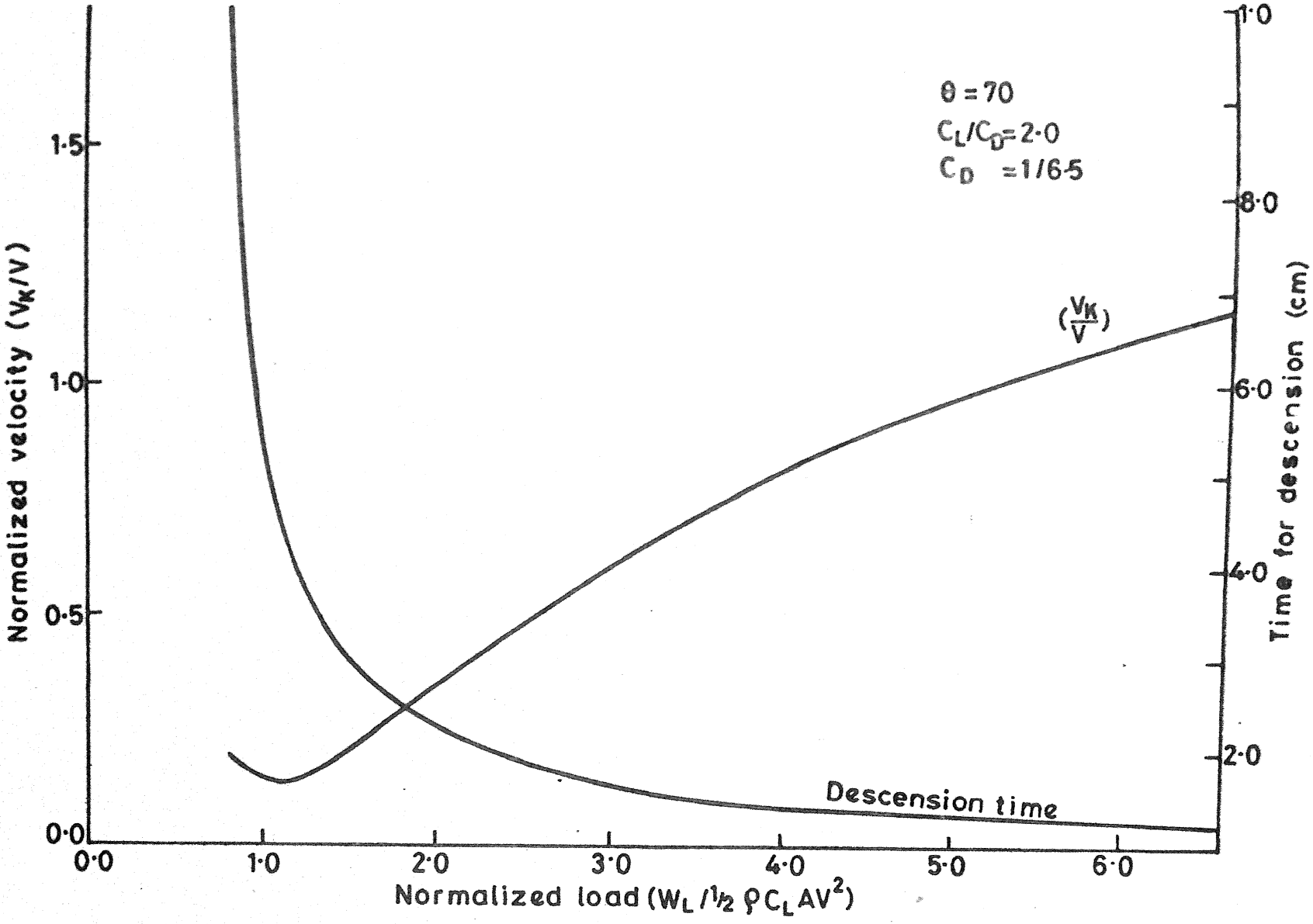

Fig. 28 Variation of velocity at the end of stroke and descension time vs load

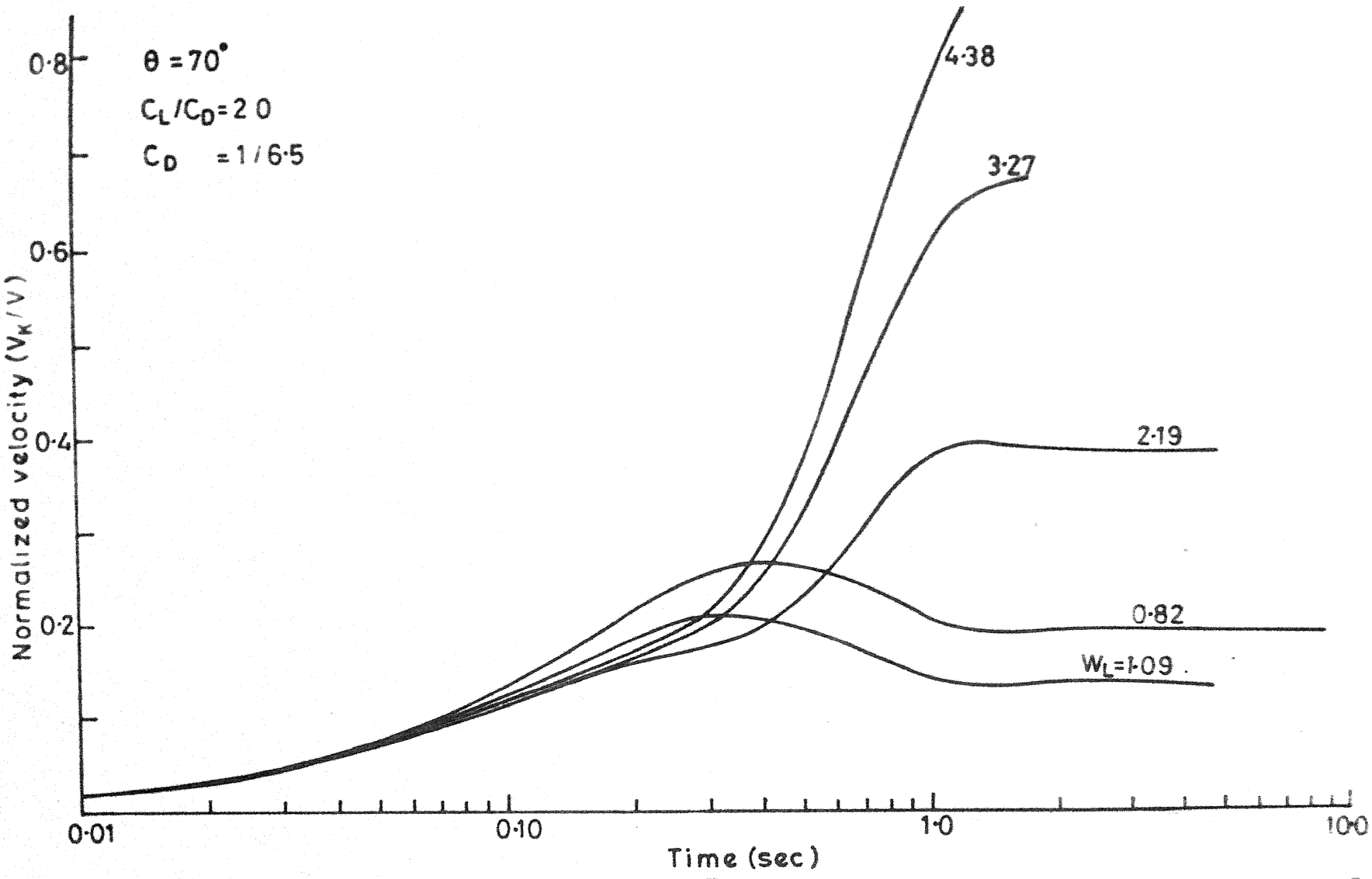

Fig. 29 Variation of kite velocity with time during descension

The kite velocity as a function of time is shown in Fig. 29. This again varifies our conclusion that V_k is the smallest when $\bar{W}_L \simeq 1.0$. The above results were obtained for initial tether angle = 70° and stroke = 5m. Similar results can be obtained for other tether angles and C_L/C_D.

5-4. Matching Ascension and Descension

After the ascension stroke in which work is done by the system, it is necessary to bring the system back to its initial position so as to begin a new cycle. This return stroke should be completed by spending less power so that there is a net gain in power from the cycle. Thus it is evident that, not only the power and time during ascension and descension are important, but the total cycle time and power are also important.

Concerning matching of profiles during ascension and descension, it is not important to match the two profiles point by point, but the descension profile should reach the same position at the end of the stroke as the starting position for ascension. Thus the two profiles can follow very different paths, but with the same end points. To see which combination of ascension and descension may lead to a matched profile resulting in a cyclic operation consider Fig. 30. In this figure the path profiles of the kite are drawn during ascension and descension keeping the stroke = 5m,

and initial tether angle = 70°. All the curves lying above x axis have been drawn taking $C_L/C_D = 6.5$ while those below x axis have been drawn taking $C_L/C_D = 2.0$. It should be noted that there is a particular value of C_L/C_D at which the system with $\epsilon = 70^{\circ}$ will be in equillibrium. We call this value of C_L/C_D as $(C_L/C_D)_{eq}$. We have used $(C_L/C_D) > (C_L/C_D)_{eq}$ for ascension and $C_L/C_D < (C_L/C_D)_{eq}$ for descension. In Fig. 30, with each profile are also given the values of normalized load and average power. We see that for small loads ($\bar{W}_L < 1$), the kite moves downwind, while for lage loads ($\bar{W} > 1$) the kite moves upwind. During ascension, as the load increases, the average power also increases till for $\bar{W}_L = 1.68$, there is a maxima in power output. During descension, however, there is no minima in the power consumed. As the load increases, the power consumed also increases. From this figure, one can clearly determine the range of profiles which could be matched properly. For matching the profiles during ascension in the first quadrant, one needs descension profiles in the third quadrant. Though this matching is possible, it may result in negative power output due to the requirement of large loads during descension. Similarly it is possible to match the ascension profiles in the second quadrant with those of descension in the fourth quadrant. In these cases the cycle power will be positive. For the calculation of cycle power in the following we have taken that profile which gives the maximum

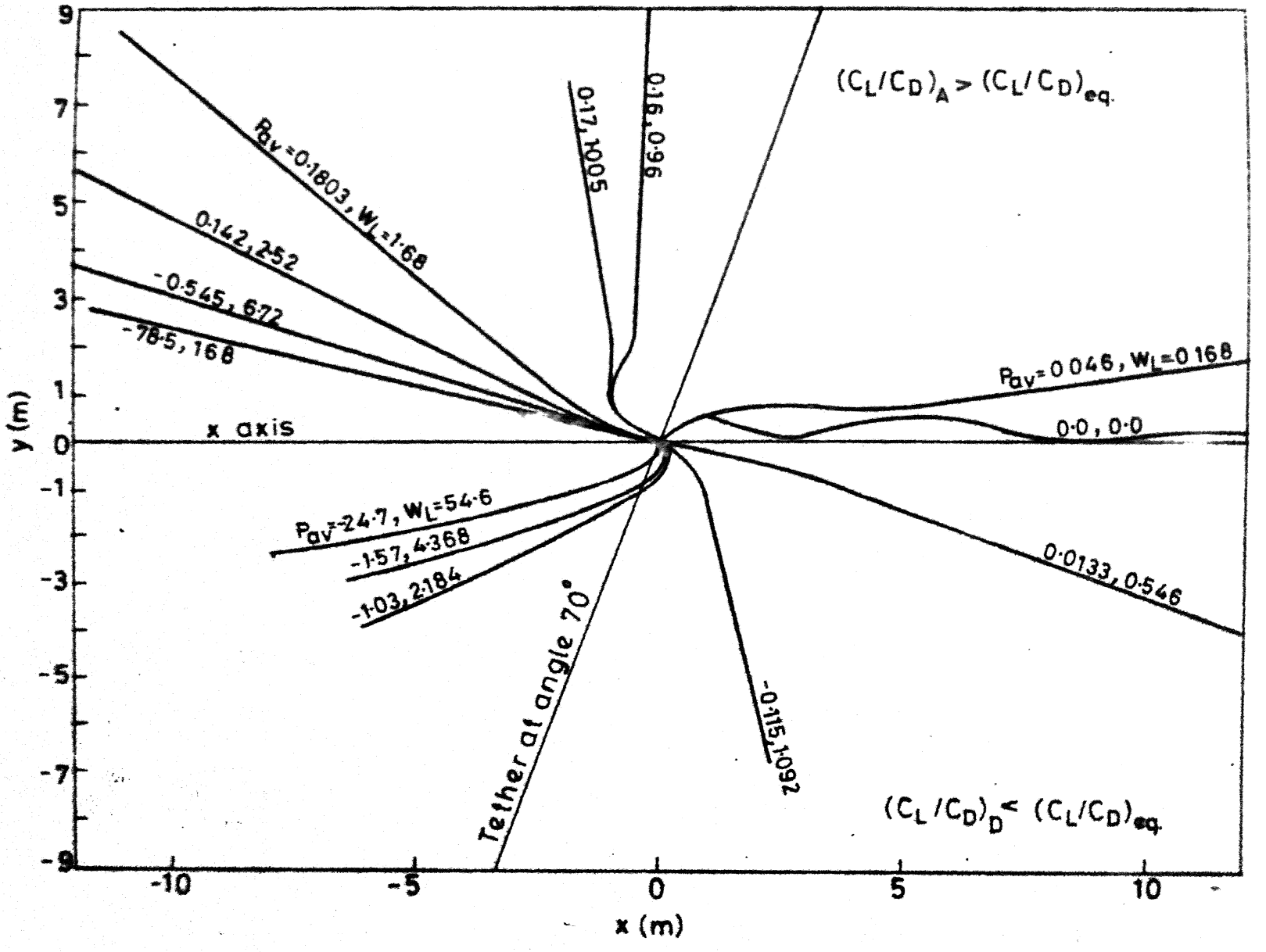

Fig.30 Ascension and descension profiles

power output during ascension. Keeping this profile and its conditions fixed, we have attempted to determine parameters during descension which will match the above profile. This is shown in Fig. 31. The ascension case that we are interested in matching has the conditions W_L = 100 kg, C_L/C_D = 6.5 and $\theta = 70^\circ$. In Fig. 31 we have kept load during descension fixed = 20 kg and varied C_L/C_D to see its effect on the profile. We see that, when C_L/C_D = 1.8 the profile is almost vertical. But as C_L/C_D increases the profile moves towards the ascension path, until at C_L/C_D = 2.4, the descension path almost exactly matches the ascension path. The ascension and descension are for a stroke of 5m.

Thus by a suitable combination of W_L and C_L/C_D during descension, it is possible to match ascension profile. Fig. 32 illustrates this point further. In this, four different combinations of C_L/C_D and load during descension which match the ascension profile are shown. We see that as load increases, we need larger values of C_L/C_D to match the ascension profile. Further we observe that as the load decreases, the deviation from the ascension profile also increases, with the end points remaining the same.

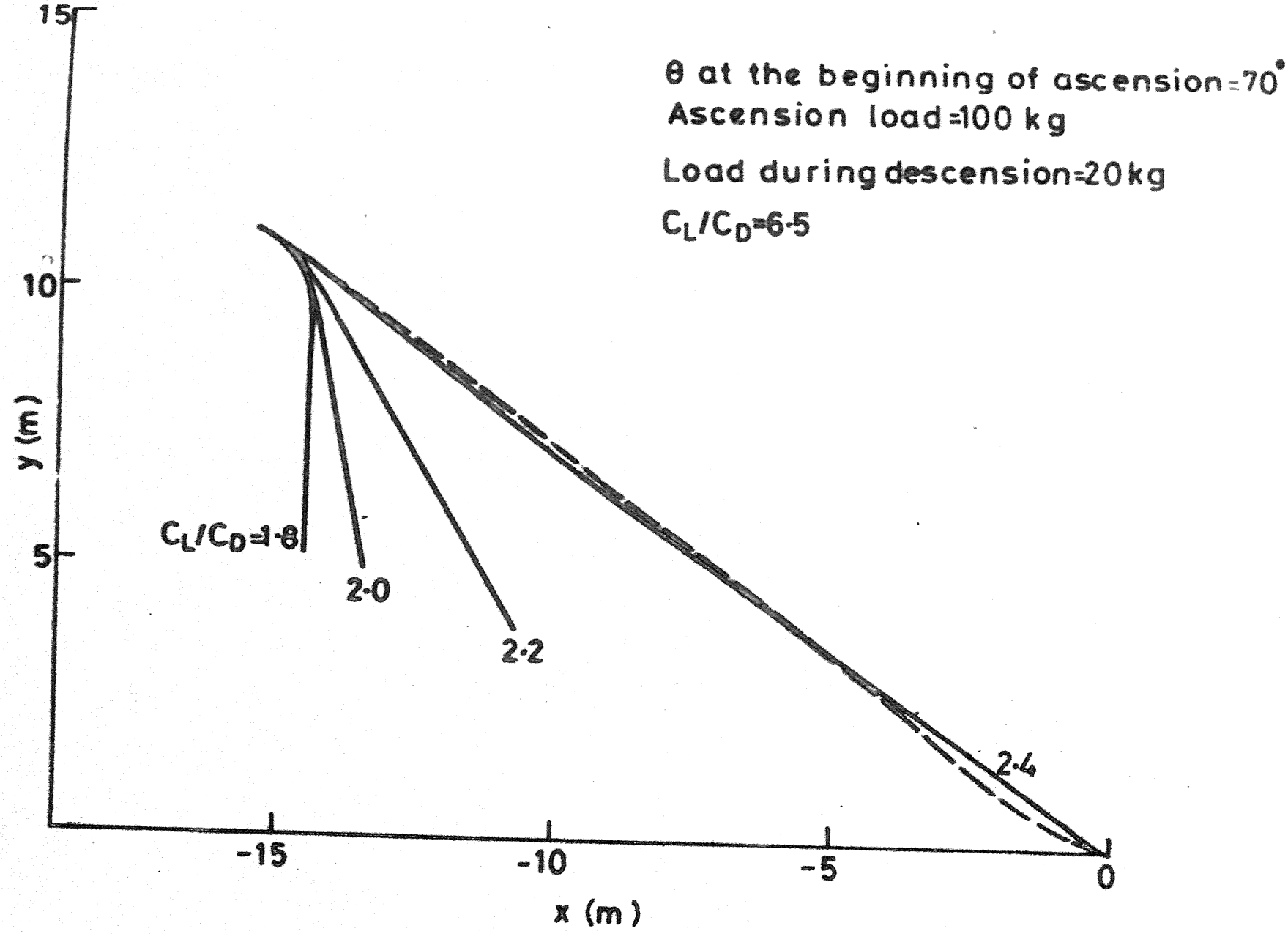

Fig.31 Path of kite during ascension & descension

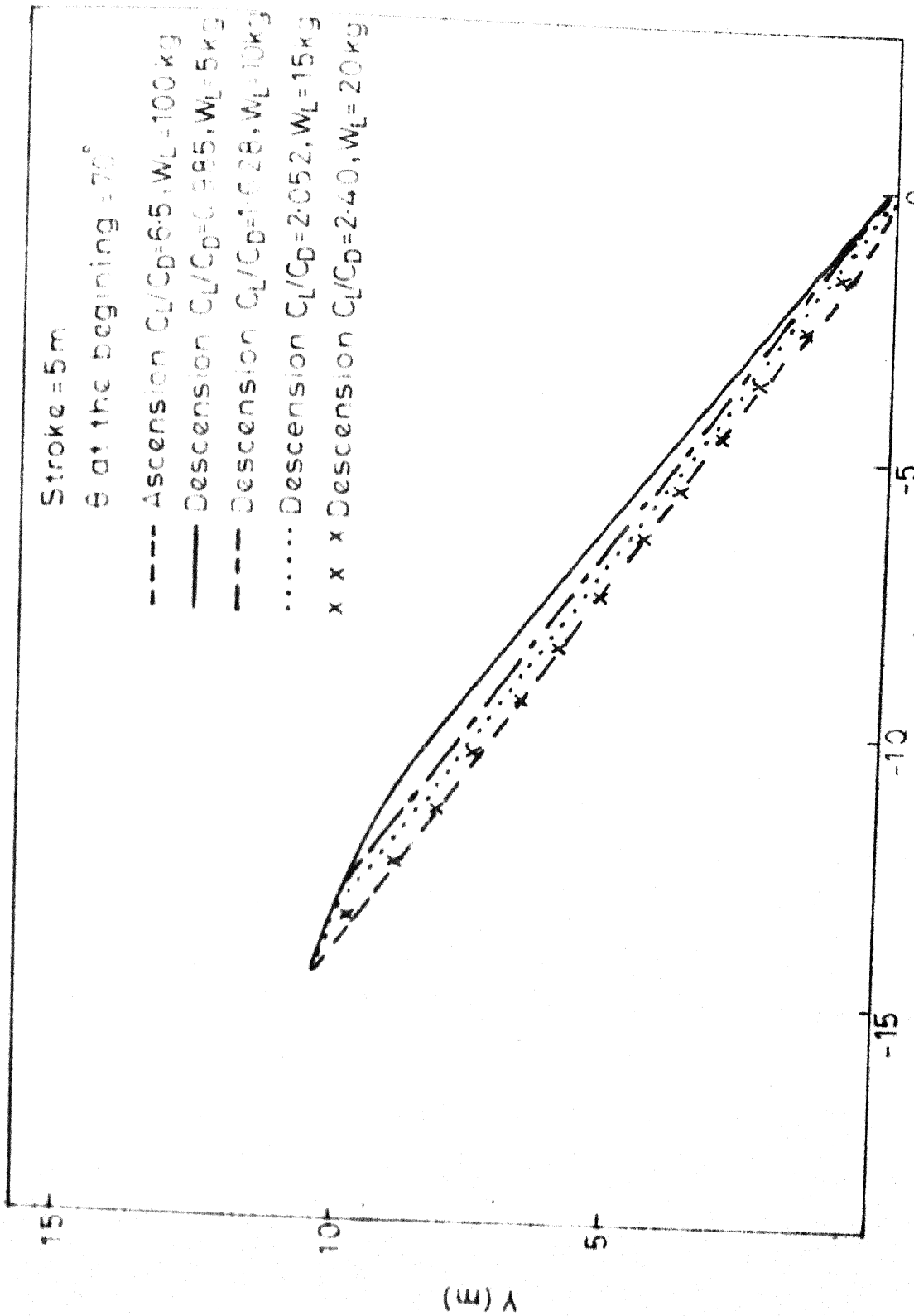

Fig.32 Ascension path and matching descension paths

C_L/C_D	Load kg	Time (s)	Cycle time (Sec.)	Effective Load kg	Cycle Power (watts)
0.985	5.0	3.42	7.65	95.0	607.5
1.628	10.0	5.675	9.91	90.0	446
2.052	15.0	8.885	13.12	85.0	317
2.40	20.0	15.315	19.35	80.0	200

Table 2: Descension data matching ascension with W_L = 100 kg, C_L/C_D = 6.5, initial $\theta = 70^\circ$ Ascension time 4.23 sec, stroke = 5m.

Since the load and descension time are different in the four cases, the choice of the matching case should be made with reference to the average power during the entire cycle. Table 2 gives the relevant data for the cyclic operation. The cycle average power was calculated as P_{av} = (W_L ascension - W_L descension) x stroke/cycle time. The same data is presented in the form of plots of cycle time, cycle power and C_L/C_D during descension Vs load during descension in Fig. 33. Both W_L for descension and cycle time decrease as C_L/C_D decreases. Thus it is best to operate at as small a C_L/C_D as possible. But this choice of C_L/C_D depends on the choice of the dead weight W_L for descension purpose.

Thus we have the situation in which during ascension the tether angle is chosen such that $\theta < \theta eq$ to maximise power, while during descension, the same tether angle should

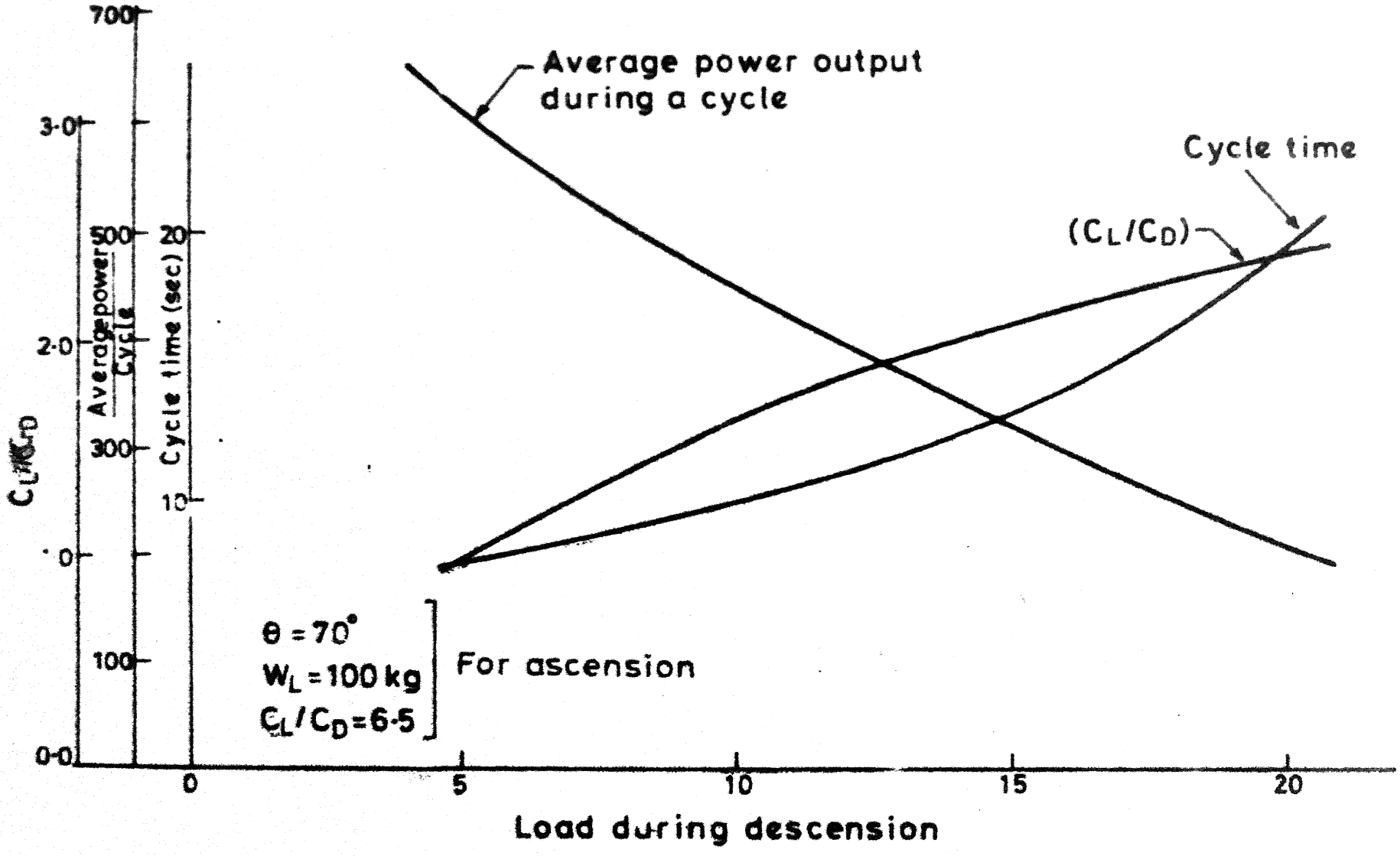

Fig. 33 Loads matching ascension curve

be > θeq. The θeq during descension depends on the choice of C_L/C_D for descension. Conversely, if $(C_L/C_D)_A$ and $(C_L/C_D)_D$ are fixed, the operating tether angle θ is so chosen such that θeq for ascension > θ > θeq for descension. Table 3 shows the effect of choice of initial tether angle θ on the cycle power. The calculations are made by considering $(C_L/C_D)_{ascension} = 6.5$ and $(C_L/C_D)_D = 1.625$. The corresponding equillibrium angles are 81° and 56° respectively.

In ascension, the loads optimising power at θ = 78°, 70° and 60° were determined. These ascension paths are matched by proper descension path with $C_L/C_D = 1.625$. Stroke = 5m for the cycle

Initial θ (degree)	Ascension		Descension		Entire cycle		
	Optimum load kg	Time sec	matching load kg	Time sec.	Net Load kg	Time sec.	Powe. watts
78	60	11.55	14.55	2.075	45.45	13.595	164
70	100	4.23	10.0	5.675	90.0	9.905	445
60	200	2.92	14.85	25.1	185.15	28.02	323

Table 3: Effect of choice of initial tether angle on the cyclic operation. $(C_L/C_D)_A = 6.5$, $(C_L/C_D)_D = 1.625$, stroke=5m.

It is observed from the data in Table 3 that, the best operating condition is initial tether angle = 70°. The other two angles are nearer to one of the equillibrium angles. For example, θ = 78° is nearer to $\theta_{eq} = 81°$ (corresponding to $(C_L/C_D = 6.5)$ and hence the performance during ascension is

affected. In this case, the optimum load is the smallest and the ascension time is the largest. Similarly when $\theta = 60^\circ$, it is descension that is affected since $\theta = 60^\circ$ is nearer to $\theta_{eq} = 56^\circ$ (corresponding to $C_L/C_D = 1.625$). In this case the descension time is large affecting the total cycle time and hence the cycle power.

5-5. Effect of Variation of Kite Weight on the Performance

So far the discussion had been restricted to a kite with W_K constant. In the following we discuss how the performance characteristics of the system changes when W_k changes. The other parameters are kept constant, i.e., stroke = 5m, initial tether length = 1000m, C_L/C_D during ascension = 6.5 and C_L/C_D during descension = 2.0, and initial tether angle $\theta = 70^\circ$.

The effect of the W_k on average power during ascension is given in Fig. 34 and 35. Since W_k is a liability on the system contributing nothing to the power generated, we expect that the least kite weight is the best for ascension. Figs. 34 and 35 verify this intuition. As $\bar{W}_k$ decreases, not only the average power is increased, but the optimum load also increases. The effect of W_k can be viewed from another angle. It may be regarded as something which reduces the lift causing a decrease in effective C_L/C_D. When $\bar{W}_k = 0$, the effective lift is maximum. But when

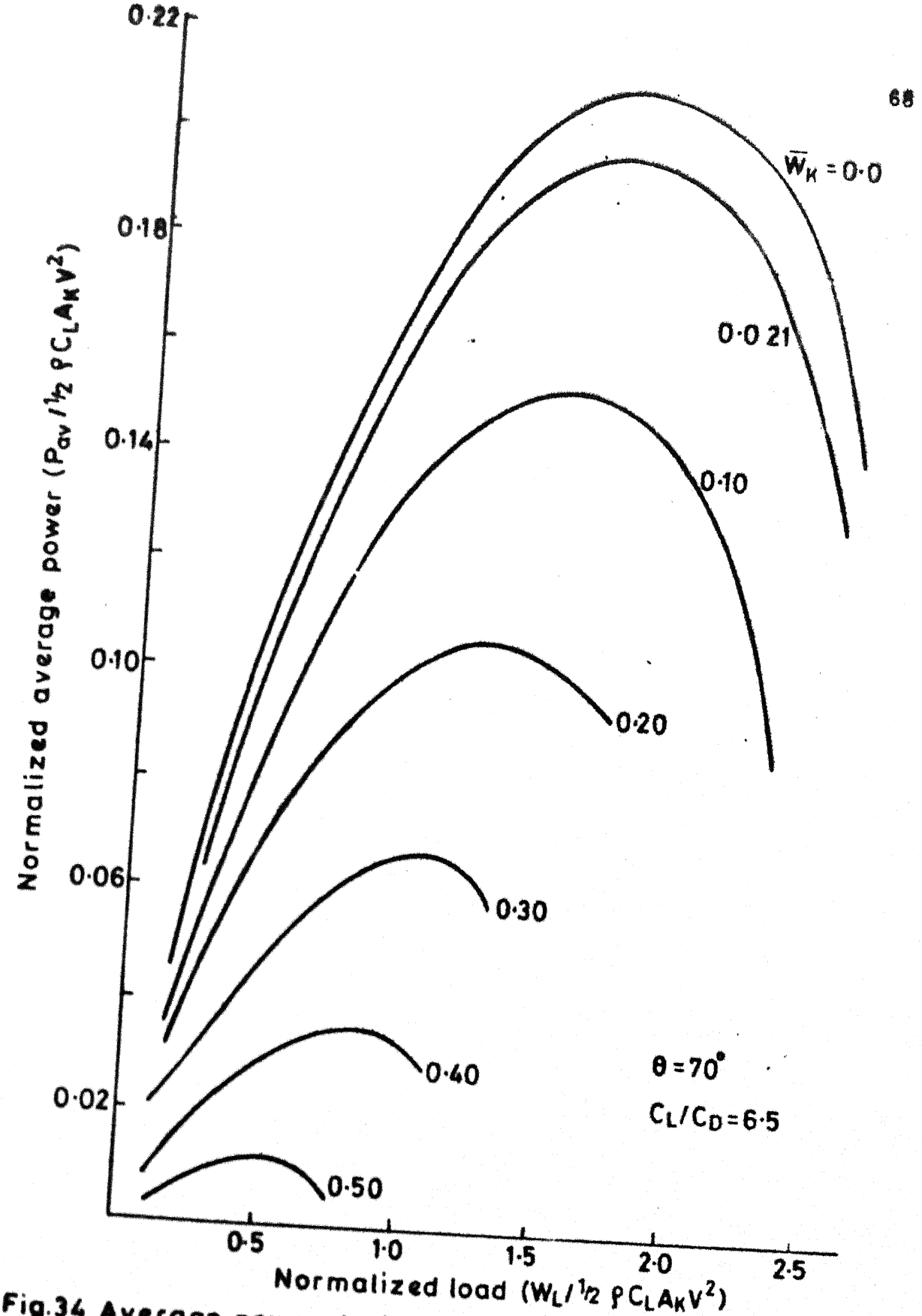

Fig.34 Average power during ascension vs load for different W_K

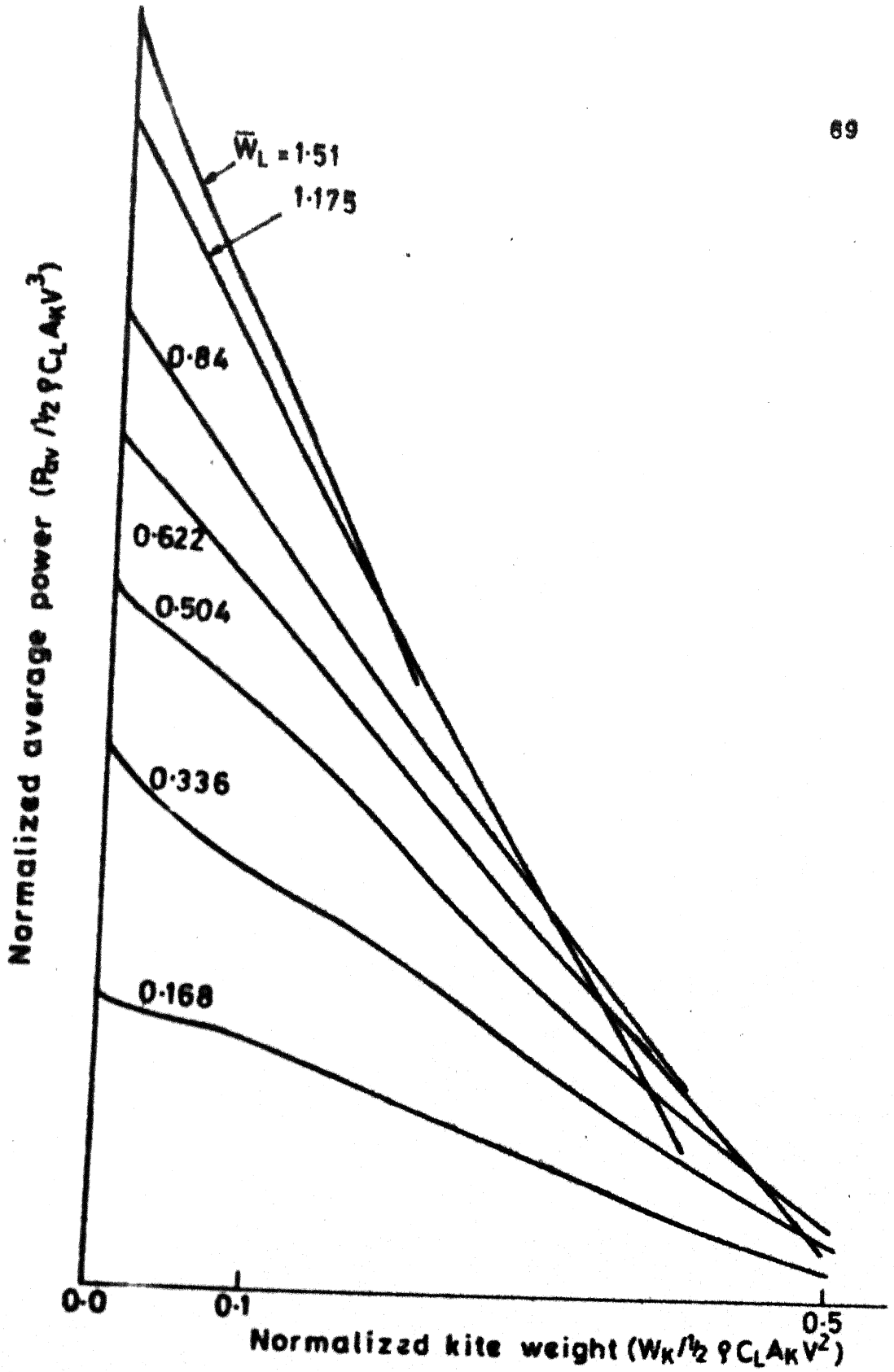

Fig.35 Average power during ascension vs $\bar{W}_K$

$\bar{W}_k = 1.0$, the entire lift is balanced by W_k and the kite cannot ascend. Further θ_{eq} also decreases as $\bar{W}_k$ increases (refer Fig. 8). This adds to the poor performance of the system at large $\bar{W}_k$.

Now to examine how the kite profiles change with W_k, refer Fig. 36. The portion above the x axis corresponds to ascension and the portion below the x axis corresponds to descension. In ascension, increase in kite weight acts in a manner similar to increasing the load in that each curve corresponding to a $\bar{W}_L$ tends to move towards the left. However, in descension, the kite weight acts in such a way as to shorten the path. This means that as the kite weight increases the system descends more rapidly, at smaller loads. Therefore, kite weight is desirable during descension, but undesirable during ascension. Obviously an optimum kite weight may be found if the entire cycle is analyzed. Fig. 37 shows the variation of cycle power with $\bar{W}_K$. The average power is obtained by first determining the optimum load during ascension and the corresponding profile and then matching it with descension for each value of kite weight considered. Kite weight is normalized by $\frac{1}{2}\rho C_L A_K V^2$ where C_L is that used for ascension and power is normalized by $\frac{1}{2}\rho A_K V^3$. It is found that the cycle power is a maximum when $\bar{W}_K = 0.133$.

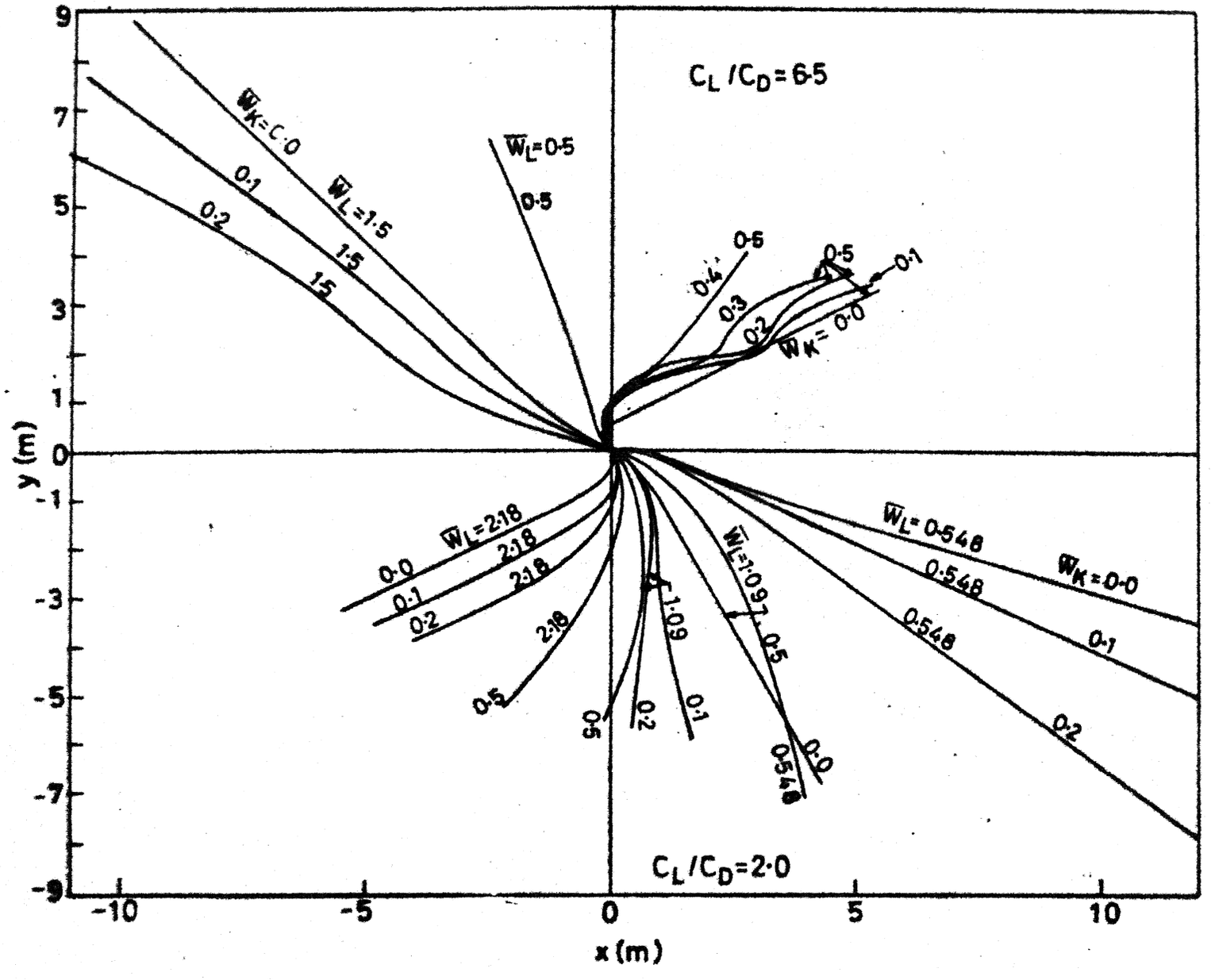

Fig.36 Kite profiles during ascension and descension for different values of $\overline{W}_L$ and $\overline{W}_K$

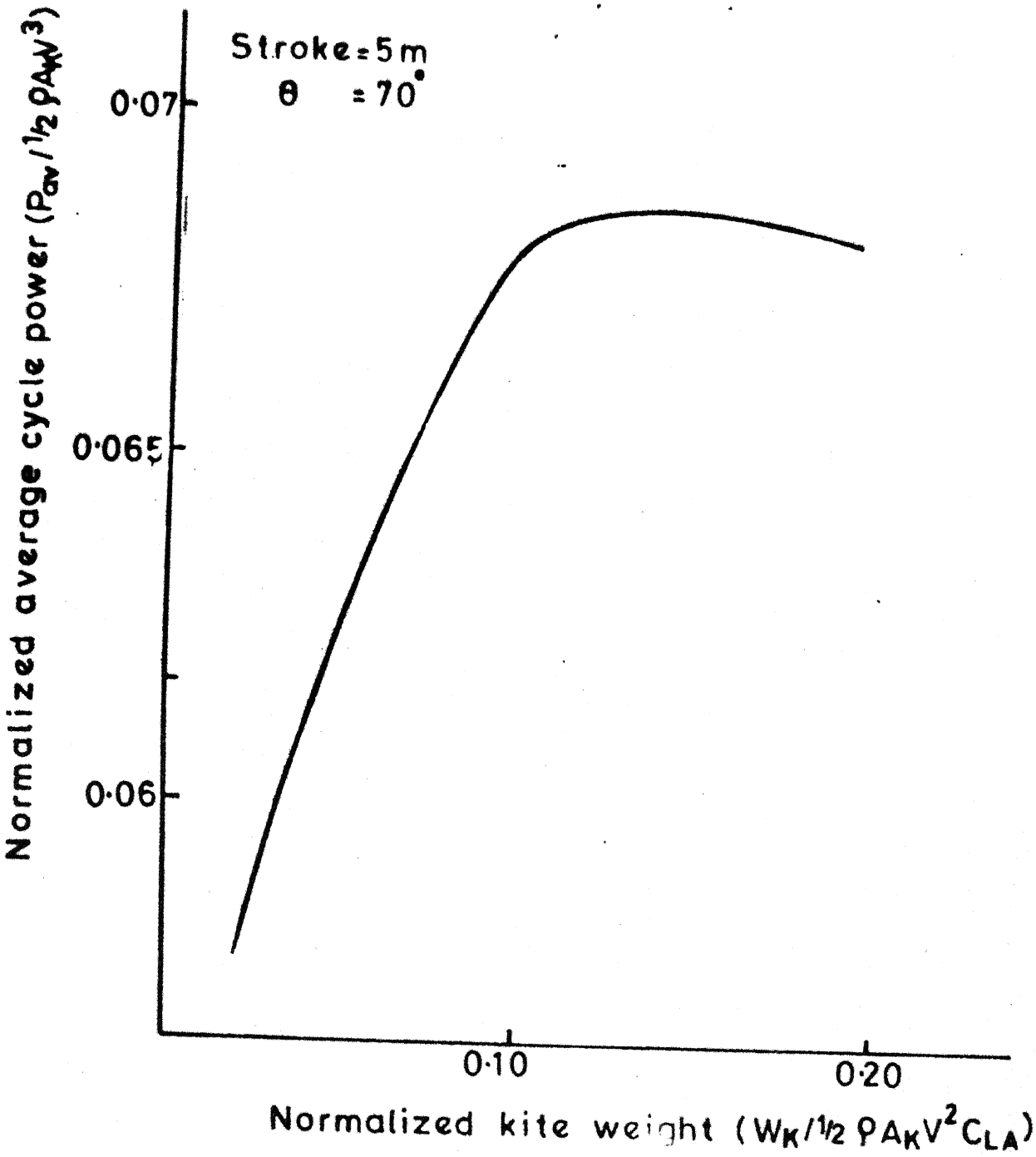

Fig.37 Average power output during a cycle vs $\overline{W}_K$

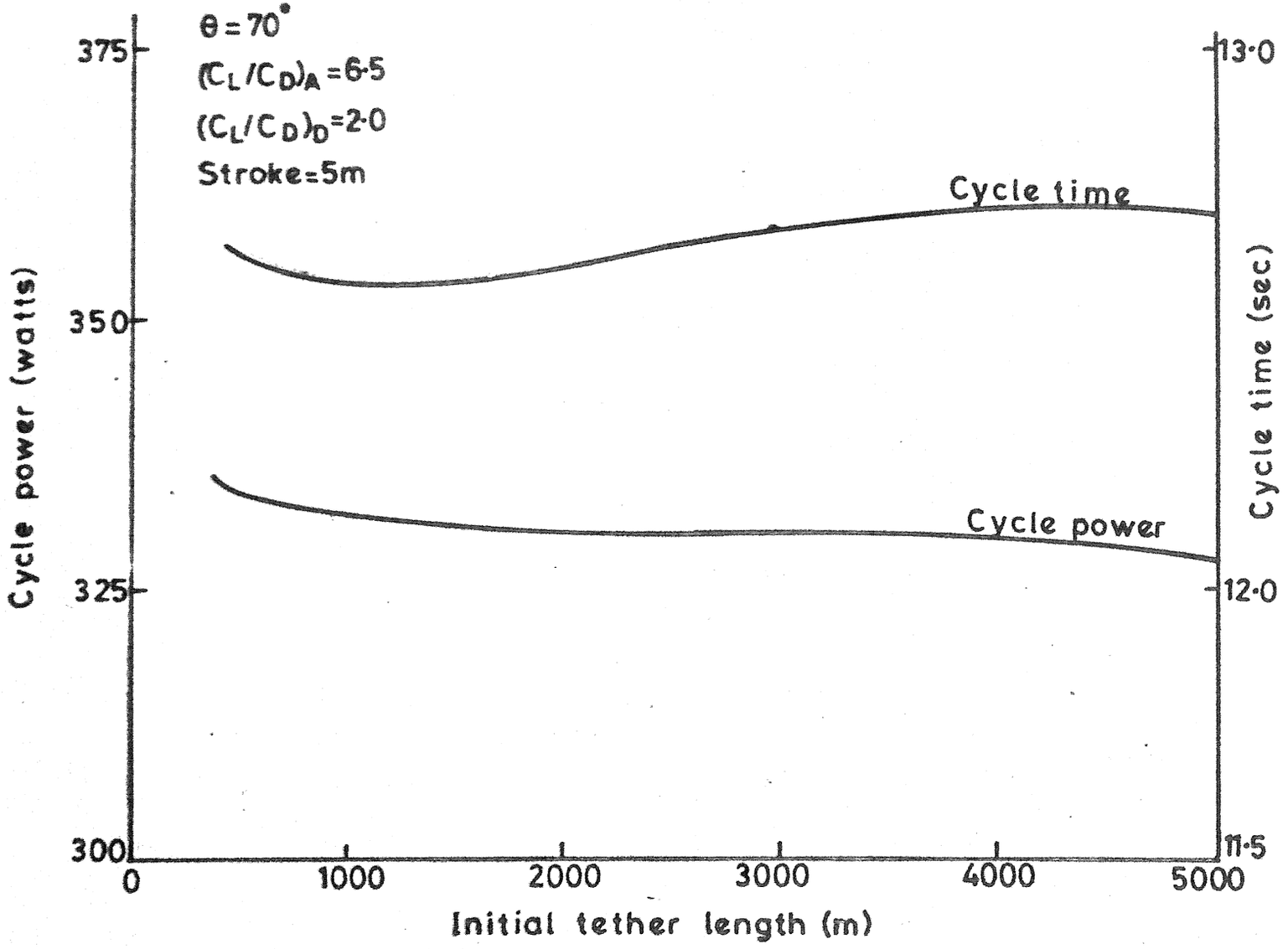

Fig. 38 Variation of cycle power and cycle time with initial tether length

5.6. Effect of Variation of Initial Tether Length

To examine whether the performance of the system changes with the initial tether length L, the average power during a cycle was evaluated for different initial tether length. During ascension C_L/C_D, θ, and $\bar{W}_L$ were taken as 6.5, 70° and 1.68 respectively. This case was matched with $(C_L/C_D)_D = 2.0$ and suitable load during descension. (It should be noted that the results with different tether length have been obtained assuming that the tether profile is a straight line. At larger tether lengths, the actual profiles may deviate considerably from the ideal straightline profile). The results of the above calculation are plotted in Fig. 38. This indicates that the cycle power and cycle time are not seriously affected by the change in initial tether length.

VI. CONCLUSION

In this thesis, the performance characteristics of a kite powered pump have been theoretically studied. The system consists of a kite which intercepts wind at a desired altitude, its tether which transmits the kite motion to the ground and a load which is attached directly to the other end of the tether. There are two strokes for the pump: the power stroke (ascension stroke) and the return-stroke (descension stroke). This cyclic operation of the system is made possible by varying the altitude of the kite at the end of each stroke. During ascension the kite pulls the load (water payload and container dead weight) while during descension the dead weight pulls the kite.

The kite powered pump has been analysed theoretically to explore the possibility of cyclic operation. Governing equations describing the motion of the system in both ascension and descension were developed assuming that the tether profile is a straight line. Non-dimensionalization of the governing equations shows that the important parameters on which the performance of the system depend are $\frac{gL_o}{V^2}$, $\frac{S}{L_o}$, $W_k/(\frac{1}{2} \rho A_k C_L V^2)$, $W_L/(\frac{1}{2} \rho A_k C_L V^2)$, C_L/C_D and $V_{initial}$ tether angle θ where L_o is the initial tether length and S is the stroke.

Numerical solutions of the equations show that cross wind kite motion ($\theta = 0^{\circ}$) will provide the maximum power during ascension. However, due to practical difficulties involved in its operation, this mode was not considered for further analysis. Instead, a system with initial tether angle = 70° was considered. For this case, it turns out that the average power output during ascension is maximized when the load is 1.68 times the static lift force. During descension, however, as the load increases the power consumed also increases and thus no minimization of power output was obtained. Further it was found that the descension path profiles and power output are functions of both C_L/C_D and load.

The cyclic operation of the system was studied keeping the conditions of the optimum ascension stroke when tether angle = 70° and varying parameters for descension stroke such that the kite returns to its initial position. The results show that a choice of the least possible load and a corresponding C_L/C_D (to match the ascension profile) during descension maximizes cycle power. Further, if C_L/C_D during ascension and descension are fixed, one should choose initial tether angle midway between the two equilibrium angles corresponding to the two given (C_L/C_D)s for maximizing cycle power.

The results obtained by varying kite weight show that cycle power can be maximized with kite weight. At initial tether angle = 70°, $C_L/C_D = 6.5$ during ascension and = 2.0 during descension, a kite weight of 8 kg gives the maximum cycle power. Further, the cycle power is a very weak function of initial tether length within the frame work of our analysis which assumes that the tether profile is a straight line.

Scope for Further Work

One may extend the above study in the following directions:

(i) Theoretical study of the dynamic behaviour of the system to include the effect of tether weight and wind drag on the performance characteristics of the system.

(ii) Theoretical analysis taking into account the variation of air density and wind speed with altitude.

(iii) In actual case, the system is to be decelerated to zero velocity before it can start the next stroke. Analysis of this situation to determine the subsequent change in the performance.

-

REFERENCES

1. C.A.J. Fletcher and B.W. Roberts, "Electricity generation from jet stream winds", J. of Energy, 3, 241-249 (July-August 1979).
2. C.A.J. Fletcher, Honan and J.S. Sapupo, "Aerodynamic platform comparison for jet stream Electricity generation", J. of Energy, 7, 17-24 (Jan- Feb. 1983).
3. G. Riegler, W. Riedler and E Horvath, "Transformation of wind energy by a high altitude power plant", J. of Energy, 7, 92-94 (Jan.- Feb., 1983).
4. M.L. Loyd, "Cross-wind Kite Power", J. of Energy, 4, 106-111 (May-June 1979).
5. J.S. Goela, "Wind power through kites', Mechanical Engineering, 42, 42-43 (June 1979).
6. J.S. Goela, "Wind Energy Conversion through Kites", Physical Sciences Inc., Report SR-S1 (1979).
7. J.S. Goela, "Project Report I on Wind Energy Conversion through Kites", No. DST/ME(JSG)/81-84/26/I, IIT Kanpur (Jan. 1982).
8. J.S. Goela, "Project Report II on Wind Energy Conversion through Kites", No. DST/ME(JSG)/81-84/26/II, IIT Kanpur (Jan. 1983).
9. K.K. Tiwari, "Design and fabrication of a kite pump", M.Tech. thesis, Dept. of Mech. Engg., IIT Kanpur (1983).
10. W. Yolen, "The complete book of kites and kite flying", Simon and Shuster, 56-66 (1976).

11. G. Pocock, "Aeroplaustic art, Fasemile", E.L. Steme, San Fransisco, 3-51 (1969).

12. C.A.J. Fletcher, "On the rotary wing concept for jet stream Electricity generation", J. of Energy, 7, 90-92 (Jan.- Feb. 1983).

13. S.K. Verma and J.S. Goela, "Effect of wind loading on the design of a kite tether", J. of Energy, 6, 342-343 (Sept.-Oct. 1982).

APPENDIX A

STATIC TETHER PROFILE AND VARIATION OF TENSION ALONG THE TETHER

(i) Governing Equations

Consider a small element of a tether of length dL, diameter d_t and weight per unit length w_t as shown in Fig. 39.

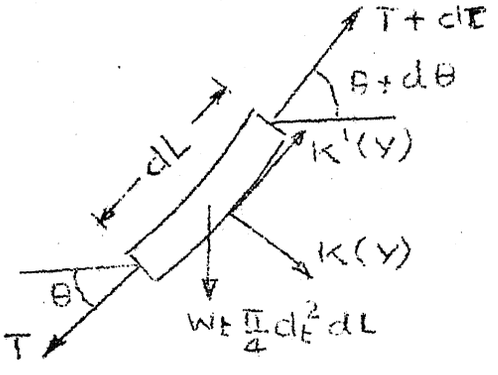

Fig. 39: Forces acting on an element of tether

Proper force balance and subsequent simplifications yields the following four equations which describe the effect of wind drag on the static profile and force transmission efficiency of a kite tether [7,8,13].

$$\frac{dT}{dL} = w_t \text{ Sin } \theta - K'(y) \text{ Cos } \theta \qquad (29)$$

$$T\frac{d\theta}{dL} = w_t \text{ Cos } \theta + K(y) \text{ Sin}^2\theta + K'(y) \text{ Sin } \theta \qquad (30)$$

$$\frac{dx}{dL} = \text{Cos } \theta \qquad (31)$$

$$\frac{dy}{dL} = \text{Sin } \theta \qquad (32)$$

where

$$K(y) = 0.55\ \rho(y)\ V^2\ d_t \tag{33}$$

$$K'(y) = 0.01\ \rho(y)\ V^2\ d_t \tag{34}$$

When it is assumed that ρ and V are not function of y, K and K' become constants. With these assumptions, Eqns. (29) to (32) after non dimensionalization become

$$\frac{d\bar{T}}{d\bar{L}} = \frac{w_t L_o}{T_k}\left\{ \text{Sin } \theta - \frac{K'}{w_t} \text{Cos } \theta \right\} \tag{35}$$

$$\frac{d\theta}{d\bar{L}} = \frac{w_t L_o}{T_k}\ \frac{1}{\bar{T}}\left\{ \text{Cos } \theta + \frac{K}{w_t} \text{Sin}^2\theta + \frac{K}{w_t} \text{Sin } \theta \right\} \tag{36}$$

$$\frac{d\bar{x}}{d\bar{L}} = \text{Cos } \theta \tag{37}$$

and

$$\frac{d\bar{y}}{d\bar{L}} = \text{Sin } \theta \tag{38}$$

where $\bar{T}$, $\bar{L}$, $\bar{x}$ and $\bar{y}$ are non-dimensional tension, length, and x and y coordinates. L_o and T_k are the characteristic length and tension (T_k is the tension at the kite end where $\theta = \theta_k$). In Equations 35-38, there are three parameters of which $\frac{K}{w_t}$ and $\frac{K'}{w_t}$ are mutually dependant. When $\frac{K}{w_t}$ (and $\frac{K'}{w_t}$) = 0, the results will be those of a catenary. Equations (35-38) are solved numerically by Runge-Kutta method for different values of the parameters $\frac{w_t L_o}{T_k}$ and $\frac{K}{w_t}$ to determine the static profile and the force transmission.

(ii) Results

Figs. (40-47) give the results. In Fig. 40, the tether profiles for four different values of $\frac{w_t L_o}{T_k}$ (= 0.01, 0.02, 0.05, 0.1) are plotted. For these plots we have taken the wind load parameter $\frac{K}{w_t} = 17.51$ and $\theta_k = 80^\circ$. This value of K/w_t corresponds to tether tension at the kite end T_k=60N, wind velocity = 10 m/s and diameter of tether designed on the basis of T_k with a factor of safety = 4. For comparison purposes, we have also shown tether profile for a catenary when $\frac{w_t L_o}{T_k} = 0.01$ and 0.1. We see that as the tether weight parameter varies from 0.01 to 0.1, the catenary behaviour shows little change but there is appreciable change when wind drag is taken into account.

For the above conditions, the variation in tether tension as a function of θ is shown in Fig. 41. The plot of T/T_k vs θ is independant of the parameter $\frac{w_t L_o}{T_k}$ in the sense that the same shape of the curve is obtained; if larger values of $\frac{w_t L_o}{T_k}$ is used one moves further on the same curve than when smaller value of $\frac{w_t L_o}{T_k}$ are taken. Different values of $\frac{w_t L_o}{T_k}$ are marked on the two curves showing how far one can go with a given value of the parameter. From Fig. 41 we again see that there is appreciate difference between a catenary behaviour and the behaviour when wind drag is taken into account.

Figs. 42 and 43 show the tether profile and variation of tether tension for different values of $\frac{K}{w_t}$. These results are obtained for $\frac{w_t L_o}{T_k} = 0.02$. We see that as $\frac{K}{w_t}$ increases, there is a reduction in tension defect. Thus the reduction in tension with θ is maximum in catenary behaviour. Another interesting point to note is that when $\frac{K}{w_t} = 100$, the tether tension at lower values of θ is larger than that at $\theta = \theta_k$. Therefore when wind velocity is large one should design the tether based on tension at $\theta = 0^o$ and $\theta = \theta_k$.

The tension at the lower end of the tether $\overline{T}_p$ is shown as a function of $\frac{w_t L_o}{T_k}$ and $\frac{K}{wt}$ in Figs. 44 and 45 respectively. It is observed that for small values of $\frac{w_t L_o}{T_k}$, the tension at the lower end is not much different from that at the kite end. For $\frac{k}{w_t} < 50$, the change in tension is as small 4% or less. All the above curves were obtained for $\theta_k = 80$.

To see how the tension changes when θ_k is changed, refer Fig. 46. The change in tether angle and tension are comparatively smaller when θ_k is small.

In this thesis, for the most part we have chosen $\theta_k = 70^o$. The optimum load at this angle is 981N. For Kevlar 29 tether of length 1000m (density = 1.44×10^3 kg/m^3 and tensile strength = 2.9×10^9 Pa), 981N tension will result in $\frac{w_t L_o}{T_k} = 0.02018$ and $\frac{K}{wt} = 0.43308$. The tether profile for the above case is shown in Fig. 47, along with

the straight line approximating it. It can be seen that the deviation of the actual profile from a straightline is small and therefore negiligible. Also, the change in tether tension is less than 4% for the case considered.

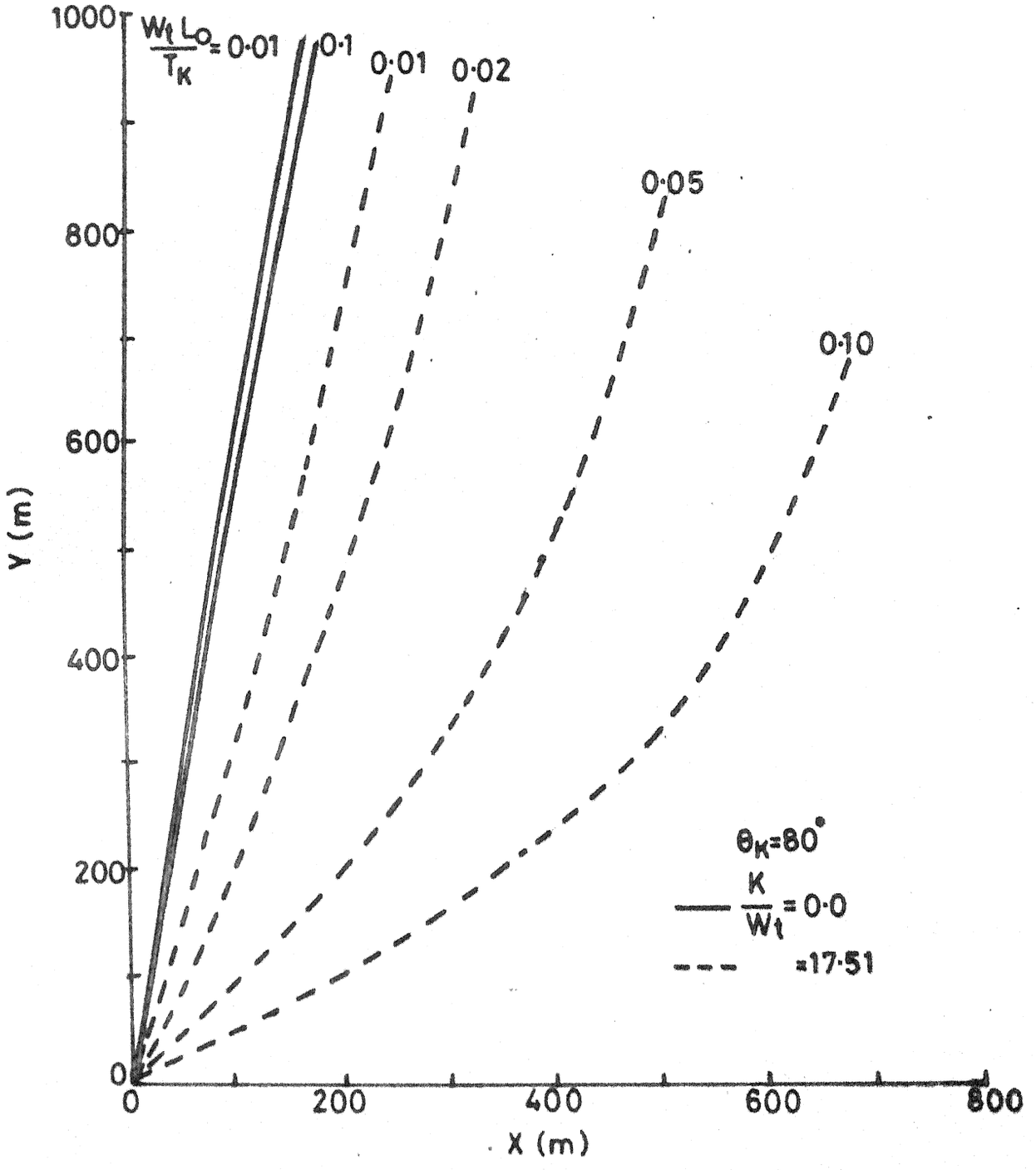

Fig. 40 Tether profiles of a 1 km tether

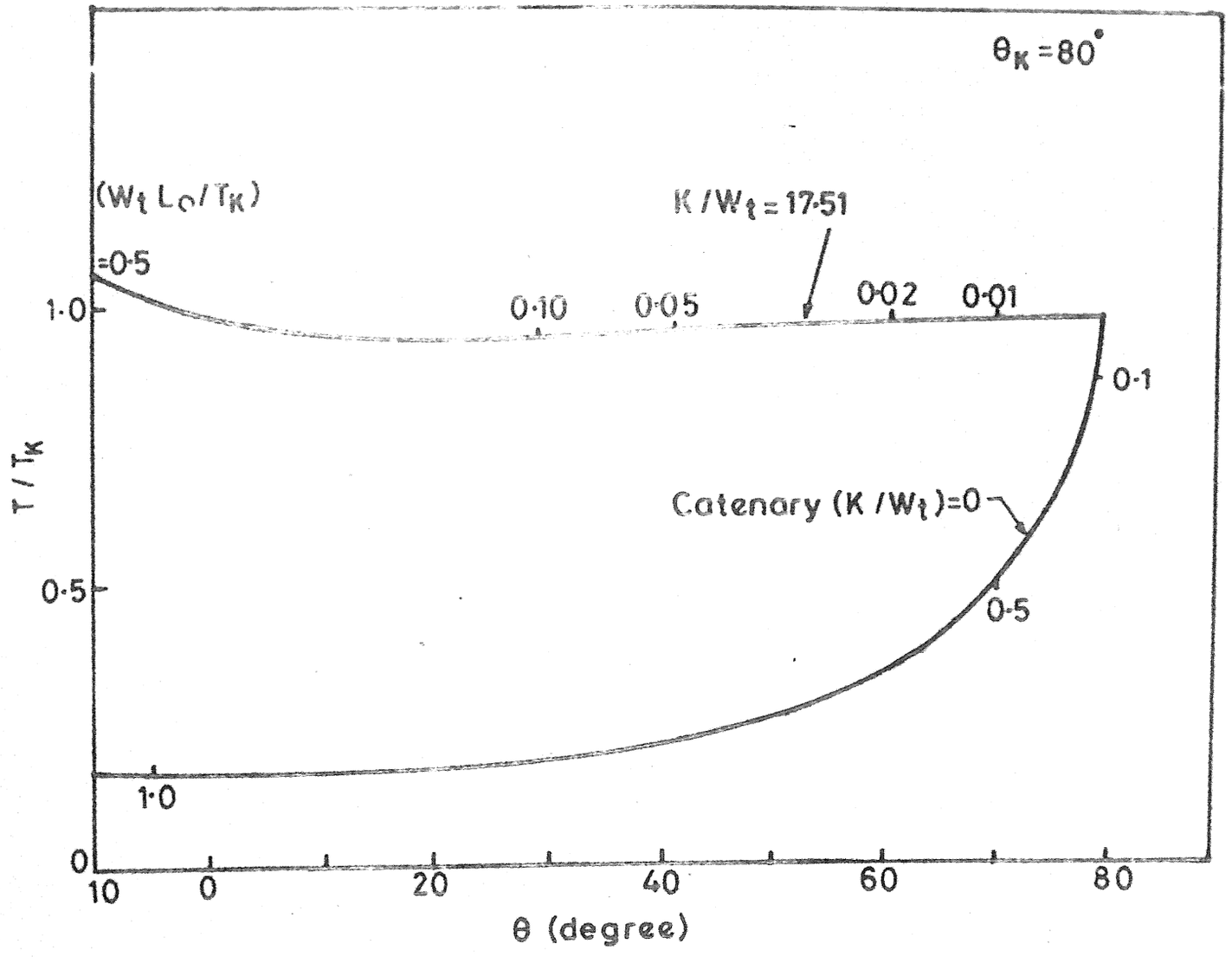

Fig. 41 Variation of tension along the tether

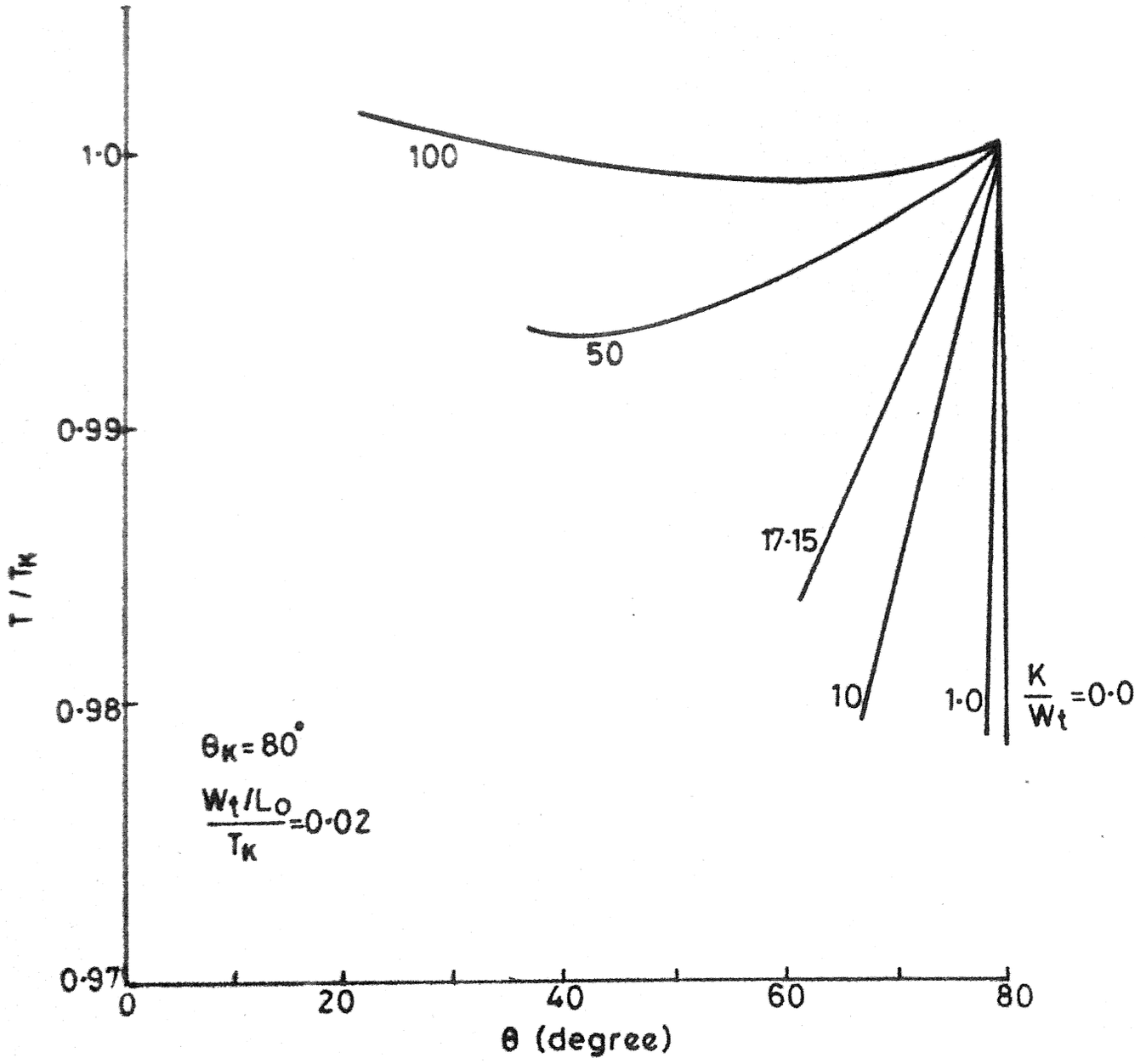

Fig. 43 Variation of tension along tether

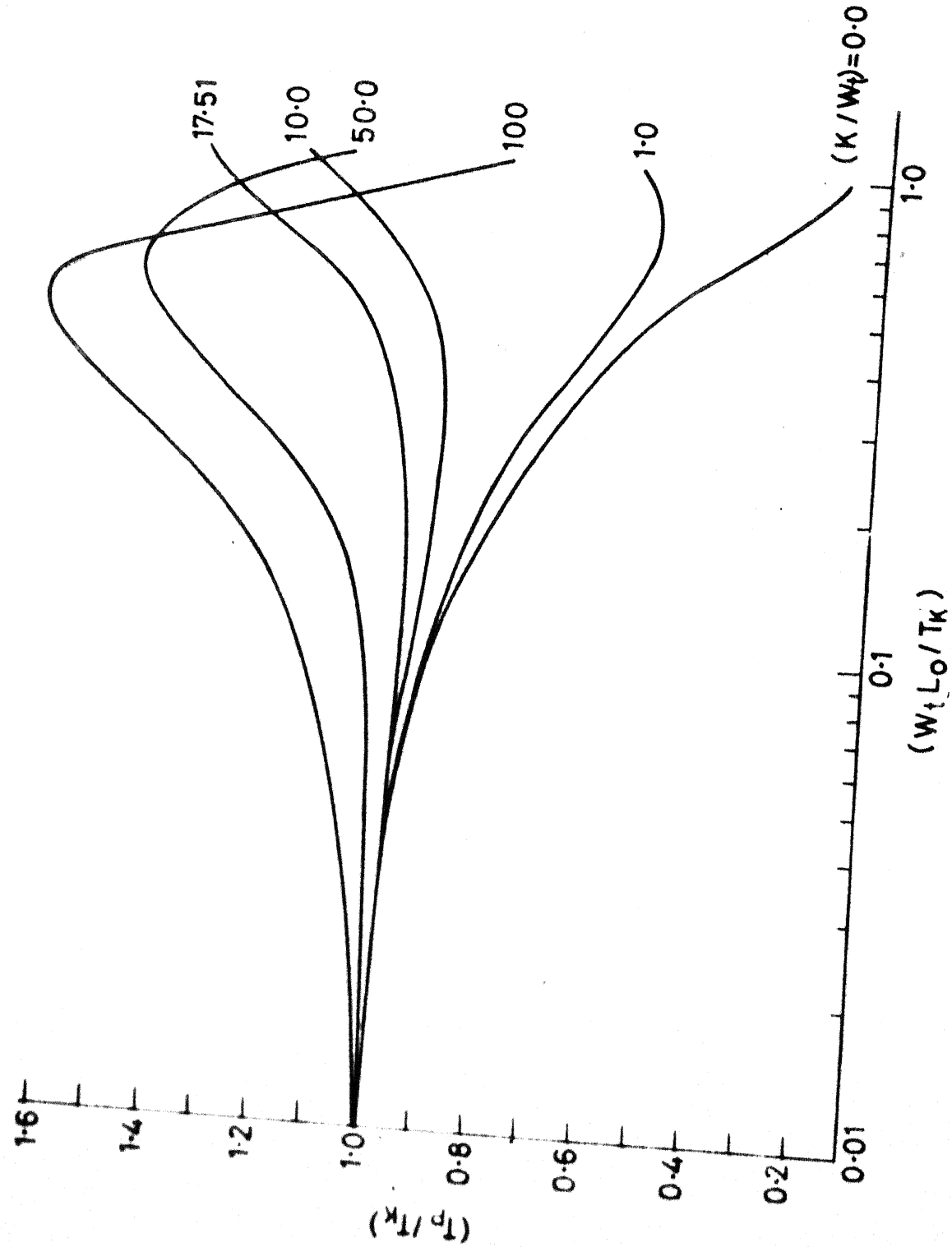

Fig.44 Variation of T_P with $(W_t L_o/T_K)$

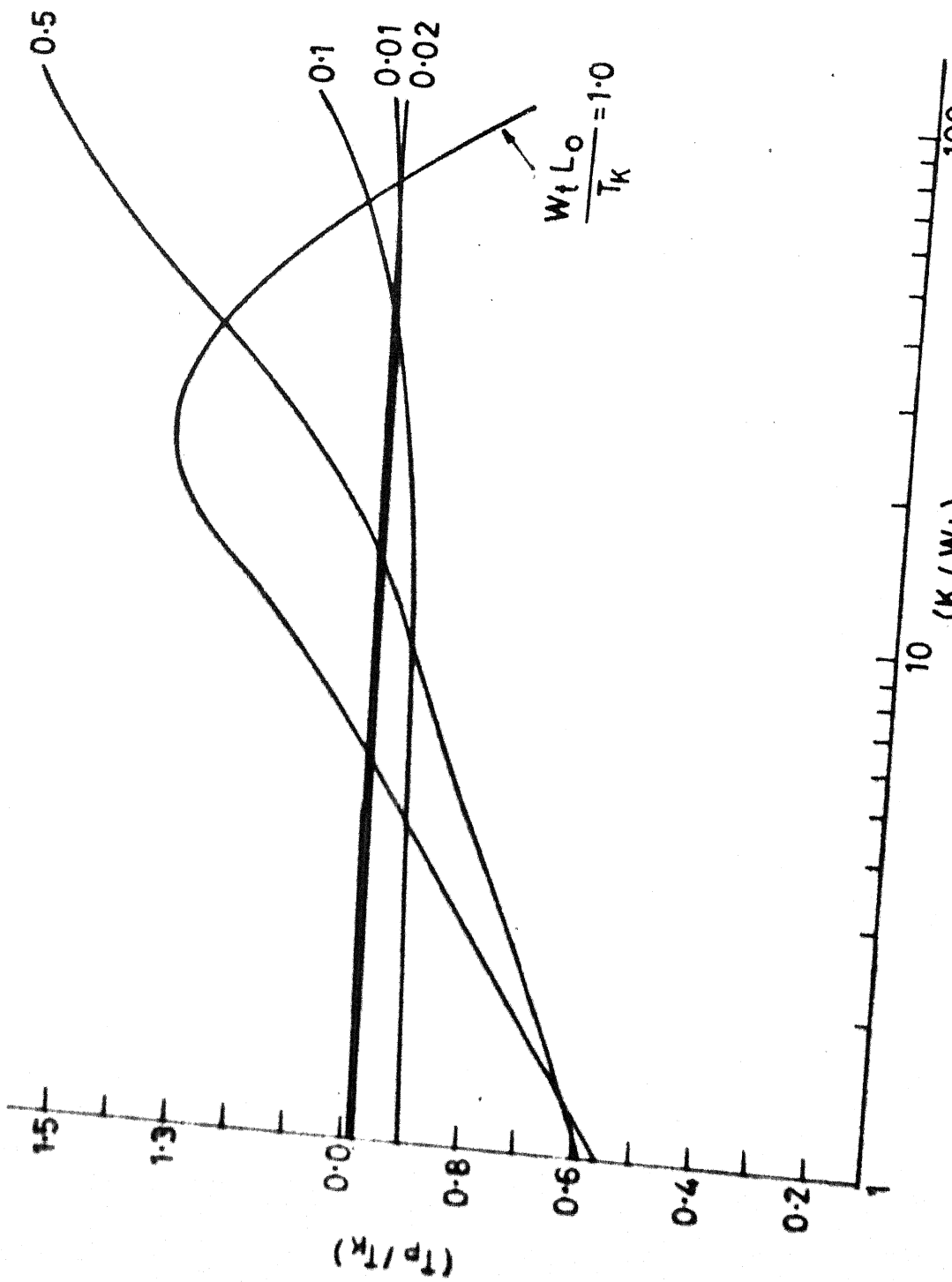

Fig.45 Variation of T_P with K / W_t

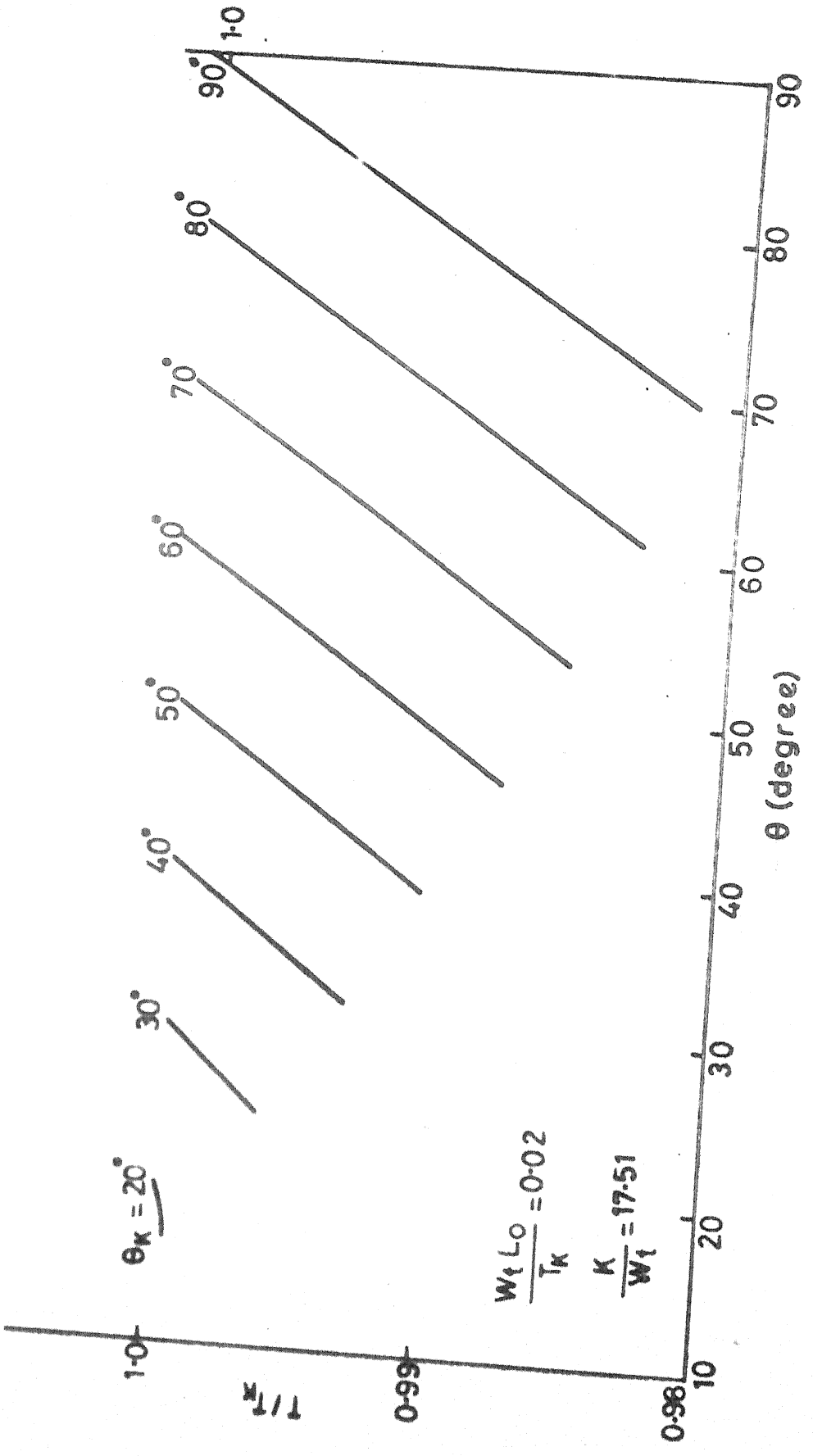

Fig. 46 Variation of tension with θ_K

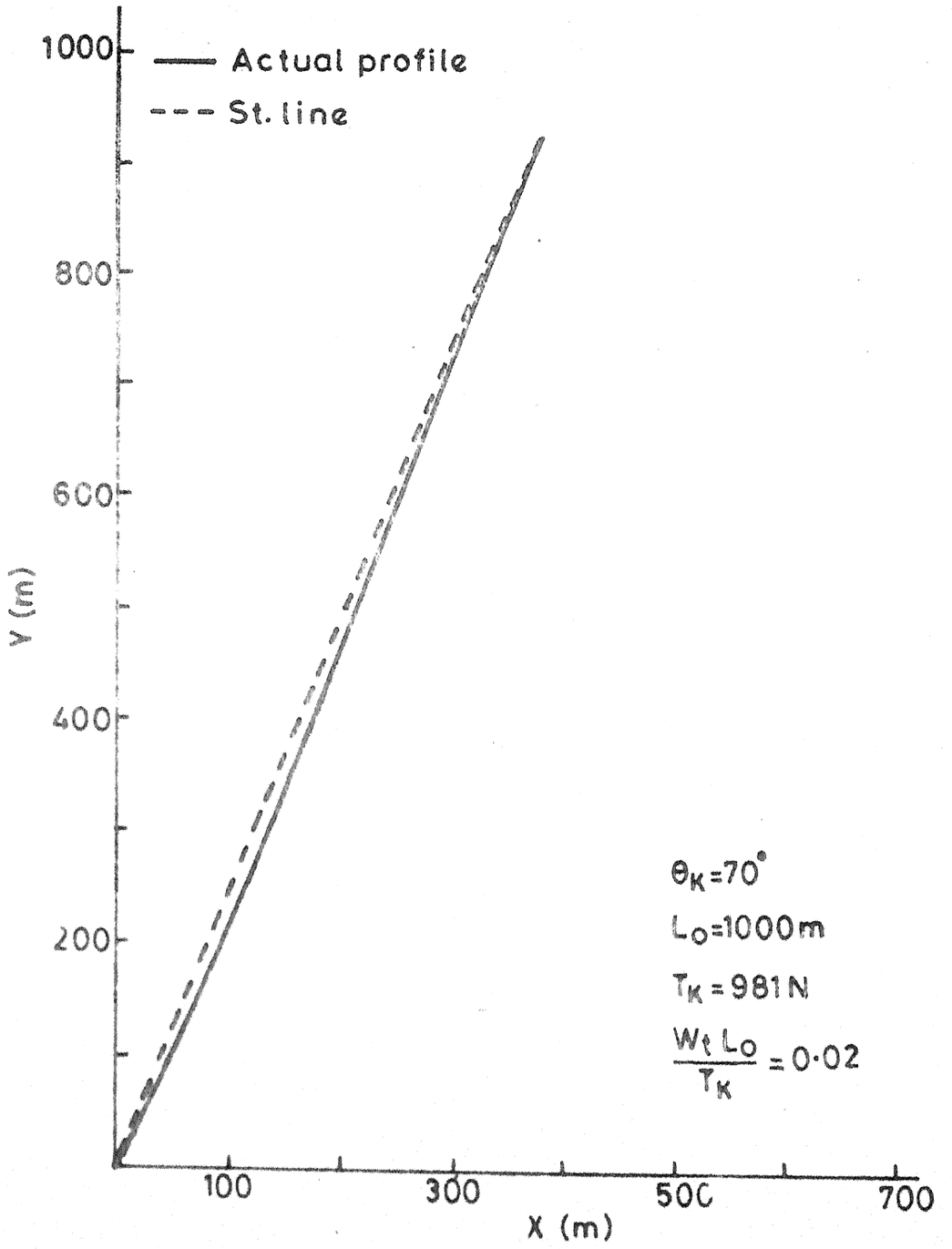

Fig. 47 Tether profile and straight line approximating the profile

```
                                                    PAGE 001:03
C     THIS PROGRAM SOLVES THE EQUATIONS OF MOTION FOR THE KITE
C     POWERED PLANE
C     LT,THETA,V1,V2 AND TAKE THE DEPENDANT AND INDEPPENDANT VARIABLES
      REAL LT,MU,MK,MLT
      DIMENSION B(5),C(5),FG(5),G(20)
      OPEN(UNIT=6,DEVICE='DSK',FILE='AB.OUT')
      DATA  AREA,RHO,V,G,PI,AMU,WLT,RATIO
     1/ 10.0,1.1670,10.0,9.81,3.141926,0.25,1.008E-03,6.5/
      WRITE(6,300)AREA,RHO,V,AMU,WLT
      RATIO=1.0/RATIO
      MU=1.0
      MK=0.3+0.1*AREA
      WK=MK*G
      FL1=0.5*CL*RHO*AREA
      FD1=FL1*CD
      FL=FL1*V**2
      FD=FD1*V**2
      WLT=WLT*G
      WLTBAR=WLT/FL
      WRITE (6,325) WLTBAR
      WRITE(6,310) THETAI,RATIO
      MU=1.0
      WRITE(6,320)MU,GPI
      W2=10*G
      THETA=THETAI
      LT=1000.
      DT=.05
      V1=0.0
      V2=0.0
      AVK=0.0
      DT=0.001
      BETA=(180.-0)/PI
      PHI=(THETA/RATIO
      X1=0.0* COS(PHI)
      Y1=0.0* SIN(PHI)
      BETA=(THETA+0.0
      X=0.0
      Y=0.0
      T=0.0
      WRITE(6,330)
      PHI=0.
      POWER=0.0
      WD=0.0
      J=2
      N=5
      A=T
      IS=0
      B(1)=LT
      B(2)=PHI
      B(3)=V1
      B(4)=V2
      B(5)=POWER
25    WRITE(6,340)T,LT,THETA,V1,V2,AVK,BETA,PHI,X,Y,POWER,WD
      STRK=B(1)-LT1
      IF(ABS(STRK).GT.S) GO TO 30
550   DO 120 I=1,10
        DO 110 NG=1,4
          G(1)=B(3)
          G(2)=-B(4)/B(1)
          IF(I.GT.2) GO TO 50
          IF(NG.GT.1)GO TO 50
          V2S0=V**2
          GO TO 90
50        VKS0=B(3)**2+B(1)**2
          VKS=SQRT(VKS0)
          BTA=B(2)=ATAN(B(4)/B(3))
          IF(B(3).LT.0.0) BTA=PI+BTA
          VRS0=V**2+VKS0-2.0 0*V*VK* COS(BTA)
          DIF=V-VK*COS(BTA)
          PHI= ATAN((VK* SIN(BTA))/DIF)
          IF(DIF.GT.0.) PHI=PI+PHI
60        ANGLE=B(2)+PHI
          SIN= SIN(ANGLE)
          COS= COS(ANGLE)
          FL=FL1*VRS0
          FD=FD1*VRS0
          FRI=EXP(AMU*(PI/2.0-B(2)))
          IF(B(3).LT.0.0)FRI=1./FRI
          G(3)=(FL*SIN+FD*COS-W1*SIN(B(2))-W2*FRI)/(MK+MLT*FRI)
          G(4)=(FD*SIN-FL*COS+W1*COS(B(2))+(MK/B(1)+WLT/3.0)*
     1    B(3)*B(4))/(MK+WLT*B(1)/3.0)
          G(5)=W2*B(3)
110     CALL RKM(A,B,C,DT,N,F,G,IS)
      STRK=B(1)-LT1
      IF(ABS(STRK).GE.S)GO TO 5
```

```
C SAVE VALUES AFTER INTEGRATION
5       LT=B(1)
        BTA=B(2)
        V1=B(3)
        V2=B(4)
        AVK=SQRT(V1**2+V2**2)
        BTA=BTA-ATAN(V2/V1)
        IF(V1.LT.0.0) BTA=BTA+PI
        X=LT*COS(BTA)-X1
        Y=LT*SIN(BTA)-Y1
        DIF=V-AVK*COS(BTA)
        THETA=BTA*CONST
        BETA=BTA*CONST
        PHI=CONST*ATAN((AVK*SIN(BTA))/(V-AVK*COS(BTA)))
        IF(DIF.LT.0.0)PHI=PHI+180.
        POWER=V2*V1
        WD=B(5)
        T=A
        I=I+1
        IF(T.LT.0.49) GO TO 25
        IF(T.LT.2.45)GO TO 35
        GO TO 45
35      DT=0.005
        GO TO 25
45      DT=0.01
        GO TO 25
30      AVPR=B(5)/A
        WRITE(6,350),AVPR
        TYPE*,AVPR
111     CONTINUE
90      CONTINUE
100     STOP
C
C
C FORMAT SPECIFICATIONS
C
300     FORMAT(20X,'KITE MOTION DURING ASCENSION'/20X,28(1H-)/15X,
     1  'AREA OF KITE=',F5.2,5X,'DENSITY OF AIR=',F5.3/15X,'VELO
     1  CITY OF AIR=',F5.2,5X,'COEFF. OF FRICTION=',F5.3/15X,'DEN
     1  SITY OF TETHER MATERIAL=',E11.4,'KG PER METER')
310     FORMAT(20X,'INITIAL TETHER ANGLE=',F4.1,5X,'CL/CD=',F6.3/
     1  20X,37(1H-))
320     FORMAT(15X,'LOAD=',F9.2,'KG',5X,'INITIAL L=',F7.1,'METER')
330     FORMAT(2X,129(1H=)/5X,'TIME',5X,'LENGTH',6X,'THETA',8X,'V
     11',10X,'V2',9X,'VK',7X,'BETA',8X,'PHI',9X,'X',10X,'Y',
     17X,'POWER',6X,'WD'/ 2X,129(1H-))
340     FORMAT(2X,F8.3,9F11.4,2F11.2)
350     FORMAT(25X,'AVERAGE POWER=',E13.6/2X,129(1H=))
325     FORMAT(20X,'NORMALIZED KITE WEIGHT=',F10.6)
333     FORMAT(2X,'TYPE IN REQUIRED LT1;K=',I2)
        END
C
C
C :::::::::::::::::::::::::::::::::::::::::::::::::::::::::::::::::::::::::::::::::::::::::
        SUBROUTINE RKM(A,B,C,DX,N,F,G,IS)
        DIMENSION  B(5),C(5),F(5),G(20)
C***************************************************************************************
        IS=IS+1
        GO TO (10,30,60,80),IS
C FIRST ENTRY
10      E=A
        DO 20 I=1,N
        F(I)=B(I)
        G(4*I-3)=C(I)*DX
20      B(I)=F(I)+G(4*I-3)/2.00
        GO TO 50
C SECOND ENTRY
30      DO 40 I=1,N
        G(4*I-2)=C(I)*DX
40      B(I)=F(I)+G(4*I-2)/2.00
50      A=E+DX/2.00
        GO TO 100
C THIRD ENTRY
60      DO 70 I=1,N
        G(4*I-1)=C(I)*DX
70      B(I)=F(I)+G(4*I-1)
        A=E+DX
        GO TO 100
C FOURTH ENTRY
80      DO 90 I=1,N
        G(4*I)=C(I)*DX
        B(I)=G(4*I-3)+2.00*(G(4*I-2)+G(4*I-1))
90      B(I)=(B(I)+G(4*I))/6.00+F(I)
        IS=0
100     RETURN
        END
```

APPENDIX C

If it is assumed that friction is absent around the pulley $T_P = T_L$ (refer page 16). The performance of the system changes slightly with this assumption. The variation of average power during ascension, ascension time and velocity at the end of a 5 m stroke during ascension with load during ascension are given in figs. (48-50). The behaviour of the curves are similar to those of figs. (10, 11 and 17). These are plotted for different values of initial tether angle.

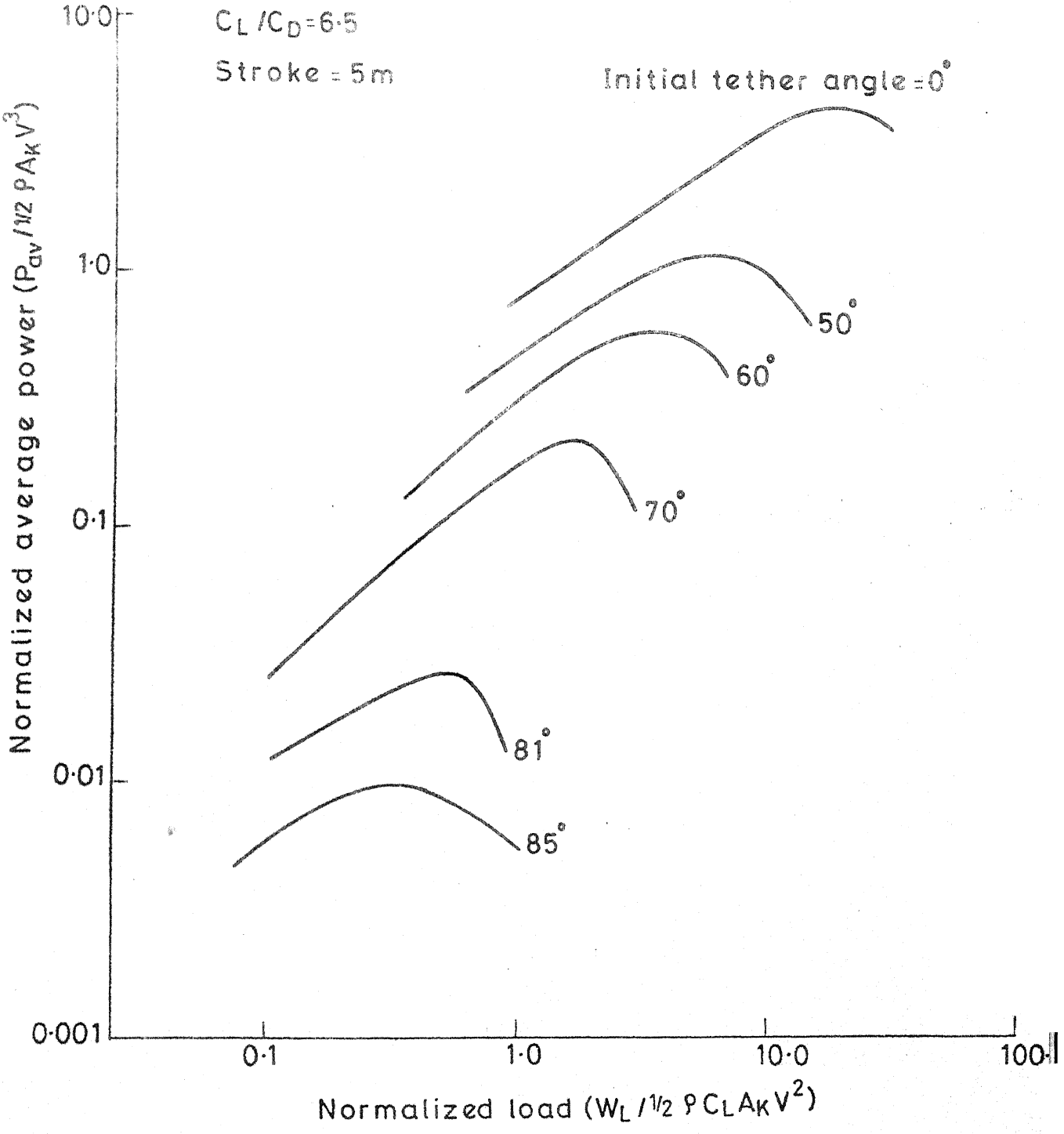

Fig 48 Variation of average power with load during ascension (friction neglected)

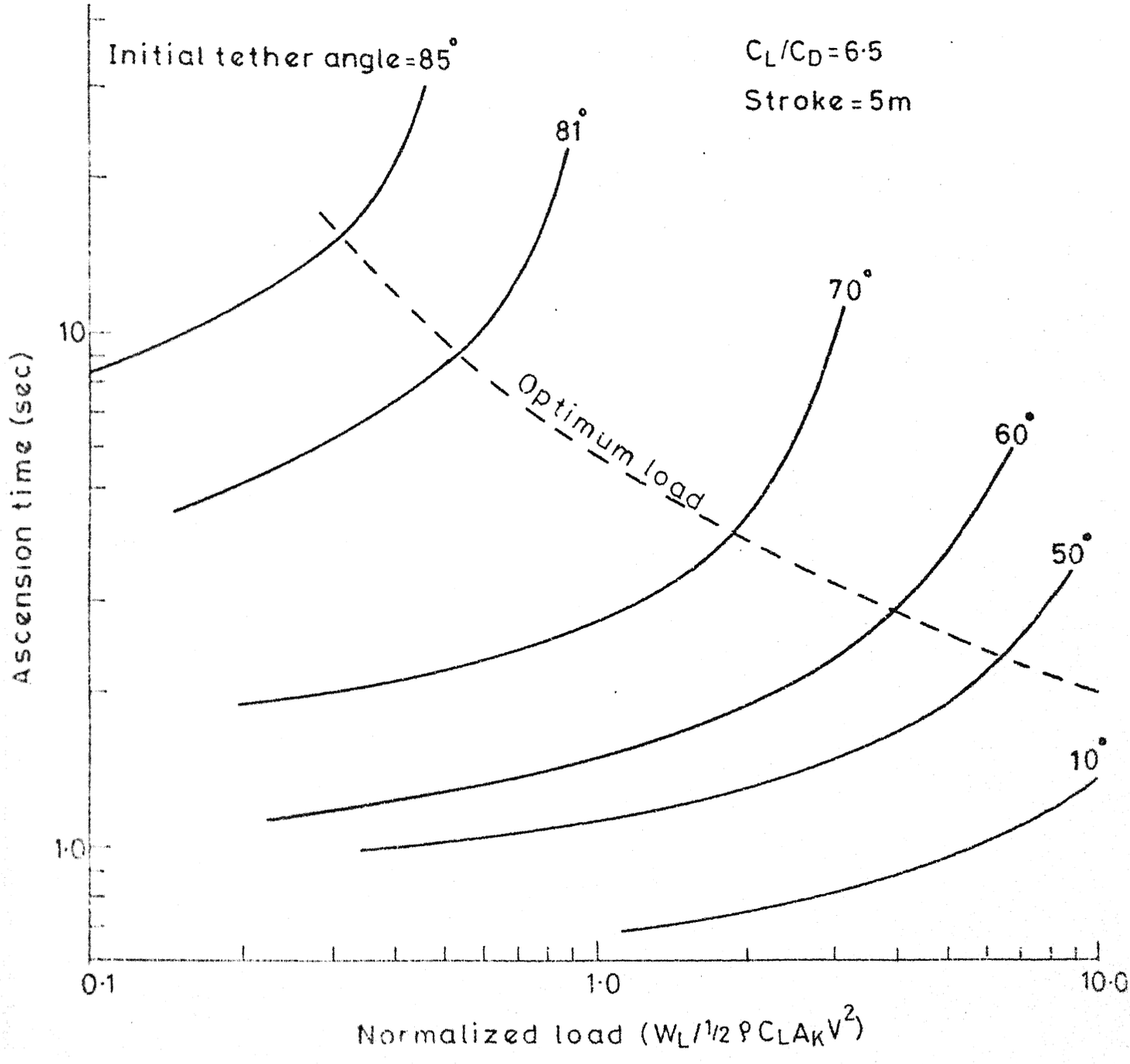

Fig. 49 Variation of ascension time with load

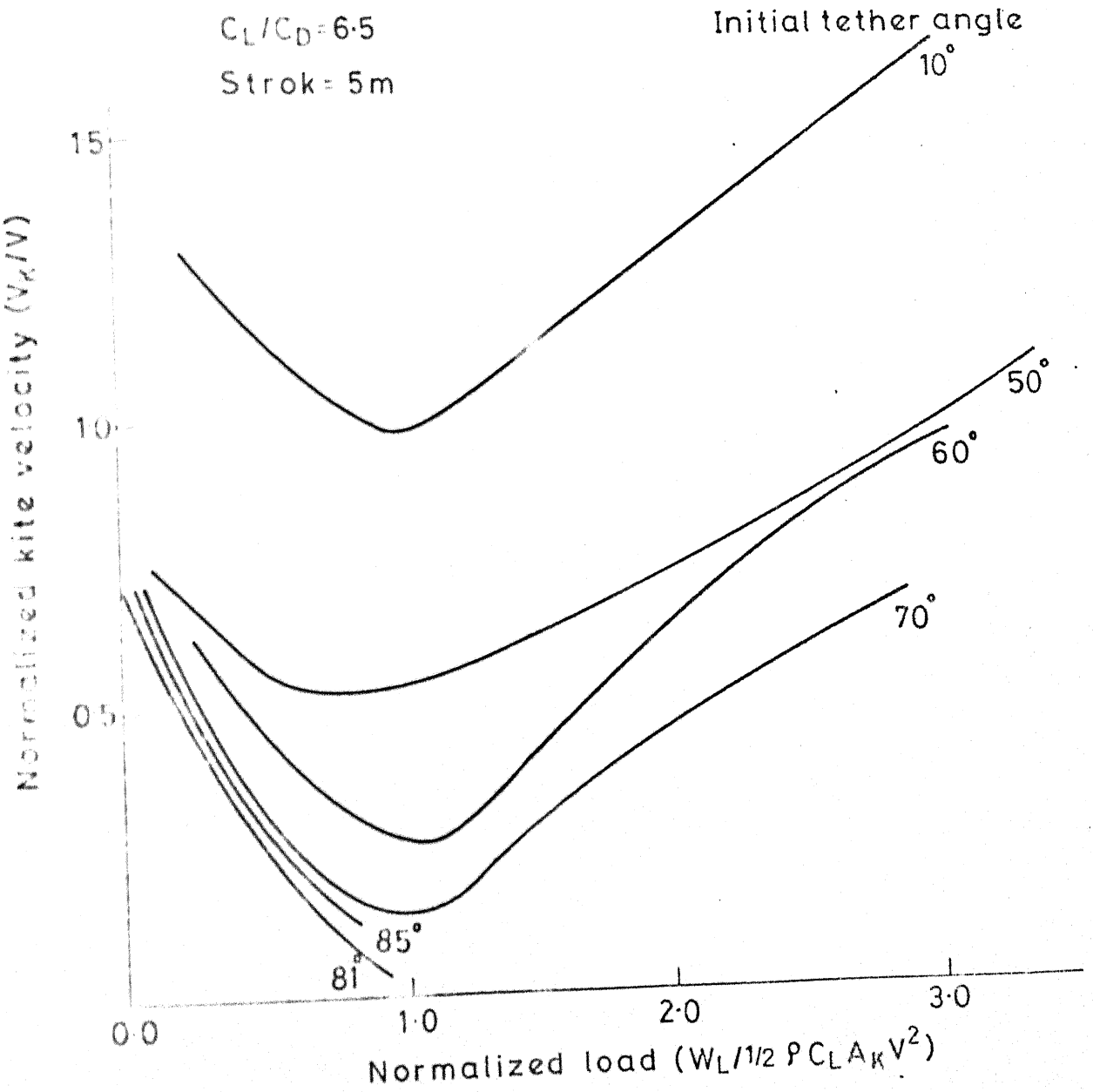

Fig.50 Load vs kite velocity at the end of ascension